Muhammad Faisal

Homo- and Heteronuclear Cold Collisions between ^{7}Li, ^{23}Na and ^{87}Rb Atoms in a Magneto-Optical Trap

DISSERTATION

zur Erlangung des akademischen Grades
Doktor der technischen Wissenschaften

Doktoratsstudium der technischen Wissenschaften
Technische Physik

Technische Universität Graz

Betreuer:

Univ.-Prof. Dipl.-Ing. Dr.techn. Laurentius Windholz

Institut für Experimentalphysik

Graz, Juni 2010

Beschluss der Curricula-Kommission für Bachelor-, Master- und Diplomstudien vom 10.11.2008
Genehmigung des Senates am 1.12.2008

EIDESSTATTLICHE ERKLÄRUNG

Ich erkläre an Eides statt, dass ich die vorliegende Arbeit selbstständig verfasst, andere als die angegebenen Quellen/Hilfsmittel nicht benutzt, und die den benutzten Quellen wörtlich und inhaltlich entnommenen Stellen als solche kenntlich gemacht habe.

Graz, am …….

…….
……..
(Unterschrift)

Englische Fassung:

STATUTORY DECLARATION

I declare that I have authored this thesis independently, that I have not used other than the declared sources / resources, and that I have explicitly marked all material which has been quoted either literally or by content from the used sources.

…… ……

date (signature)

ABSTRACT

Homo- and Heteronuclear Cold Collisions between ^{7}Li, ^{23}Na and ^{87}Rb Atoms in a Magneto-Optical Trap

^{7}Li and ^{23}Na atoms as well ^{87}Rb and ^{23}Na were trapped simultaneously in a two-species magneto optical trap (MOT). The laser frequencies needed to capture ^{87}Rb atoms were generated by a ring dye laser, which was stabilized at D_2 resonance line using saturation spectroscopy. The locking frequency could be shifted by a variable static magnetic field which was modulated in order to generate the first derivate for locking. To our knowledge it is the first time that this method of locking was used when trapping Rb atoms. Steady state atom numbers, density and volume of the atomic cloud and the fraction of excited atoms were determined for each element in order to characterize the MOT. Goal of the investigations was the measurement of homo-and heteronuclear collisional loss rate coefficients 'β' and '$\hat{\beta}$' between same and different species of atoms.

ABSTRACT

Homo- and Heteronuclear Cold Collisions between ^{7}Li, ^{23}Na and ^{7}Rb atoms in a Magneto-Optical Trap

^{7}Li und ^{23}Na Atome sowie ^{87}Rb und ^{23}Na Atome konnten gleichzeitig in einer für zwei chemische Elemente geeigneten Magnetooptischen Falle (MOT) gefangen werden. Die Frequenzen für das Einfangen der ^{87}Rb Atome wurden mittels eines Farbstoff-Ringlasers erzeugt. Dieser wurde mittels Sättigungsspektroskopie stabilisiert, wobei der Stabilisierungspunkt mit Hilfe statischer, modulierter magnetischer Felder verschoben werden konnte. Die stationäre Atomanzahl, die Dichte und das Volumen der Atomwolke und der Anteil der angeregten Atome wurde für jedes Element getrennt bestimmt, um die MOT zu charakterisieren. Ziel der Untersuchungen war die Messung der Ratenkoeffizienten ‘β’ und ‘$\hat{\beta}$’ für Stöße zwischen gleichartigen bzw. verschiedenen Sorten von kalten Atomen (homo- bzw. heteronukleare Stoßraten).

Declaration

This dissertation is submitted to the Institute of Experimental Physics, Graz University of Technology, Graz Austria, in partial fulfillment of the requirement for the degree of Doctor of Technical Sciences.
The thesis is entitled:

Homo- and Heteronuclear Cold Collisions between ^{7}Li, ^{23}Na and ^{87}Rb atoms in a Magneto-Optical Trap

written by Muhammad Faisal and has been approved by the Institute of Experimental Physics, Graz University of Technology, Graz Austria.

The final copy of this thesis has been examined by the under signed authority, and find that both the content and the form meet acceptable presentation standards of scholarly work in the above mentioned discipline.

_____
Univ. Prof. Dip.-Ing. Dr. tech. Laurentius Windholz

Date _____

Acknowledgments

In pre eminent, I would like to offer my exuberance gratefulness special esteem and honor to my supervisor, Prof. Dr. Laurentius Windholz, for his extraordinary support and guidance during my entire period of research. I am profoundly impressed with his noteworthy and incredible ability of correlating theoretical interpretation of experimental observations. I enormously regard and respect him with core of my heart. I would strive hard to acquire this unique ability in my coming life and able to produce such a high quality of scientific understanding for my team members. This transparency and conciseness of understanding is also reflected in his teachings and experimental works. His methods and tireless steps of ownships to improve my professional and communication skills by attendance of useful lectures as well demonstration of experimental setup have paved a major hallmark in my life. During my entire stay at the institute, I never felt hesitate in communicating with him and he is always able to take some time out of his busy schedule for listening to my queries. I consider myself lucky to have such a keen advisor, honest in nature, hard worker and a real gentleman.

I am specially gratefull to the head of the institute, Prof. W. E. Ernst for giving me this opportunity to work here as a research student. I am really impressed for his high quality of leadership. He is highly natural, qualified and above all a loving attitude to share and guide maximum for students.

I am grateful to Dr. Roland and Dr. Auböck for valuable discussions about my experiments. I am thankful to people from machine and electronic workshops for providing me technical supports during my stay.

I am highly thankful to Ivan Vasari for his assistance to develop a stabilization system for Rb repumping beam and analysis of experimental data.

I am also greatful to Imran and Shamim for nice co-operation.

I am thankful to Higher Education Commission (HEC) Islamabad, Govt. of Pakistan for funding my studies.

Dedicated to my

Teachers

Parents and Family

.

1. Introduction

Einstein explained the concept of spontaneous and stimulated emission in 1917. He suggested that spontaneous emission process can transfer a momentum to the atoms (Einstein, 1917). Frisch demonstrated the deflection of a Na atomic beam with the ordinary resonance light (Frisch, 1933). This was a great achievement for the manipulating of Na atomic motion before the laser was invented. The dream of cooling and trapping atoms below mK range with the laser light was suggested by the T. Hänsch & A. Schawlow (Hänsch and Schawlow, 1975) and Wineland & Dehmelt (Wineland and Dehmelt, 1975) in the same year. This dream came true in 1985, when Chu demonstrated to cool the atoms of Na (Chu *et al.*, 1985) by using absorption and spontaneous emission of laser light in three dimensions by creating optical molasses and be reached the temperatures in the μK range.

By introducing a spatially varying magnetic field with opposite circularly polarized laser beams in three dimensions, Raab *et al.*, 1987 demonstrated successfully to cool and trap neutral atoms in a magneto optical trap (MOT). Magneto optical trap was loaded in different ways. At the beginning, the MOT was loaded by slowing an atomic beam (Walker *et al.*, 1990). The MOT apparatus became simpler when vapor cells were used to load the atoms. In a vapor cell, atoms from the velocity edge of the Maxwell-Boltzman Distribution (Monroe *et al.*, 1990) can be captured by laser light.

The captured atoms in MOT have a certain volume and density in the range of 10^9 -10^{10} cm^{-3}. Collisions with background gas, collisions with fast vapor atoms, cold binary interaction of atoms, laser induced collisions, the repulsive force between the atoms and collisions between trapped atoms in the ground state and their excited state in MOT are limiting factors in the achievement of number, high density and storage time (Vigue, 1986; Pritchard, 1986; Prentiss *et al.*, 1988; Sesko *et al.*, 1991) of cold atoms.

There are two types of collisions, elastic collisions and inelastic collisions. Inelastic collisions occur when the atoms absorb light. Further, inelastic collisions reduce the density of the atoms due to fine structure changing collisions (FSCC) and radiative decay (RE)

mechanisms. Section 2.2.2 describes inelastic collisions and loses mechanism in more detail.

Hyperfine Structure Changing Collisions (HFSCC) are also one of the loss mechanisms which occur only in the ground state atoms for all alkali elements at low intensity (Wallace *et al.*, 1992; Ritchie *et al.*, 1995; Weiner *et al.*, 1999). During the elastic collisions, both colliding atoms remain in the ground state. These collisions are essential for ground state atoms for the rethermalization of cold atoms.

At low temperature, following interesting features are observed:

- Domination of long range interaction.
- A long De-Broglie wavelength λ_D at low temperature.
- Collision time is comparable to radiative life time of the excited state atom (Telles *et al.*, 2000).
- Excited state interaction potential for heteronuclear atoms is smaller compared to the excited state potential of homonuclear atoms (Schlöder *et al.*, 1999).

Globally, diverse groups have studied homonuclear and heteronuclear trap losses on different alkali atoms especially sodium, cesium, rubidium, lithium, potassium, sodium-potassium, lithium-sodium. A summery of theoretical and experimental aspects of cold collisions is provided by (Weiner *et al.*, 1999).

1n 1998, our group successfully trapped lithium and sodium atoms simultaneously in a magneto optical trap (Scherf, 1998). This research focused to study cold atom photo-association spectroscopy as well as trap losses due to homo- and heteronuclear cold collisions. (Auböck *et al.*, 2006), measured heteronuclear inelastic cold collisions in a mixed-species ^{7}Li–^{23}Na magneto-optical trap and calculated. The trap depth was calculated by (Szczepkowski *et al.*, 2007).

The scope of this dissertation is to enhance the existing setup by incorporating a new larger chamber (having a large number of ports) and upgrade the existing optical setup. The optical setup for trapping ^{87}Rb atoms was also designed. The updated setup can now be used for trapping ^{23}Na and ^{87}Rb atoms simultaneously, in addition to trapping ^{7}Li and ^{23}Na atoms. Section 3.4 describes the complete set up.

Furthermore the setup has an extra advantage that the three species of atoms ^{7}Li, ^{23}Na and ^{87}Rb can be trapped either independently or in groups of two or three, simultaneously. The experimental results for trap losses for homonuclear and heteronuclear atom pairs i.e. ^{7}Li-^{7}Li, ^{23}Na-^{23}Na, ^{87}Rb-^{87}Rb, ^{7}Li-^{23}Na and ^{87}Rb-^{23}Na are described in (Chapter 4).

2. Theory

This chapter will give an overview of laser cooling and trapping and theoretical background for the cold collisions and existing models to explain the trap loss channels. It is a short review. All theories, the mathematical equations and models can be found in more comprehensive way in a book and a review paper (Weiner, 2003; Weiner, 1999).

2.1 Laser Cooling and Trapping

2.1.1 Light Force

There are two types of light forces exerted on the atom, one is called the spontaneous force and other is called the dipole force. The spontaneous force comes from the impulse of the absorption and emission of the photons. It means that during absorption, a photon transfers the momentum $\hbar k$ to the atom along the propagation direction (where $\hbar = h/2\pi$ and $k = 2\pi/\lambda$). Due to absorption of photons, spontaneous and stimulated processes occur. The average force due to absorption and emission cycle is zero during spontaneous emission (as shown in figure 2.1) but net spontaneous force acting on the atom in the direction of laser propagation is present.

The dipole force is created during the stimulated process such that momentum is conserved but net exchange of energy between atom and photon is zero. Keeping momentum conservation during stimulated process, a net recoil force is transferred to atom.

During collisions energy is transferred such that

$$U = -\mu.\mathbf{E} \qquad (2.1)$$

where μ is transition dipole moment, $\mathbf{E}$ is the electric field of laser light. But the negative of the spatial gradient of potential energy gives a force which is

$$\mathbf{F} = -\nabla_R.\mathbf{U} = \mu\nabla_R\ \mathbf{E} + E\nabla_R\mu \qquad (2.2)$$

but $\nabla_R \mu$ is zero because there is no spatial variation of dipole over the length of optical field.

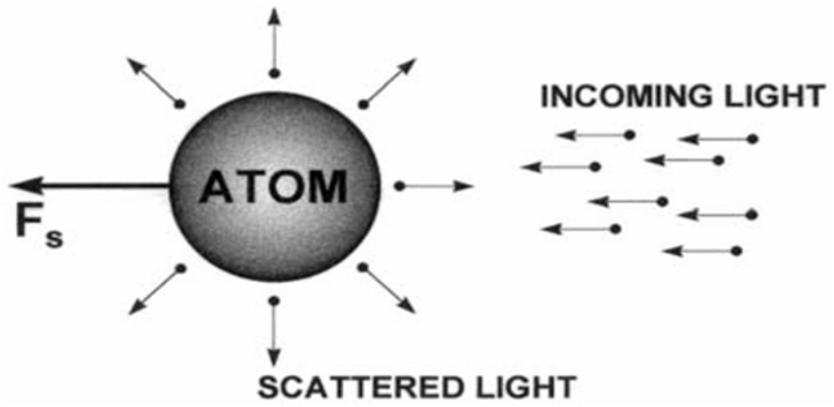

Figure 2.1:.Light coming in one direction but spontaneous emission occurs in all directions (Weiner, 1999).

Average force during the optical-cycle is

$$\langle F \rangle = \langle \mu \nabla_R E \rangle = \mu \{ (\nabla_R E_0) \mu + (E_0 \nabla_R (k_L R) \nu) \} \qquad (2.3)$$

where μ and ν are obtained from the steady state solution of the Optical Bloch Equations (OBE). R is internuclear distance.

$$\mu = \frac{\Omega}{2} \frac{\Delta\omega_L}{(\Delta\omega_L)^2 + (\Gamma/2)^2 + \Omega^2/2} \qquad (2.4)$$

and

$$\nu = \frac{\Omega}{2} \frac{\Gamma/2}{(\Delta\omega_L)^2 + (\Gamma/2)^2 + \Omega^2/2} \qquad (2.5)$$

Here $\Delta\omega_L = \omega - \omega_0$ is detuning of laser from the atomic transition frequency ω_0 and Γ is natural width of atomic transition.

The Rabi frequency Ω tells the strength of the coupling between laser field and atom such as

$$\Omega = -\frac{\mu . E_0}{\hbar} \qquad (2.6)$$

and light intensity

$$I = \frac{1}{2}\varepsilon_0 c E_0^2 \qquad (2.7)$$

Consider equation (2.3) which shows that time average dipole μ and ν are in phase.

$$\langle \mu \rangle = 2\mu(u\cos\omega_L t - v\sin\omega_L t) \qquad (2.8)$$

Classically electric field of light is

$$E = E_0[\cos(\omega t - k_L R)] \qquad (2.9)$$

According to equation (2.3), the force depends upon the gradient of electric field amplitude as well as gradient of the phase.

$$\langle F \rangle = \mu(\nabla_R E_0)\frac{\Omega}{2}\left[\frac{\Delta\omega_L}{(\Delta\omega_L) + (\Gamma/2)^2 + \Omega^2/2}\right] + \mu[E_0 \Delta_R(\ k_L R)]\frac{\Omega}{2}\left[\frac{\Gamma/2}{(\Delta\omega_L)^2 + (\Gamma/2)^2 + \Omega/2}\right]$$

_____ (2.10)

First term in equation (2.10) represent the trapping force $\langle F_T \rangle$

$$\langle F_T \rangle = \mu(\nabla_R E_0)\frac{\Omega}{2}\left[\frac{\Delta\omega_L}{(\Delta\omega_L) + (\Gamma/2)^2 + \Omega^2/2}\right] \qquad (2.11)$$

and

$$U_T = -\int F_T dR = \frac{\hbar\Delta\omega_L}{2}\ln\left[1+\frac{\Omega^2/2}{(\Delta\omega_L)^2+(\Gamma/2)^2}\right] \qquad (2.12)$$

The trapping force is conservative and defines the trapping potential of the atom.

Second term in equation (2.10) is a cooling force $\langle F_C \rangle$.

$$\langle F_C \rangle = \mu E_0 k_L \frac{\Omega}{2}\left[\frac{\Gamma/2}{(\Delta\omega_L)^2+(\Gamma/2)^2+\Omega/2}\right] \qquad (2.13)$$

Spontaneous force in nature is a dissipative force which is used to cool atoms.

The dipole force in Equation (2.10) can also expressed in terms of the saturation parameter

$$F_T = \frac{1}{2\Omega}\nabla\,\Omega^2\,\hbar\,\Delta\,\omega_L\left(\frac{s}{1+s}\right) \qquad (2.14)$$

Where ‘s’ is called saturation parameter, It can be expressed as

$$s = \frac{\Omega^2/2}{(\Delta\omega_L)^2+(\Gamma/2)^2} \qquad (2.15)$$

Equation (2.15) explains criteria to compare the time required for the stimulated and spontaneous process. If $s \ll 1$ then the spontaneous emission is stronger than stimulated Rabi oscillation. If $s \gg 1$ then Rabi oscillation is stronger than spontaneous emission.

By using equation (2.7), the trapping force F_T can be expressed in term of gradient of light intensity, the saturation parameter and detuning i.e.

$$F_T = \frac{1}{4\,I}(\nabla\,I)\,\hbar\,\Delta\omega_L\left(\frac{s}{1+s}\right) \qquad (2.16)$$

Where $\Delta\omega_L < 1$ (red detuning) and $\Delta\omega_L > 1$ (blue detuning) generates attractive and repulsive forces respectively.

The cooling force or spontaneous force in terms of saturation parameter and spontaneous emission rate are

$$F_C = \frac{\hbar k_L \Gamma}{2}\left(\frac{s}{1+s}\right) \qquad (2.17)$$

Equation (2.17) shows that the spontaneous force is only due to emission and absorption of photons having momentum $\hbar k_L$ (Weiner, 1999).

2.1.2 Doppler Cooling

Spontaneous force in nature is dissipative force which is used to cool atoms. According to section 2.1.1, equation (2.13) shows the cooling force on a single atom. Now consider two counter propagating laser beams which are traveling in opposite direction towards an atom as shown in figure (2.2). Polarization, frequency and intensity of these laser beams are same. If the atom is at rest then the net force according to equation 2.13 is zero because the wave vector k is opposite for both beams. Now let the atom is moving with a velocity v, the net force acting on it is proportional to its velocity where as its direction depends on the laser frequency. When the atom and laser beam are moving in opposite direction, the laser frequency is Doppler shifted towards blue to the atomic rest frame, if the laser beam frequency is below the atomic resonance frequency. On other hand, if the atom and laser beam are moving in the same direction i.e. are parallel to each other then the laser frequency is Doppler shifted towards red and is out of resonance (Weidemüller and Zimmermann, 2009). It shows that during interaction of atom with laser beams, the velocity of atoms is reduced and alternatively they are cooled down. So this dissipative or cooling force is responsible to reduce the velocity of atoms and this process is known as optical molasses. If there are three pairs of laser beams in opposite direction in x, y and z directions and intersecting in a certain point, than the atoms are restricted in the intersection points. These restricted atoms are cooled due the dissipative or cooling force in three directions (Chu *et al*., 1985). This process is called Doppler cooling.

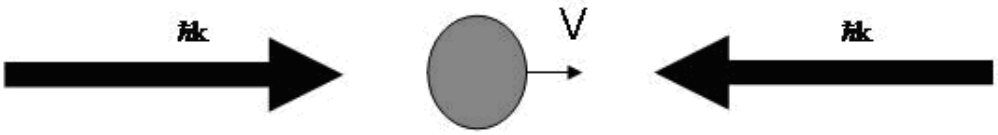

Figure 2.2: Two counter propagating laser beams reducing the velocity of an atom.

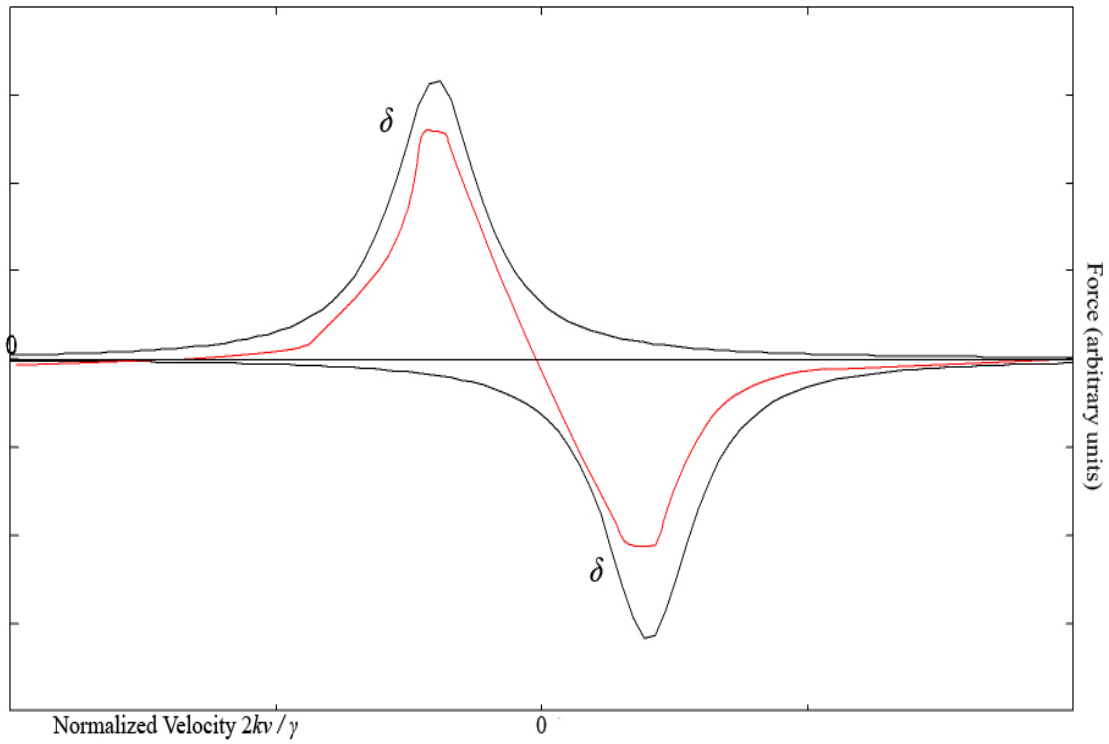

Figure 2.3: Force on moving atom during Doppler Cooling (Metcalf and van der Straten, 1999).

2.1.3 Magneto Optical Trap

Spontaneous force can be used to cool the neutral atoms (Pritchard *et al.*, 1986). This was first time demonstrated in 1987 in a magneto optical trap (MOT). It consists of inhomogeneous magnetic field and an optical field produced by three polarized laser beams (Raab *et al.*, 1986).

Consider a two level system, having a transition from $J=0 \rightarrow J=1$ moving along the z-direction. A magnetic field B (z) is applied which increases linearly in $\pm z$ directions from the center of the trap where B =

0. Due to inhomogeneous magnetic field, the energy levels of atom are Zeeman shifted. This Zeeman shift depends upon the strength of magnetic field ($\Delta M = +1$ and $\Delta M = -1$ are shifted up and down, respectively as shown in figure 2.4).

Atoms are also excited with counter propagating circular polarized beams. The frequency of laser beams is red detune (Δ) to atomic transition. A laser beam traveling from right hand side as well as left hand side of trap are σ^- polarized (see figure 2.5). Sign of polarization of laser beams ($\sigma^{\pm}$) are related to the direction of magnetic field as shown in figure 2.4. A σ^- laser beam is more in resonance (due to red detuning) with $\Delta M = -1$ transition, scattering more light compare to σ^+ laser beam at certain position of atom x' according to figure 2.4. Atom is always pushed towards the center of trap due to this net spontaneous force (The direction of the force is also towards the center of magneto optical trap) (Auböck, 2004). Force acting on the atom traveling in $+z$ direction, with red tuning Δ and magnetic field B is given by

$$F_{+z} = -\frac{\hbar k}{2}\Gamma \frac{\Omega^2/2}{\left(\Delta + kv_z + \frac{\mu_B}{\hbar}.\frac{dB}{dz}.Z\right)^2 + (\Gamma/2)^2 + \Omega^2/2} \qquad (2.18)$$

Similarly force acting on the atom traveling in $-z$direction where laser is red detuned

$$F_{-z} = +\frac{\hbar k}{2}\Gamma \frac{\Omega^2/2}{\left(\Delta - kv_z - \frac{\mu_B}{\hbar}.\frac{dB}{dz}.Z\right)^2 + (\Gamma/2)^2 + \Omega^2/2} \qquad (2.19)$$

Net restoring force on atom is always towards the spatial center where B = 0. So atoms always push toward the center where the magnetic field is zero. The restoring force is velocity dependent due the Doppler shift of atomic motion.

Restoring force can be written in term of velocity and displacement

$$F(v,z) = F_{+z} + F_{-z} = -\alpha \dot{z} - Kz \qquad (2.20)$$

According to equation (2.20), the behavior of atom is damped harmonic oscillator

$$\ddot{z} + \frac{2\alpha}{m} z + \frac{K}{m} z = 0 \qquad (2.21)$$

Where $\alpha = \hbar k \Gamma \dfrac{16|\Delta'|(\Omega')^2 (k/\Gamma)}{\left[1+2(\Omega')^2\right]^2 \left[1+\dfrac{4(\Delta')^2}{1+2(\Omega')^2}\right]^2}$ is damping constant

and

$$K = \hbar k \Gamma \frac{16|\Delta'|(\Omega')^2 (d\omega_o / dz)}{\left[1+2(\Omega')^2\right]^2 \left[1+\dfrac{4(\Delta')^2}{1+2(\Omega')^2}\right]^2}$$ is known as spring constant

By considering six laser beams, this two dimension scheme is easily converted into three dimensions.

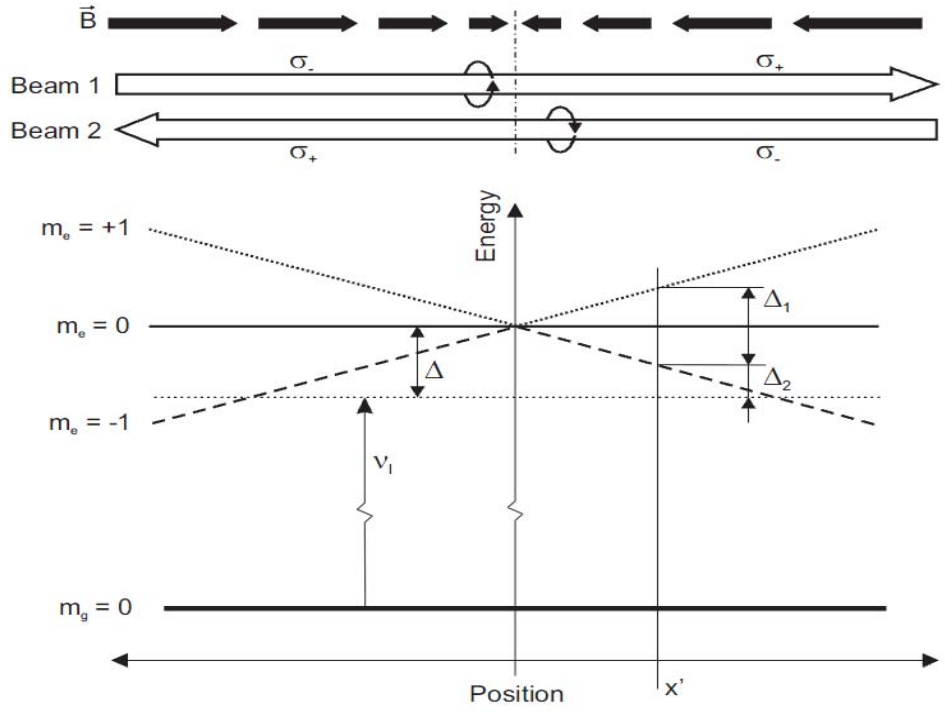

Figure 2.4: One dimensional magneto optical trap. Magnetic field and laser beams are shown separately. Dashed line indicates the laser frequency seen by an atom at rest. Δ_1 and Δ_2 are detuning for σ^+ and σ^- polarized light at position x'.

Due to the velocity damping, the kinetic energy is released by the atoms

$$\frac{E}{E_o} = e^{-\frac{2\alpha}{m}t}$$

Where E_0 is initial kinetic energy before starting the cooling process and

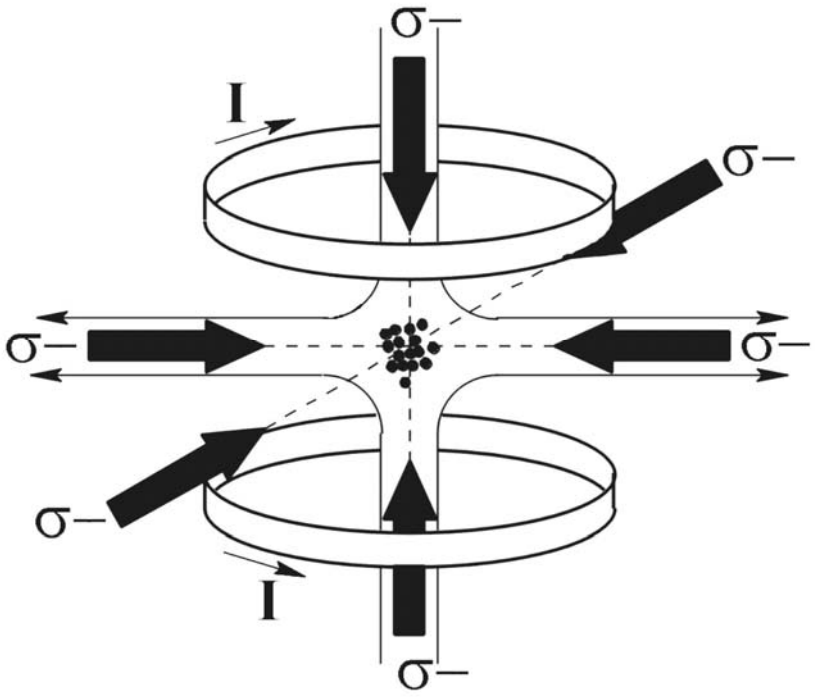

Figure 2.5: Sketch of magneto optical trap. Atoms are trapped in center

m is the atomic mass and $\tau = \frac{m}{2\alpha}$ where τ is damping time. So the spontaneous force as well as the dissipative force is used to cool and confined atoms in the magneto optical trap (Wiener *et al.*, 1999).

2.1.4 Doppler Cooling Limit

In principle, MOT should be capable to cool the atom to absolute temperature zero according to the equations (2.18) & (2.19) but due the atomic recoils and spontaneous emission creates the heating effect (Phillips, 1998). Suppose, there are N number of absorption and re-emission of atoms, the average momentum of all atoms will be zero $< p > = 0$. But there is the recoil effect due to emission of the photons so $< p^2 > \neq 0$. There is a equilibrium state after a certain time due to cooling and heating process. This is temperature limit of Doppler cooling and called Doppler limit.

Consider a velocity of the atom such as

$v = \frac{\sqrt{< p^2 >}}{M}$ after absorption of photon, change in p^2 is

$$(p - \Delta p)^2 \approx -2p\Delta p = -2Mc\hbar k \qquad (2.22)$$

But the number of decelerating photon s = $\frac{kv}{\gamma}$ where $kv << \gamma$

Therefore cooling is

$$\left(\frac{\partial < p^2 >}{\partial t}\right)_{cooling} \approx N\frac{kv}{\gamma}2Mv\hbar k = NM\frac{\hbar k^2}{\gamma} \qquad (2.23)$$

By considering the random walk phenomenon, the heating process can be calculated such as

$$\left(\frac{\partial < P^2 >}{\partial t}\right)_{heating} \approx N\Delta p^2 = N\hbar^2 k^2 \qquad (2.24)$$

When the processes are in equilibrium

$$\left(\frac{\partial < p^2 >}{\partial t}\right)_{cooling} + \left(\frac{\partial < p^2 >}{\partial t}\right)_{heating} = 0 \qquad (2.25)$$

So

$$T_D \propto Mv^2 = \frac{\hbar\gamma}{2} \qquad (2.26)$$

Hence

$$k_B T_D = \frac{\hbar\gamma}{2} \qquad (2.27)$$

Where T_D is the Doppler temperature.

When laser frequency is tuned such as $\delta = \frac{\gamma}{2}$ then the Doppler limit is reached. For example ^{23}Na, ^{87}Rb and ^{7}Li have the Doppler temperature of approximately 240 μK ,143 μK and 142 μK, respectively (Metcalf and van der Straten, 1999).

In polarization gradient cooling, optical molasses depends upon the circularly polarized light, Zeeman levels of atom and the light shift. (Dalibard and Tannoudji, 1989).

Below Doppler cooling limit, there is a recoil limit where a minimum energy of photon is absorbed and atom is decayed spontaneously in a magneto optical trap. Mathematically it can be expressed as

$$E_{rec} = k_b T_{rec} = \frac{\hbar^2 k^2}{2M} \qquad (2.28)$$

Where E_{rec}= recoil energy, k_b = Boltzman constant. T_{rec}= recoil temperature. Recoil limit for ^{87}Rb atom is 4μK which is ten times less than Doppler limit.

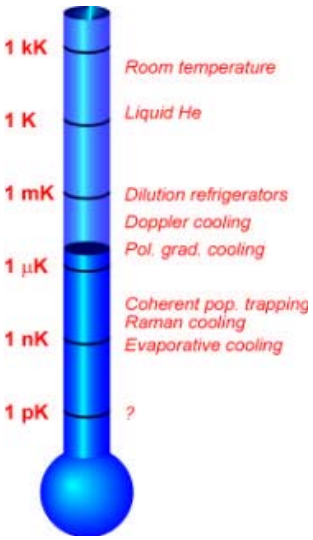

Figure 2.6: Temperature scale starting from room temperature to evaporating cooling

.Velocity-selective coherent population trapping is another technique in which one can achieve a temperature below the recoil limit. The atoms cannot absorb the resonance light if they are in coherent superposition of their two ground states. The reason for this is the velocity selective population which results in a decay to non–absorbing coherent superposition of states. (Aspect *et al.*, 1988).

2.2 Cold Collisions

2.2.1 Quasi Molecular Potential

Two atoms of the same element or different element approach each other and interact for short interval of time and form a quasi-molecule.

Interaction potential can be described as

$$U_{eff}(R) = U(R) + \frac{\hbar l(l+1)}{2\mu R^2} \qquad (2.29)$$

Where R is inter atomic separation and μ is the reduced mass of the colliding atoms. For the long range interaction potential is given by

$$U(R) = D - \sum_n \frac{C_n}{R^n} \qquad (2.30)$$

Where D is known as dissociation energy and $\frac{C_n}{R^n}$ shows the multiple interactions of interacting atoms. The value of C_n is calculated and well explained with perturbation theory (Bussery, 1987). During collision if one atom is in the excited state and other atom is in ground state then nature if interaction depends upon colliding partner (belongs to same element or different element).

For the homonuclear quasi-molecule, the interaction potential is $\frac{C_3}{R^3}$ and is called the resonant dipole-dipole interaction, whereas for the heteronuclear quasi-molecule, the induced dipole-dipole potential $\frac{C_6}{R^6}$ is due to van der Waals interaction (Schlöder *et al.*, 1999).

On other hand when pair of atoms are in ground state then the interaction potential is van der Waals that is $\frac{C_6}{R^6}$.

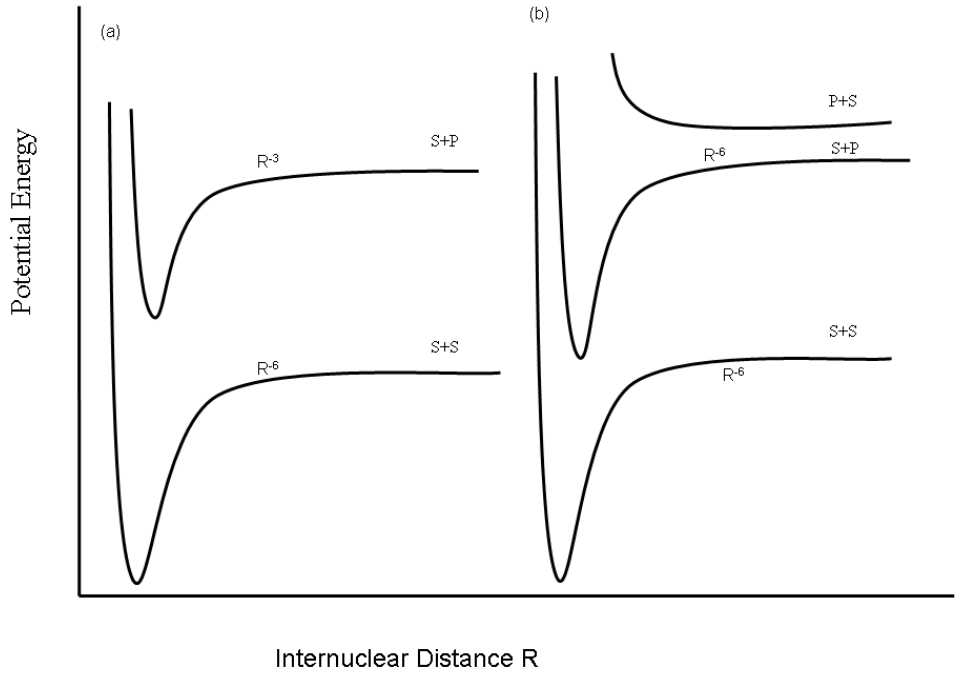

Figure 2.7: Ground and excited state interaction potential for homonuclear (a) and heteronuclear (b) quasi-molecule.

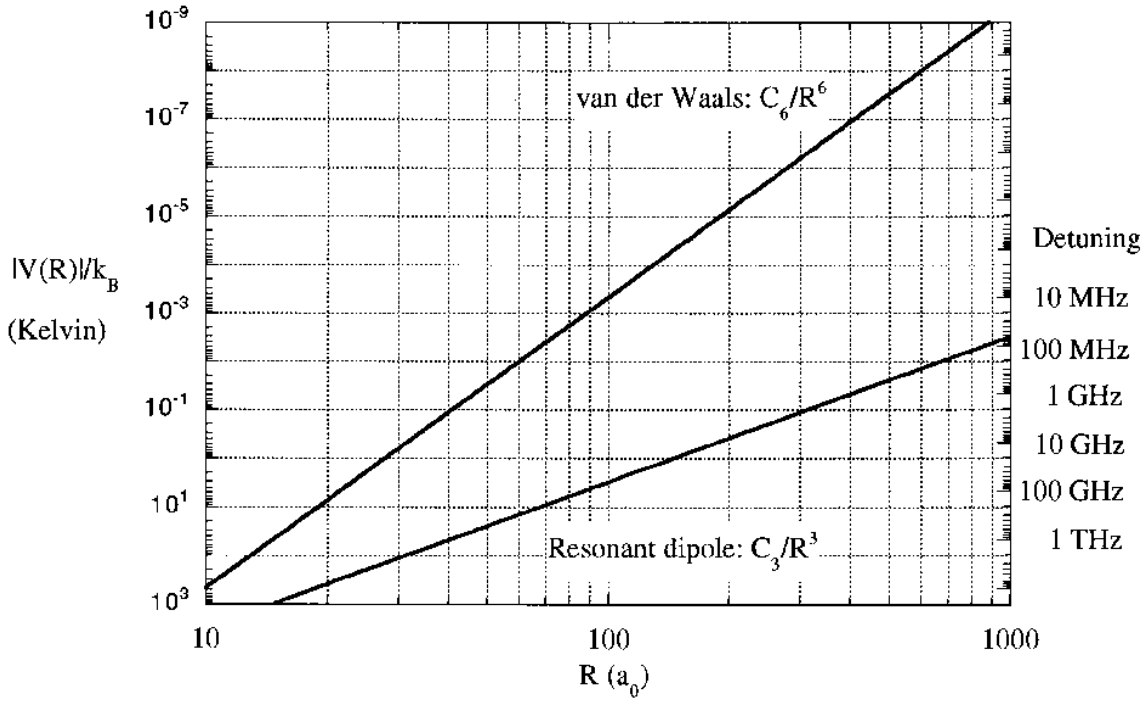

Figure 2.8: Interaction of Na atom in ground and excited states potentials due to van der Waals and resonate dipole forces (Julienne, 1996).

2.3 Inelastic Collisions in MOT

Cold collisions can be distinguished as elastic and inelastic collisions. In elastic collisions the momentum and the kinetic energy are conserved. During inelastic collisions the internal energy is non conserved and this energy is converted into the kinetic energy of the interactive atoms. If the kinetic energy of the single atom or pair is greater then the trap depth, the atom will escape from the MOT.

Main trap escape mechanisms are Radiative Escape (RE) and Fine Structure Changing Collisions (FSCC). These mechanisms occur when one atom is in the ground state and other is in the excited state and they travel towards each other due to the attractive potential at large internuclear distance. So during cold collision, absorption, spontaneous or stimulated emission processes can occur. Cold collisional time between colliding pair of atom is longer as compared the interaction time between colliding atoms at normal temperature. Excited state atom have a certain decay time, if this decay time is shorter then the collisional time (interaction time between the colliding atoms), extra energy is released. This released kinetic energy is divided equally between the colliding atoms. If this shared kinetic energy of atoms is greater then magneto optical trap depth then trap loss occurs.

If both atoms are in the ground state then a change in the hyperfine structure may occur and due to this change the trap loss occur. This mechanism is called the Hyperfine Changing Collision (HFSCC). These mechanisms are well explained by the Gallagher-Pritchard and Julienne-Vigue model described sections 2.3.1, 2.3.2.

2.3.1 Gallagher – Pritchard Model

Gallagher and Pritchard (Gallagher and Pritchard, 1989) developed a semi classical model to explain trap losses due to Fine Structure Changing Collisions (FSCC) and Radiative Escape (RE) for ultra cold collisions in a MOT and estimated that FSCC is the dominant trap loss process compared to RE trap loss process. Consider a photon is absorbed by an atom when they are at a far apart from each other and they are excited from ground state to a long range attractive molecular state. Suppose that two ground state atoms mentioned as S + S are approaching

each other or one atom is in excited state and other is in the ground state represented as $S+P_{1/2}$ or ($S+P_{3/2}$, respectively) as shown in figure (2.9).

Fine structure changing collisions, the process can be described as

$$A+A+\hbar\omega \rightarrow A^{*}\left(P_{3/2}\right)+A \rightarrow A^{*}\left(P_{1/2}\right)+A+\Delta E_{FS} \qquad (2.31)$$

Where $\Delta E_{FS}/2$ for each atom is transferred to kinetic energy.

Radiative escape process during collision is represented as

$$A+A+\hbar\omega \rightarrow A_2^{*} \rightarrow A+A+\hbar\omega' \qquad (2.32)$$

Energy $E_{RE}=\hbar(\omega-\omega')/2$ is distributed to each atom after collision

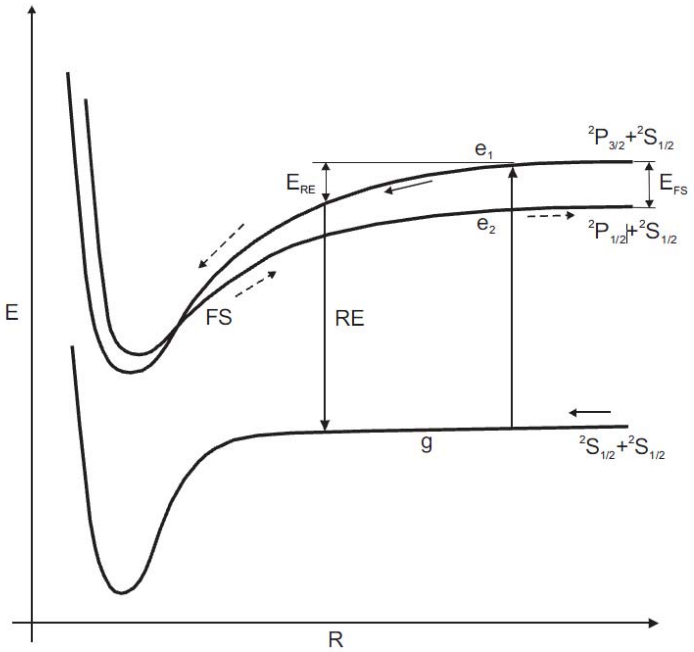

Figure 2.9: Schematic diagram showing the potential energy versus internuclear distance of quasi-molecule. In Fine Structure changing collisions, atom is excited from 'g' to 'e_1' state and then it travel towards small R and then it transferred to 'e_2' state and trap losses occur. Radiative Escape process, the excited atom decayed from 'e_1' state to 'g' state after gaining enough energy to escape from the MOT and trap losses occur (Suominen et al., 1998)

In this model, they consider two atoms having inter nuclear separation R_0, interacting with the laser having frequency ω_L and intensity I, atom is excited and there rate of excitation represented as

$$\Re(R_0,\omega_L,I)=\left[\frac{(\Gamma_M/2)^2}{(\Delta_M)^2+(\Gamma_M/2)^2}\right]\frac{I}{\hbar\omega_L}\frac{\lambda^2}{2\pi}=\varepsilon(\omega_L,R_0)\frac{I}{\hbar\omega_L}.\frac{\lambda^2}{2\pi} \qquad (2.33)$$

With

- $\Delta_M=[\omega_L-\omega(R_0)]$ where resonance frequency $\omega(R_0)=\omega_A - C_3/\hbar R_o^3$
- ω_A is atomic resonance frequency
- C_3 is constant of excited molecular potential
- $\frac{\lambda^2}{2\pi}$ is photo absorption cross section for all attractive molecular states.
- Γ_M is molecular spontaneous decay rate

The colliding atoms start to accelerate on the C_3/R^3 potential and approaching a region where trap loss occur due to RE or FSCC process.

The time required to start the RE or FSCC process is the same as to reach R = 0 and can be calculated such as

$$t(R_0)=\left(\frac{M}{4}\right)^{1/2}\int_0^{R_0}dR\left(\frac{C_3}{R_3}-\frac{C_3}{R_0^3}\right)^{-1/2}=0.747\left(\frac{MR_0^5}{4C_3}\right)^{1/2} \qquad (2.34)$$

Where M = atomic mass.

Using parameters, $\Delta=\omega_A-\omega_L$ is laser detuning, $\tau=\Gamma_M^{-1}$, R_τ= interaction separation and Δ_τ = Detuning at R_τ. The time for the atom to reach the short range zone can be calculated as

$$t(R_\tau)=\left(\frac{\Delta_\tau}{\Delta}\right)^{5/6}\Gamma_M^{-1} \qquad (2.35)$$

The probability of survival against spontaneous emission is

$$\gamma=e^{\left[-\Gamma_M t(R_0)\right]}=e^{\left[\left(-\Delta_\tau/\Delta\right)^{\frac{5}{6}}\right]} \qquad (2.36)$$

Before radiating, a pair A^*-A reaches at that region where FSCC take place. The probability for FSCC is

$$\eta_J = 2P(1-P).$$

Here P = Landau-Zener single transit curve crossing probability.

For repeated oscillation of atoms, total probability P_{FSCC} is the sum of individual transversal probability

$$P_{FSCC} = \eta_J\gamma + \gamma_J(1-\eta_J)\gamma^3 + \ldots.$$
$$= \frac{\eta_J\gamma}{(1-\gamma^2+\eta_J\gamma^2)} \qquad (2.37)$$

Consider 'n' is the total atomic density, the number of pair with separation $R_0 \to R_0 + dR_0$ is $4\pi n^2 R_o dR_o/2$ and total rate of FSCC per unit volume is

$$R_{FSCC} = \frac{n^2}{2}\int_0^\infty dR_0 4\pi R_0^2 \Re(R_o, \omega_L, I) P_{FCC}(R_0) \qquad (2.38)$$

Rate constant between two colliding ground state atoms is

$$K_{FSCC} = \frac{1}{2}\int_0^\infty dR_0 4\pi R_0^2 \Re\left(R_{0,}, \omega_L, I\right) P_{FCC}(R_0) \qquad (2.39)$$

Equation (2.38) can be written in terms of binary collisions between pairs of one excited and one unexcited atom

$$R_{FSCC} = nn^* k'_{FSCC} \qquad (2.40)$$

Where n^* is excited state density, at the steady state, the rate of atom photo excitation is the product of photon flux, atom density and absorption cross section gives the rate fluorescence.

$$\left(\frac{I}{\hbar\omega_L}\right) n\left(\frac{\lambda^2}{\pi}\right)\left[\frac{\Gamma_A^2/4}{(\Delta_M)^2+\Gamma_A^2/40}\right] = n^*\Gamma_A \qquad (2.41)$$

By using equation (2.33), (2.38), (2.39) and (2.41) we get

$$k'_{FSCC} = \frac{1}{4}\left[\frac{(\Delta_M)^2 + \Gamma_A^2/4}{\Gamma_A/4}\int_0^\infty dR_0\, 4\pi R_0^2 \varepsilon(\omega_L, R_0) P_{FCC}(R_0)\right] \qquad (2.42)$$

Radiative escape per unit volume can be calculated from equations (2.39 and 2.42), by replacing $P_{FCC}(R_0)$ by $P_{RE}(R_0)$. Consider the probably of spontaneous emission during transition region where $R < R_E$. R_E is the inter-nuclear separation at which the kinetic energy of colliding pair is enough to escape from MOT.

Probability $P_{RE}(R_0)$ at inter-nuclear separation $R < R_E$ spending time $2t_E(R_0)$ is

$$P_{RE}(R_0) = \frac{2t_E(R_0)\Gamma_{M\gamma}}{1-\gamma^2+\eta_j\gamma^2} \qquad 2.43)$$

Rate constant for RE is analogous to equation (2.39)

$$k_{RE} = \frac{1}{2}\int_0^\infty dR_0\, 4\pi R_0^2 \Re\left(R_{0,}, \omega_L, I\right) P_{FCC}(R_0) \qquad (2.44)$$

Also alternate expression as analogous to equation (2.42)

$$k'_{RE} = \frac{1}{4}\left[\frac{(\Delta_M)^2 + \Gamma_A^2/4}{\Gamma_A/4}\int_0^\infty dR_0\, 4\pi R_0^2 \varepsilon(\omega_L, R_0) P_{FCC}(R_0)\right] \qquad (2.45)$$

For sodium collision, Gallagher and Pritchard calculated $\eta_J = 0.2$ and measured the probability for homonuclear losses in magneto optical trap is $P_{FSCC}/P_{RE} \approx 20$ (Gallagher and Pritchard, 1989).

2.3.2 Julienne-Vigue Model

In 1991, Julienne and Vigue also worked on the facts of cold collision losses and purposed a model in which they considered angular momentum and thermal averaging procedure. They considered the effect of retardation on molecular spontaneous emission but without consideration of the molecular hyperfine structure (Julienne and Vigue, 1991).

The rate of FSCC or RE transition per unit volume is given by

$$\frac{\text{rate}}{\text{volume}} = kn^2 = \frac{1}{2d_g^2}\frac{\pi v}{k^2}\sum_{l,\varepsilon}(2\ell+1)P_{TL}(\varepsilon,\ell)P_{ES}(R,\varepsilon,\ell,\Delta,I)n^2 \qquad (2.46)$$

With

- n = ground state density
- v=Asymptotic velocity for atoms
- k = Wave vector
- I = Light Intensity
- d_g = Ground state degeneracy and factor 1/2 shows the homo nuclear symmetry.
- $P_{TL}(\varepsilon,\ell)$ = Probability trap losses due to FSCC or RE mechanism.
- $P_{ES}(R,\varepsilon,\ell,\Delta,I)$ = Excitation and survival excitation probability is due to the excited state ε produced at the rate G(R′) at $R' > R$

The excitation and survival probability $P_{ES}(R,\varepsilon,\ell,\Lambda,I)$ can be expressed as

$$P_{ES}(R,\varepsilon,\ell,\Lambda,I) = \int_R^\infty G(R',\varepsilon,\Delta,I)S_{Ei}^l(R,R',\varepsilon)\frac{dR'}{v_{Ei}^l(R')} \qquad (2.47)$$

Hence

$S_{Ei}^l(R,R',\varepsilon)$ = survival factor

ε= excited state

angular momentum = l and

E_i= kinetic energy initialized by ground state.

$G(R',\varepsilon,\Delta,I)\ \frac{dR'}{v_{Ei}^l(R')}$ is excitation probability in term of excited rate $G(R',\varepsilon,\Delta,I)$.

Julienne and Vigue calculated the trap loss coefficient β by examining FSCC and RE of Na, Rb, Li, K and Cs as shown in the figure (2.10) (Julienne and Vigue, 1991).

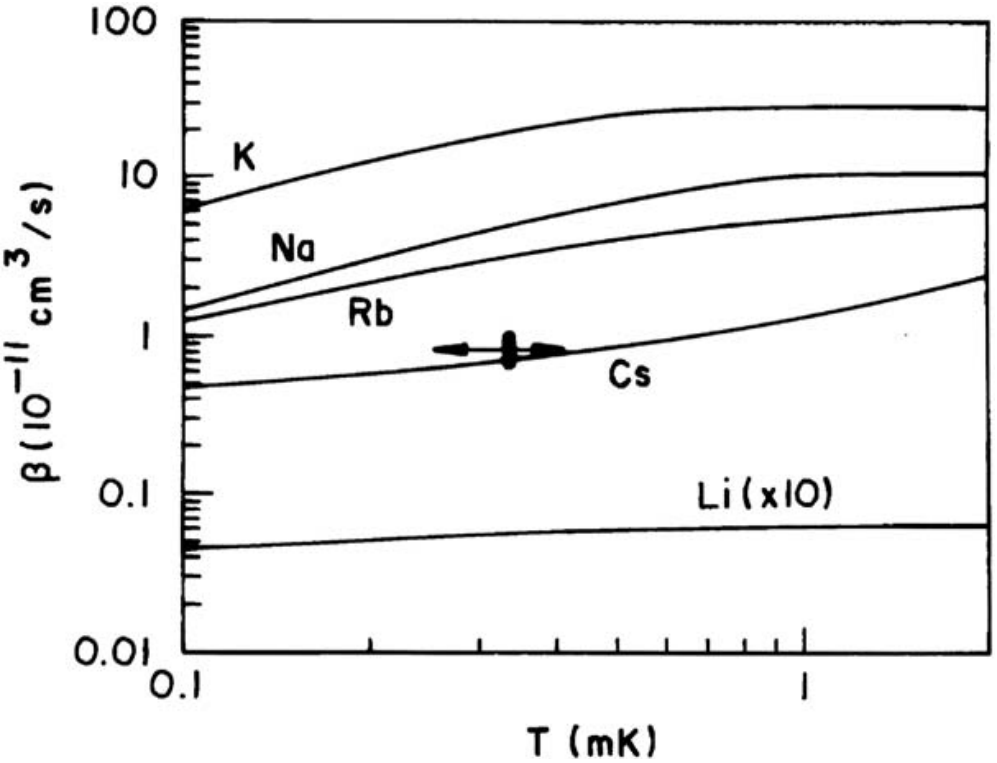

Figure 2.10: Trap loss rate coefficient β of K, Na, Rb, Cs and Li versus temperature calculated by (Julienne and Vigue, 1991).

2.3.3 Method of Complex Potential

Method of complex potential is developed for cold collisions, thus for measuring the losses in a MOT at weak field (low intensity) where optical cycling of population between ground and excited state can be ignored (Boesten *et al.*, 1993; Julienne *et al.,* 1994) developed a method of complex potential to verify the semi classical theories. In this method, they explained the trap losses due to small detuning of laser light which are not explained in semi classical theories.

By using this method some one can also calculate the probability for trap losses for long range excitation as well as probability for survival $J(E,l,\ell,\Delta,I;\Gamma)$ and short range loss processes $P_X(E,\ell)$ such as

$$P(E,\ell,\Delta,I;\Gamma) = P_X(E,\ell)J(E,l,\ell,\Delta,I;\Gamma) \qquad (2.48)$$

Where E, ℓ, Δ, I and Γ represent total collision energy, angular momentum, detuning, intensity and spontaneous decay rate, respectively. The X subscript stands for FSCC or RE mechanism in equation (2.48). Julienne also introduced a three state model having ground state entrance channel, an optically excited molecular state and a fictitious probe state. This model explains the collision losses due to FSCC or RE processes (Julienne *et al.*, 1994). The total probability for losses in term of S matrix having to ground state ' g ' to probe state 'p' is

$$P(E,\ell,\Delta,I;\Gamma) = \left|S_{gp}(E,\ell,\Delta,I;\Gamma)\right|^2 = P_{XQ}(E,\ell).J_Q(E,\ell,\Delta,I;\Gamma) \qquad (2.49)$$

Subscript Q in equation (2.49) represents the "quantum closed coupling". Julienne in his model compared J_Q with J_{JV} (probability of trap losses in Semi classical JV model) J_{BJ} (probability of trap losses calculated by OBE method).

By using J_{BV} and J_{LZ}, the Landau-Zener formula can be written as

$$J_{LZ} \cong S_a e^{-A} \qquad (2.50)$$

Where S_a = survival factor, A = LZ (Landau Zener) arguments

$$A = \frac{2\pi\left|V_{ag}(I)\right|^2}{\hbar\left|\frac{dV_a}{dR} - \frac{dV_g}{dR}\right|_{R_c} v_a} \qquad (2.51)$$

where ' V_{ag} ' = optical coupling . By laser intensity, optical coupling is also increased.

OBE calculation, Landau-Zener model and LZ model of Julienne, respectively.(Julienne et al., 1994).

The product of $\left|\frac{dV_a}{dR} - \frac{dV_g}{dR}\right|$ at Condon point R_c and local velocity v_a and trap loss probability depends upon trend of $J_Q(E,\ell,\Delta,I;\Gamma)$.

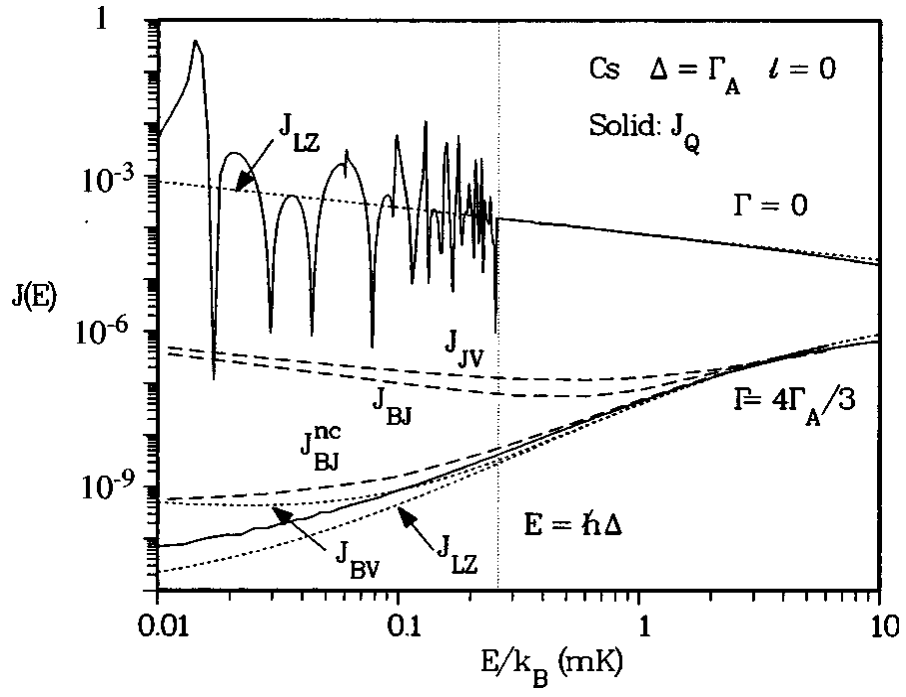

Figure 2.11:. Trap loss probabilities J's versus collisional temperature for Cs atoms. Trap loss probability of J_{JV}, J_{BJ}, J_{BV} and J_{LZ} from semi classical JV model, OBE calculation, Landau-Zener model and LZ model of Julienne, respectively.(Julienne et al., 1994).

2.3.4 Two- Photon Distorted Theory

An advanced version of the method of complex potential theory is two-photon wave theory. This theory explains cold collision losses in weak field, two photon spectra, collisional induced energy distribution and radiative escape. This theory also includes hyperfine states (Solts *et al.*, 1995).

The main focus of theory is the treatment of the RE trap loss collision in which Solts et al., considered the radiative coupling as weak perturbation.

$$A + A + \hbar\omega_L \rightarrow \left[A + A^*\right] \rightarrow A + A + \hbar\omega_S \qquad (2.52)$$

Where A is alkali atom and $A + A^*$ is a bound excited quasi molecule, ω_L & ω_S are circular frequencies of exciting and re-emitted photons. When $\omega_L \approx \omega_0$ and $\Delta_L = \omega_L - \omega_0$, corresponding to very small red detuning

near to the atomic transition then the spectrum $\hbar\omega_S$ is continuous and asymmetric, it is controlled by the pair distribution function related to Δ_L and radiative damping such as shown in the figure (2.12), in which $|\Delta_L|$ is inversely proportional to the density of the excited bound states. If E_i and E_f are energies of 'i' and 'f' states than state to state cross-section for energy states $(E_f - E_i)$ are

$$\frac{d\sigma(E_i, E_f)}{dE_f} = \frac{2\pi^2}{k_i^2}\hbar\gamma|V_L|^2 Y(E_i, E_f) \qquad (2.53)$$

Where $k_i^2 = \frac{2\mu E_i}{\hbar^2}$, V_L is known as exciting laser coupling strength.

Equation (2.53) explains that the state to state redistribution cross section is depending upon the characteristic strength function. The 'characteristic strength' function $Y(E_i, E_f)$ is calculated by using partial wave expansion such as

$$Y(E_i, E_f) = \sum_{l=0}^{l_{max}} (2\ell + 1)\left|\Theta_{fi}^{(l)}\right|^2 \qquad (2.54)$$

Where $\Theta_{fi}^{(l)}$ = two photon T_{fi} matrix element $\left(E_f, l\left|T^{fi}\right|E_i, \ell\right)$ / $(\Delta_L.\Delta_S)$ and $\Delta_S = \omega_s - \omega_0$. The trap loss rate constant $\beta_{RE}(T)$ can be calculated

$$\beta_{RE}(T) = \left(\frac{2\pi\hbar^2}{\mu k_B T}\right)^{3/2} \gamma|V_L|^2 \int_0^\infty dE_i I(\Delta_{RE}) e^{-\frac{E_i}{k_B T}}$$

where

$I(\Delta_{RE}) = \int dE_f Y(E_i, E_f)$ and k_f = Boltzman constant

So, β_{RE} is directly proportional to intensity of field $|V_L|^2$. Figure (2.12) shows the spectrum of Na_2 molecule in excited state potential where is the 'characteristic strength' $Y(K^{-4})$ and detuning Δ_L is plotted at y & x axis, respectively which shows clearly that density of resonance is inversely proportional to detuning (Weiner, 1999).

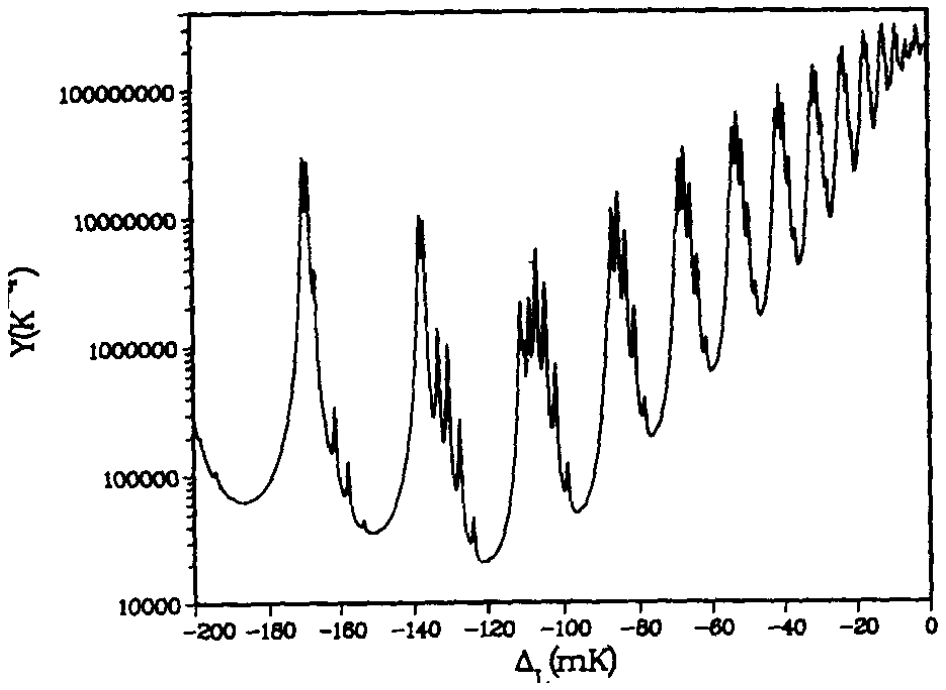

Figure 2.12: 'characteristic function' Y versus laser detuning Δ_L where 1mK= 30 MHz (Solts *et al.*, 1995)

2.3.5 Optical Bloch Equations

Optical Bloch Equation method is used when we have to explain complex optical pumping phenomena during the cold collisions. GP (Gallagher and Pritchard) and JV (Julienne and Vigue) models, complex potential method and two photon distorted theory depends upon initial optical excitation and are valid for low laser intensity region. JP and JV also consider that decay population further can not participate in cold collisional process and explained the FSCC or RE phenomenon. For stronger laser field Optical Bloch equation gives more comprehensive results. At high laser intensity region the decay population is re-excited, calculation of the excitation probability is also changing at different points on the collision trajectory as well as the ground state kinetic energy.

Also for the low temperature regime, "Optical Bloch equations are further improved and calculated on the adiabatic basis where field interaction is diagonalized and interaction coherence eliminated" (Band *et al.*, 1994). Suominen published a complete derivation of diabatic optical Bloch equation (Suominen *et al.*, 1998).

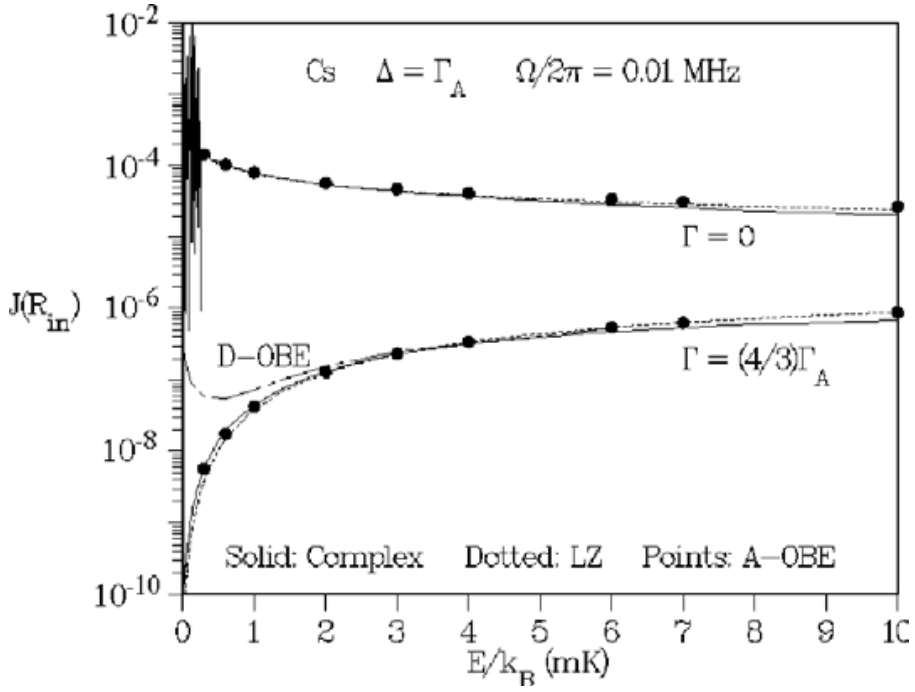

Figure 2.13: Trap loss probability versus Temperature (Band and Tuvi, 1995)

2.5 Ground State Trap Loss Collisions

Elastic collisions and Hyperfine Structure Changing Collisions (HFSCC) are main ground state collisions. Hyperfine changing collisions occur during cold collisions when both atoms are in ground states. There is transition from the upper hyperfine level to lower hyperfine level during the interaction or vice versa of two ground state atoms. If the released kinetic energy is greater than the energy of trap depth, HFSCC leads to trap losses.

There are two processes to be considered in which the hyperfine level changes one is spin exchange and other is the spin dipole-dipole interaction.
Consider two atoms having hyperfine state F_1 with projection M_{f1} and F_2 with projection M_{f2} respectively. The asymptotic limit for the internuclear separation, the product of atomic hyperfine state $\left|F_1 M_{f1}\right\rangle\left|F_2 M_{f2}\right\rangle$ is the molecular hyperfine states. The molecular energies

are the sum of the individual atomic hyperfine energies as shown in figure 2.14.

In case of sodium, the ground state have two hyperfine levels, F=1, 2, with energy difference of 1772 MHz. There are three molecular hyperfine asymptotes levels such as 1+1, 1+2, and 2+2. The energy difference in each asymptotic level is 1772 MHz respectively (Weiner, 1999). If during collision the hyperfine state changes from upper to lower level then the extra energy is released and distributed to the colliding partners and increase their velocity

$$V_{HCC} = \sqrt{\frac{\Delta E_{HCC}}{m}} \qquad (2.69)$$

If the increased velocity is greater than the trap depth, then due to hyperfine structure changing collisions (HFSCC), a trap loss is created.

Hyperfine Changing Collisions are only of interest for shallow traps where as Fine Structure Changing collision and Radiative Escape are dominating trap loss mechanisms for deep traps (Santos *et al.*, 1999).

2.6 Excited State Trap Loss Measurement

In trap losses caused by cold collisions, internal energy is converted to kinetic energy. The reaction rate can be measured by observing the time evolution of the number of trapped atoms *N* as load or decay process of magnet optical trap (Telles *et al.*, 2000). For a single element, the rate equation for the decay process is given by

$$\frac{dN}{dt} = L - \alpha N - \beta \int_V n^2(r) dr^3$$

where L is capture rate, α is linear loss rate constant due to collisions of trapped atoms with thermal background gas in chamber. β is the rate constant due to collision between trapped atoms. $n(r)$ is the number density of atoms inside the trapping volume.

(2.55)

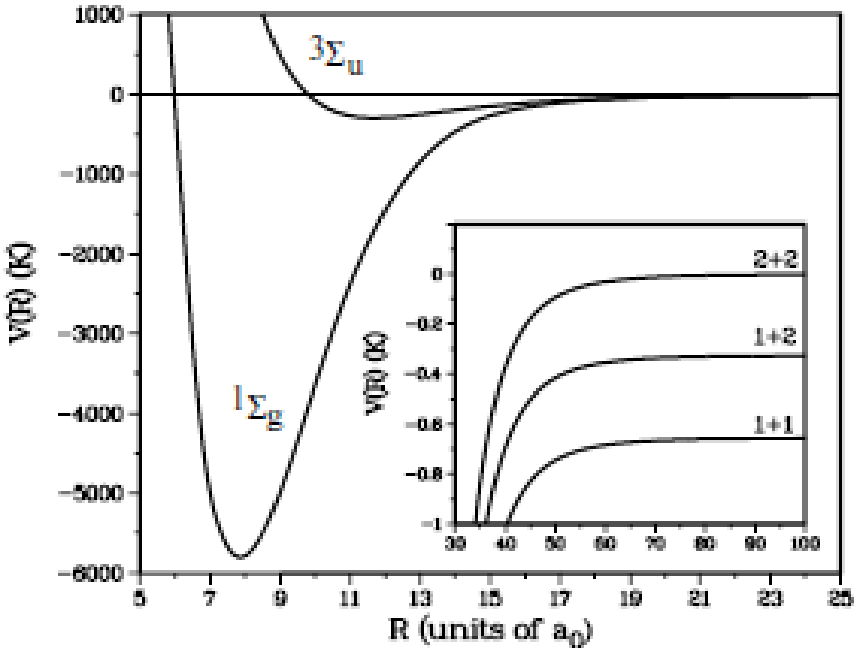

Figure 2. 14: Potential energy curve of Rb_2, inset shows hyperfine levels. (Weidemüller and Zimmermann, 2009)

If β is negligibly small then behavior of decay curve is pure exponential. Equation (2.55) becomes

$$\frac{dN}{dt} = L - \alpha N \qquad (2.56)$$

and its solution is

$$N(t) = N_0 e^{\frac{-t}{\tau_d}} \qquad (2.57)$$

Where $\tau_d = \frac{1}{\alpha}$ is time constant and it is reciprocal to linear loss rate coefficient.

The measurements in cold collisions depend upon the density distribution of the cloud of trapped atoms between the atoms in magneto optical trap. The density distribution is divided into two regimes, called temperature limited regime and density limited regime. Details are in sections (2.6.1 and 2.6.2).

The measurements in cold collisions depend upon the density distribution of the cloud of trapped atoms between the atoms in magneto optical trap. The density distribution is divided into two regimes, called

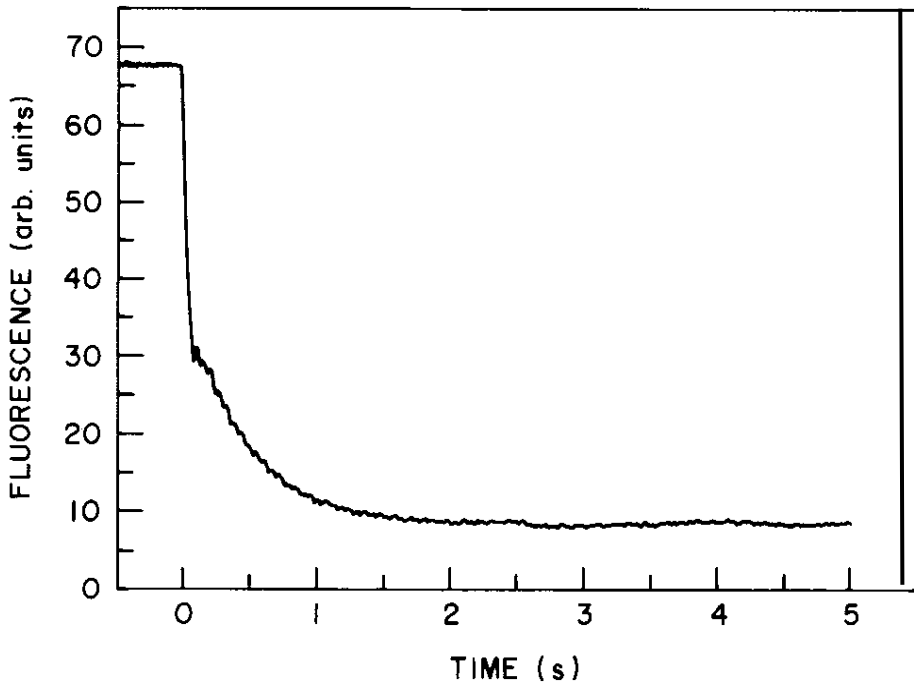

Figure2.15: The vertical decay of curve shows change in light intensity with out varying of number of trapped atoms (Santos *et al.*, 1998).

temperature limited regime and density limited regime. Details are in sections (2.6.1 and 2.6.2).

2.6.1 Temperature Limited Regime

In temperature limited regime, by increasing the number of trapped atoms, density (n) is increases until a critical density value n_c (peak value of Gaussian distribution) while atomic cloud size remains constant in a magneto optical trap (Reinaldo *et al.*, 2003).

The density distribution of cloud is approximated by Gaussian function.

$$n(r) = n e^{\frac{-r^2}{a^2}} \qquad (2.58)$$

Where n is peak density and 'a' is Gaussian width as shown in figure (2.16).

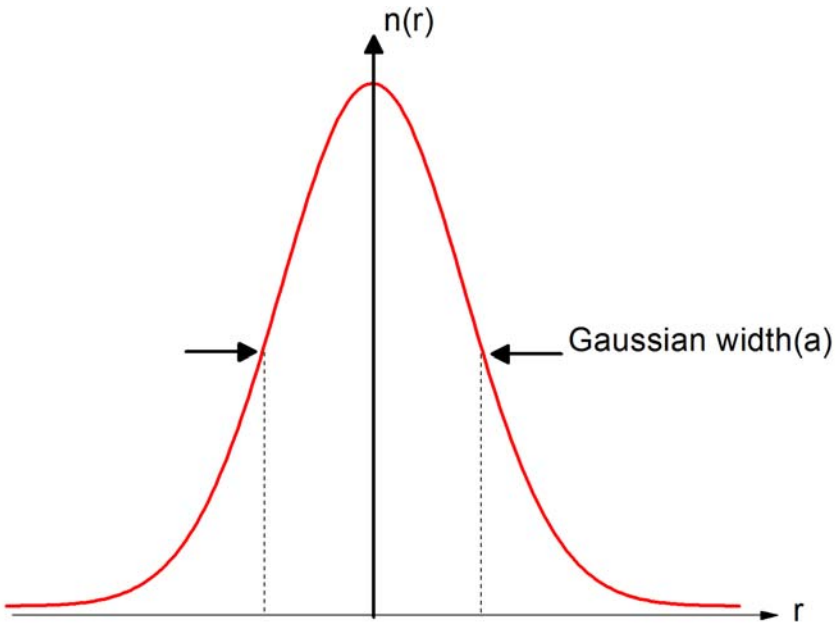

Figure 2.16 : Gaussian profile of the cloud when n(r) ≤ n(c) where ' n ' is peak density and ' a ' is width of cloud.

By putting equation (2.58) in equation (2.55)

$$\frac{dN}{dt} = L - \alpha N - \frac{\beta N^2}{(2\pi)^{3/2} a^3} \tag{2.59}$$

Equation (2.59) has a solution

$$N(t) = \frac{\sqrt{4LB+\alpha^2}}{2b}\left[\tanh\left[\frac{1}{2}\sqrt{4LB+\alpha^2}\,t - \frac{1}{2}\ln\left[-\frac{\alpha-\sqrt{4Lb+\alpha^2}}{\alpha+\sqrt{4Lb+\alpha^2}}\right]\right] - \frac{\alpha}{\sqrt{4Lb+\alpha^2}}\right] \tag{2.60}$$

Where $b = \frac{\beta}{a\pi^{3/2}}$

According to equation (2.58), cold collision loss rate is

$$\frac{1}{N}\left(\frac{dN}{dt}\right)_{CC} = \frac{\beta n_0}{2^{3/2}} \tag{2.61}$$

Fraction of total losses due to cold collisions are

$$\xi = \frac{\left(dN/dt\right)_{CC}}{\left(dN/dt\right)_{losses}} = \frac{1}{1+\sqrt{8}\,\frac{\alpha}{\beta n_0}} \tag{2.62}$$

But

$$N_0 = \frac{L}{\alpha}(1-\xi) \tag{2.63}$$

If filling of trap is stopped at time $t = 0$, than solution of equation (2.58) given by

$$N(t) = N_0 \frac{(1-\xi)\, e^{-\frac{t}{\tau_D}}}{1-\xi\, e^{-\frac{t}{\tau_D}}} \tag{2.64}$$

where time constant $\tau_d = 1/\alpha$.

If $\xi << 1$ then behavior of the decay curve is almost exponential.

2.6.2 Density Limited Regime

By increasing number of trapped atoms in a chamber, volume of atomic cloud size is increased as well as density (n) crosses the critical density limit ($n \geq n_c$), this limited distribution is known as density limited regime. During this regime, shape of the atomic cloud is Gaussian but the volume as well as size of cloud is increased as shown in figure (2.17). During measurements in density limited regime, Gaussian shape as well as the size of cloud are well concerned.

If density ' n ' is high then peak density ' n_c ', with width **'a'** such as

$$n(r) = n_c \text{ for } 0 \leq r \leq a$$

With $n_c = \text{const}$ and $a = a(t)$

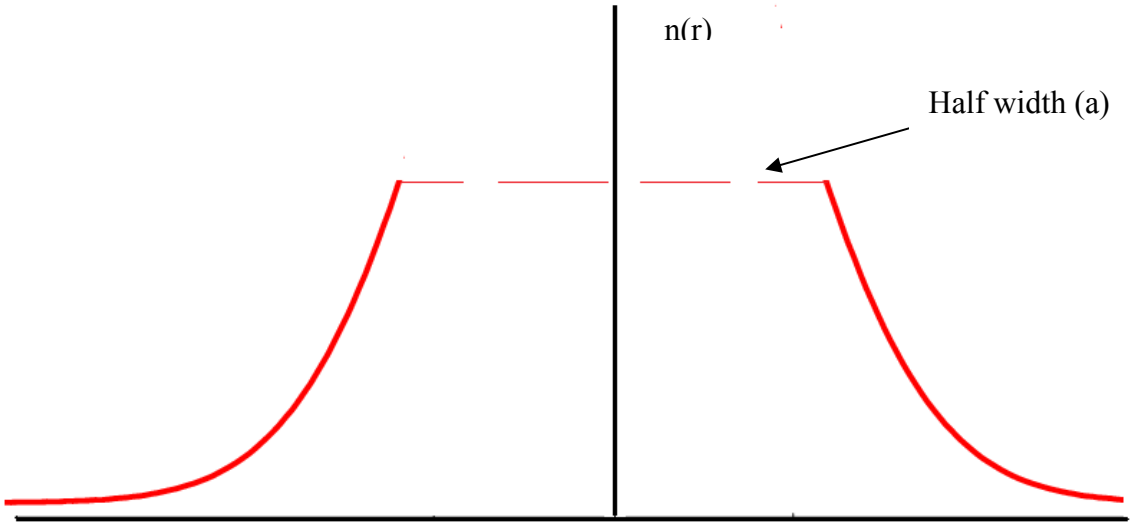

Figure 2. 17: Gaussian profile of the cloud when the n(r) ≥ n(c). in density limited regime. Size of cloud is increasing; alternatively the width 'a' is also increasing.

Equation (2.55) becomes

$$\frac{dN}{dt} = L - \delta N \qquad (2.65)$$

In equation (2.65),

$\delta = (\alpha + \beta n_C)$ where α and β are linear and collisional losses.

Feng and Walker measured rubidium decay curve for different density distributions (Walker and Feng, 1994), shown in figure. (2.18). The decay curve is divided into three parts. In first and second part, decay curve holds density limited regime ($n > n_C$) and temperature limited regime ($n < n_C$), respectively. At the end of curve, the density of cloud is small which also shows exponential behavior but with lager time constant because of the interaction with background gases.

For heteronuclear cold collision losses are determined as

$$\frac{dN_A}{dt} = L - \alpha N_A - \beta \int_V n_A^2(r) dr^3 - \hat{\beta} \int_V n_A(r) n_B(r) dr^3 \qquad (2.66)$$

$\hat{\beta}$ is the rate coefficient for losses of atom species 'A' due to the interaction of atom 'B', 'n_A' and 'n_B' are the number density for the

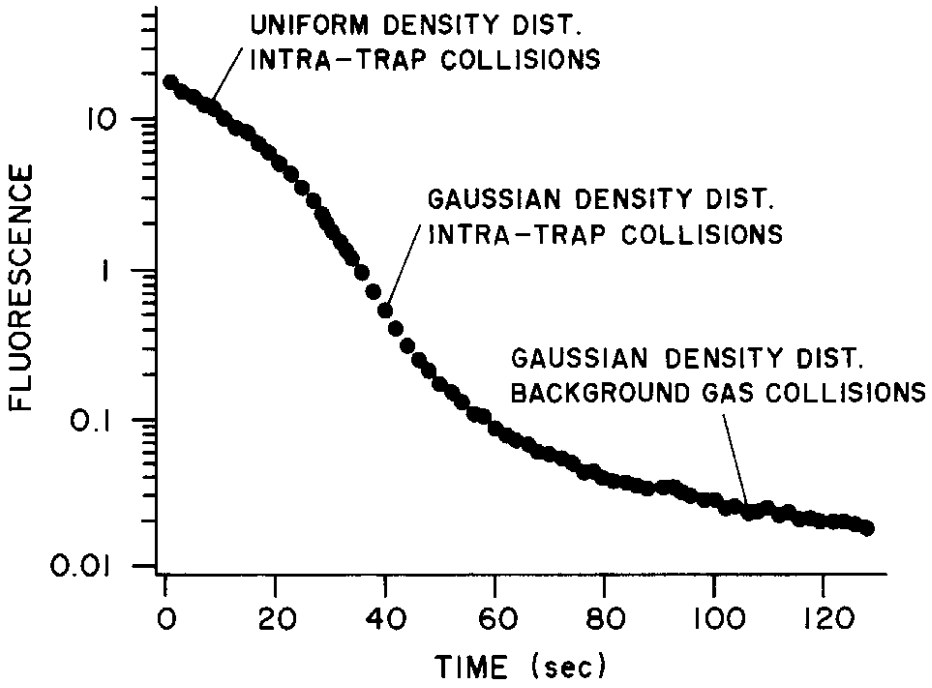

Figure 2.18: MOT decay curve at different density distribution of atoms (Walker and Feng, 1994).

element 'A' and element 'B', respectively.

For the temperature limited regime, consider that the both elements are perfectly overlapped and their shapes are Gaussian, so the rate equation becomes

$$\frac{dN_A}{dt} = L - (\alpha + \Delta\alpha)N_A - \frac{\beta}{\left(\sqrt{2\pi}a\right)}N_A^2 \qquad (2.67)$$

With

$$\Delta\alpha = \hat{\beta}\frac{N_B}{\left(\pi^{3/2}a^3\right)\left[1+\left(\frac{b}{a}\right)^2\right]^{3/2}} \qquad (2.68)$$

$\alpha + \Delta\alpha$ is sum of linear losses of back ground gases and linear losses due to the interaction of element 'A' to element 'B. By using decay curve, $\Delta\alpha$ is measured by difference of the results of linear losses of element 'A' with and without the presence of element B.

3. Experimental Setup

3.1 Rubidium Magneto Optical Trap

The laser cooling system is consisted of Kr ion laser, ring dye laser, lambda meter, spectrum analyzer.

3.1.1 Cooling Laser

For cooling beam, a laser light is generated by cw ring dye laser which is pumped by krypton ion laser. Maximum power of Kr^+ at all-line red (647-676 nm) is 4 Watt. Rhodamine 700 (LD 700) dye is used which has a emission range 690-785 nm. LD 700 is stable dye and long life. Ring dye laser is consisted of thick etalon, thin etalon, galvo plate and birefringent filter. These elements are used for the selection of appropriate wavelength. In current setup, with out these selective elements, the ring dye laser has an out power of 1.2 W, with selective elements; maximum power is about 700 mW at 740 nm. But maximum output single mode power at 780 nm of our ring dye laser is 200-250 mW when it is pumped by Kr^+ laser at 4 watt. One major limitation in output power of ring dye laser is LD-700 dye which has the absorption line at 780.024 nm almost on the edge of emission band as shown in Figure (3.19). 10% of light from the output power of ring dye laser is coupled out by beam splitter (BS) and used for the saturation spectroscopy to stabilize the frequency of laser. Remaining laser light is passed through the half wave plate $\left(\lambda/2\right)$ to keep the required polarization with respect to direction of the magnetic field and then sent to main chamber as cooling beam.

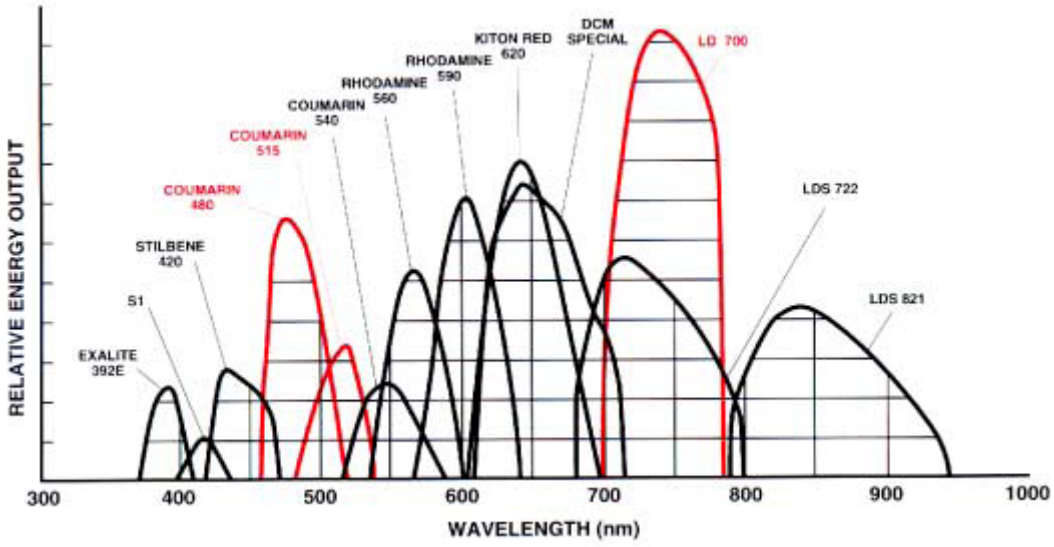

Figure. 3. 19: Tuning Curve Argon-Ion & Krypton-Ion PUMPED DYES (Exciton data sheet)

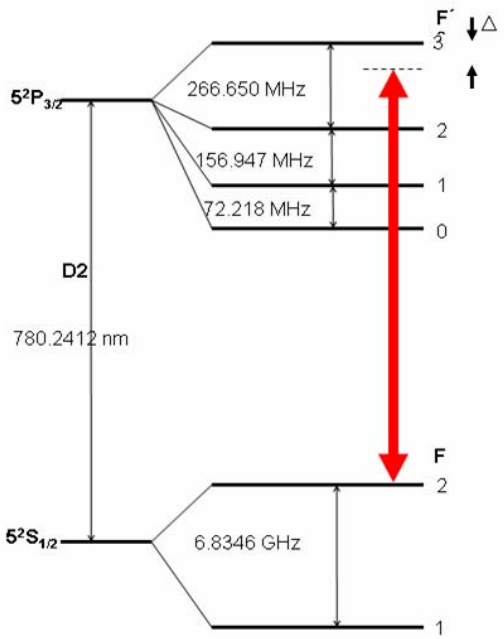

Figure 3.20: Hyperfine structure of D_2 line of ^{87}Rb. Where Δ (= 18MHz) is red detuning.

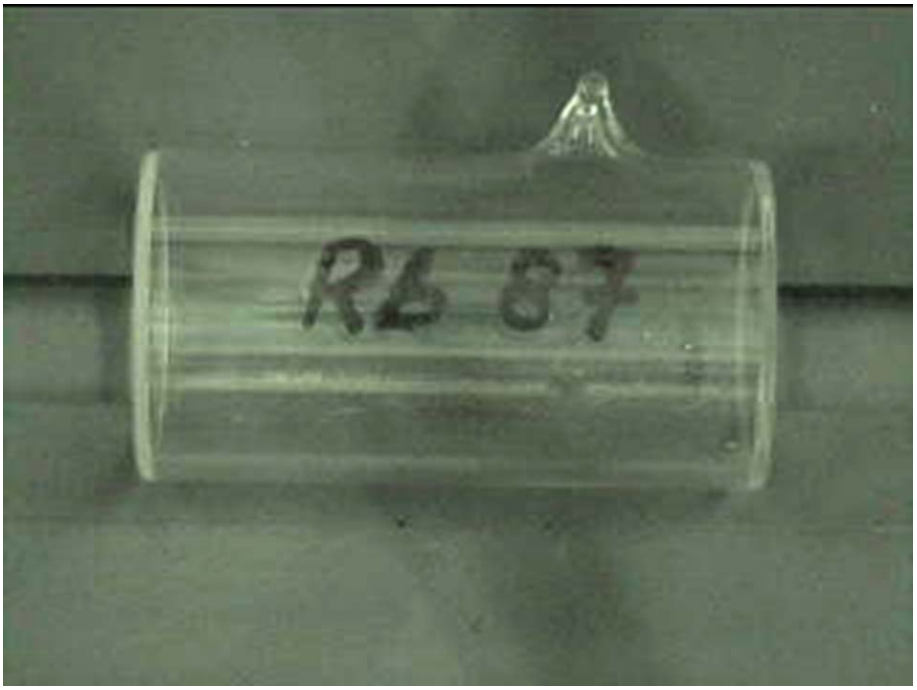

Figure 3.21:. Rubidium vapor cell

3.1.2 Stabilization System

For laser cooling and trapping experiment, two things are very important. First of all laser frequency should be very stable, controllable and of minimum line width (Metcalf and van der Straten, 1999) and secondly the cooling beam should be red shifted a certain amount. For very stable laser frequency and locking at the particular frequency at long time, the internal standard frequency stabilization system of the dye laser is not sufficient, therefore an external active stabilization system is required.

For locking and red shifting of the laser cooling beam, saturation spectroscopy is used with combination of static and alternating magnetic fields. These magnetic fields are generated by two coils which are wounded around the ^{87}Rb cell. DC or static magnetic field is able to change the resonance due to Zeeman shift.

By using this locking technique, it is easy to lock the laser frequency for a long period, also laser beam can be red shifted without any extra device such as AOM. There are four main advantages to use this technique (Dinneen *et al*., 1992).

- Modulation free ring dye laser frequency is used.

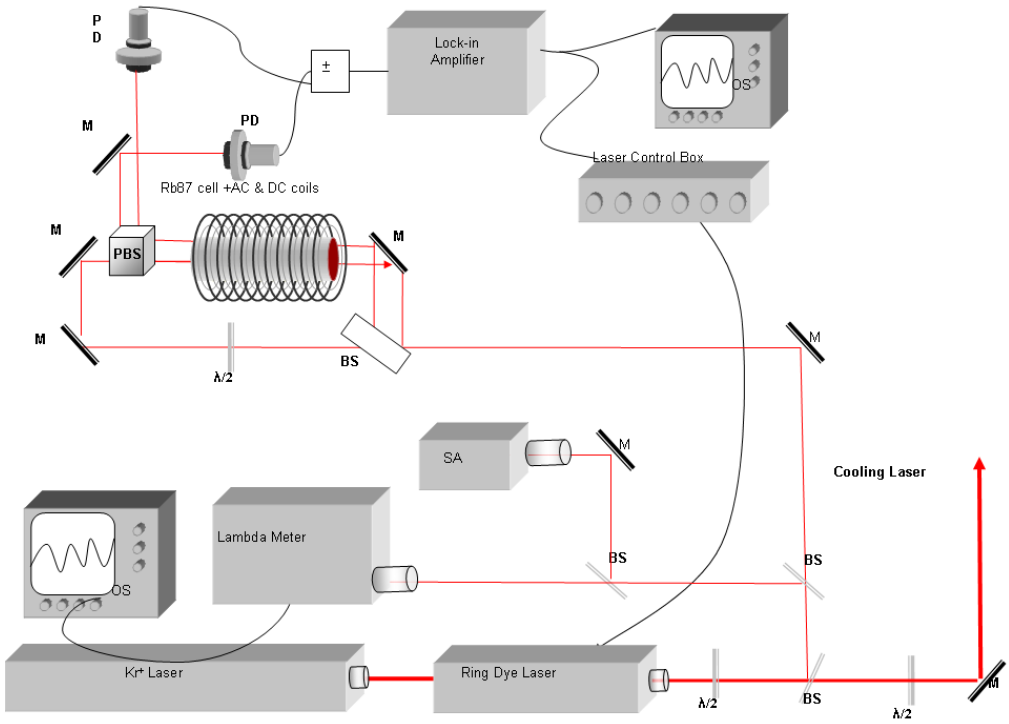

Figure 3.22: Schematic diagram of stabilization laser system of ^{87}Rb cooling beam, PD…photodiode, M…Mirror; OS…Oscilloscope; BS….Beam Splitter, SA… Spectrum Analyzer; Kr^{+}…. Krypton Ion Laser; $\lambda/2$ …Half wave plate.

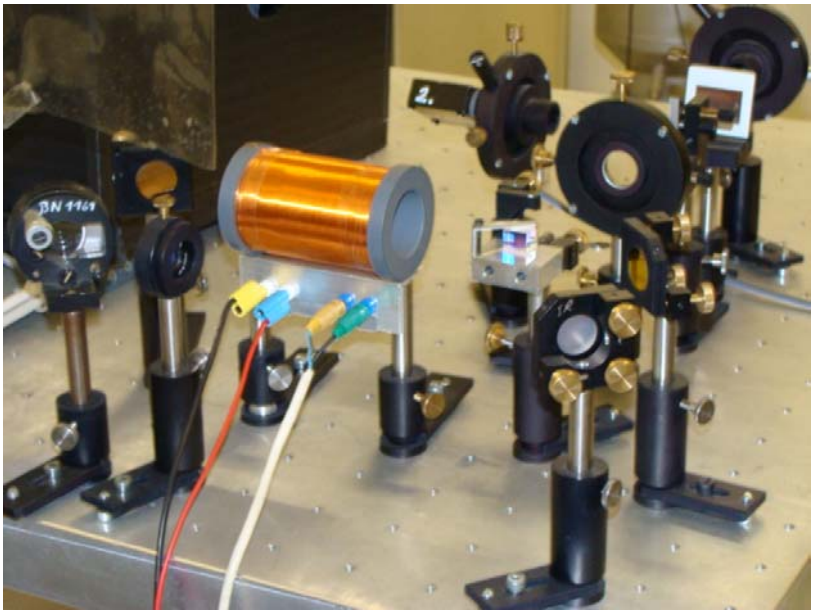

Figure 3.23: Photograph of saturation spectroscopy setup for ^{87}Rb cooling beam.

- The frequency of a ring dye laser is tune able across the locking point.
- The laser frequency can be stabilized at or near the atomic resonance for a long period of time.
- Easy to lock due to tunable locking point.

Laser frequency is locked at crossover resonance of the transition $F=2 \rightarrow F'=3$ and $F=2 \rightarrow F'=2$ of D_2 line of ^{87}Rb where laser frequency is 18 MHz red detuned. The level scheme is shown in the figure (3.20).

3.1.3 Magnetic Coils for Locking

Rubidium saturation cell is consisted of commercial Rb cell (^{87}Rb = 27.8% and ^{85}Rb = 72.2%) surrounded by magnetic coils. ^{87}Rb cell is CE RB 25 from Toptica Photonics. This cell is filled with natural rubidium without buffer gas. Its length is 25mm and has optical quality windows. The inner diameter of the coil is 50 mm and length is 90 mm.

A copper wire having diameter 0.71 mm is used for winding. There are two magnetic coils, offset coil and oscillating coil, which are surrounding around the cell. The offset coil and the oscillating coil have six layers with ohmic resistance of $4.8\,\Omega$ and three layers with ohmic resistance of $2.4\,\Omega$, respectively. Both the coils are connected separately. Offset coil can produce a maximum magnetic field of 100 Gauss at 1 ampere dc current. Oscillating coil can produced a ac magnetic field which is used for modulation.

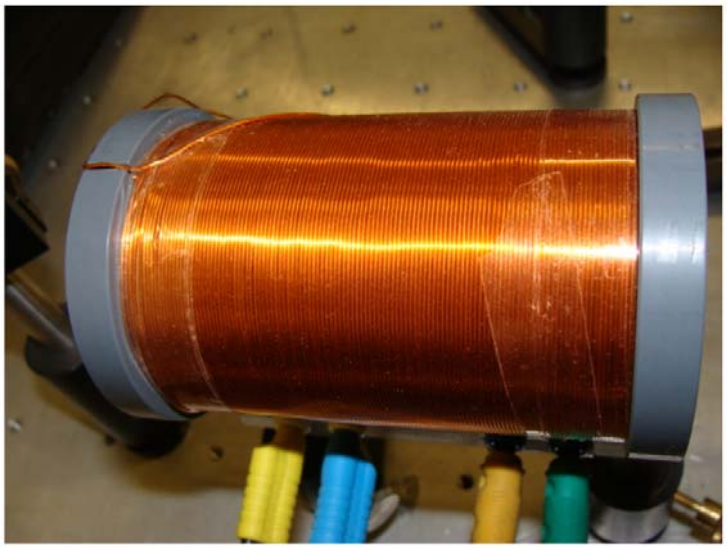

Figure 3.24: Magnetic coils around the ^{87}Rb cell.

3.1.4 Locking By Saturation Spectroscopy

The electronic system for the stabilization system is consisting of stablizatation box, reference box, magnetic field box, a low pass filter and the two magnetic coils surrounding across the rubidium cell as shown in figure (3.24).

Reference box contains a dual frequency generator (543 Hz) with adjustable phase difference for keeping the optimum magnitude of signal. Where one frequency of 543 Hz is used for lock in detection, other is used as the reference signal for ac magnetic field. The magnetic box is basically the power supply which distributes ac and dc current to the coils. The reference frequency is resonant with ac current and alternately produced the ac magnetic field in the oscillating coil. A dc current between 0-1 amperes from magnetic control box is used for the offset coil to produce dc magnetic field. This magnetic field is used for shifting of the atomic transition of ^{87}Rb and alternatively shifting locking point within a certain limit. The low pass filter is used to prevent the dc current from the influence of the ac circuit.

Saturation spectroscopy is used to get a Doppler free signal for the locking point. A thick glass plate is used to split the incident beam into two beams known as the probe and the reference beam which pass through the ^{87}Rb cell having equal intensities. The pump beam which is more intense is passing the cell in opposite direction in such a way that it overlaps completely with the probe beam. The polarization of pump beam is controlled by the $\lambda/2$ wave plate. Two photodiodes are used to measure the intensity of the each probe and reference beam. Only reference beam has the Doppler broadened absorption spectrum and the probe beam inform about the Lamb dips and crossover resonances. By taking the difference of the signal of the probe and the reference beams electronically in the reference box, the Doppler free signal is generated. A dc magnetic field is used to shift the spectrum where as ac magnetic field is used to modulate the magnetic field with frequency at 543 Hz. The change in energy levels due to the Zeeman shift of the absorption frequency is modulated with same frequency of magnetic field and produced the first derivative signal having zero crossing which is used for the locking of the laser at the desired frequency. As shown in figure (3.25).

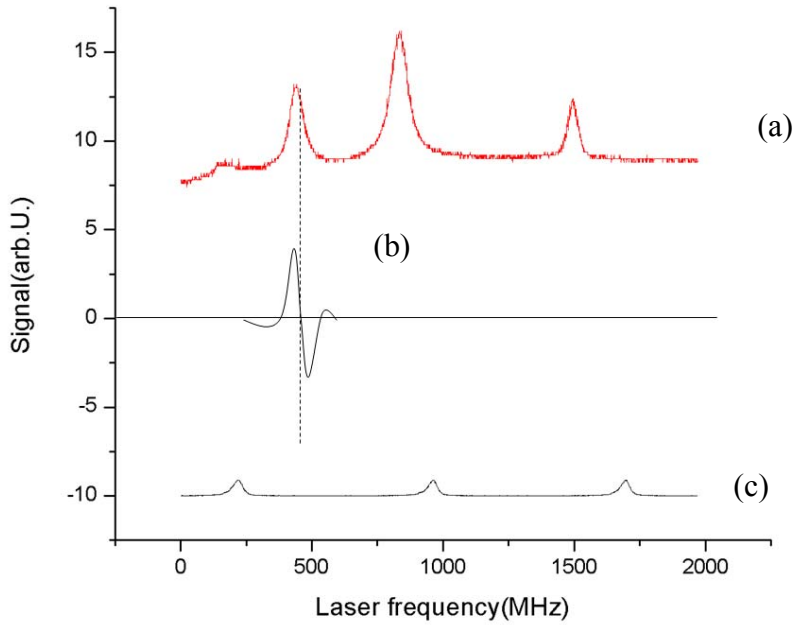

Figure 3.25: A locking scheme for ^{87}Rb (a) Saturation absorption signal. (b) 1st derivative signal at zero crossing is used for locking. (c) Etalon signal having FSR 150 MHz. A current 0.5A produced approximately 20 gauss magnetic field.

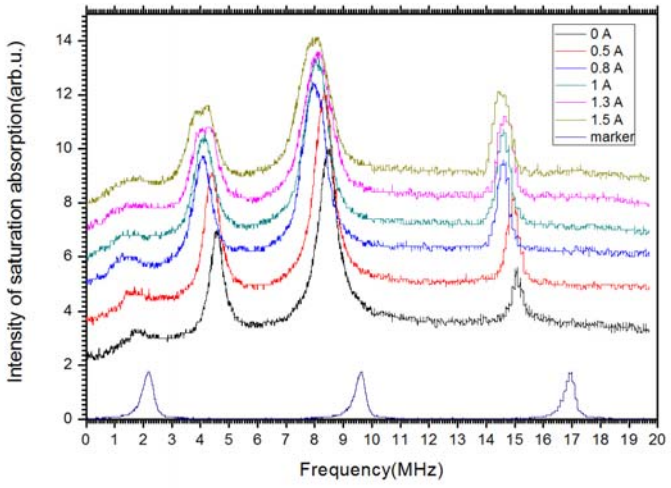

Figure 3.26: Saturation absorption signal at different magnetic field strength. Along x-axis, frequency shift relative to zero field $F = 2 \rightarrow F' = 3$ transition in ^{87}Rb.

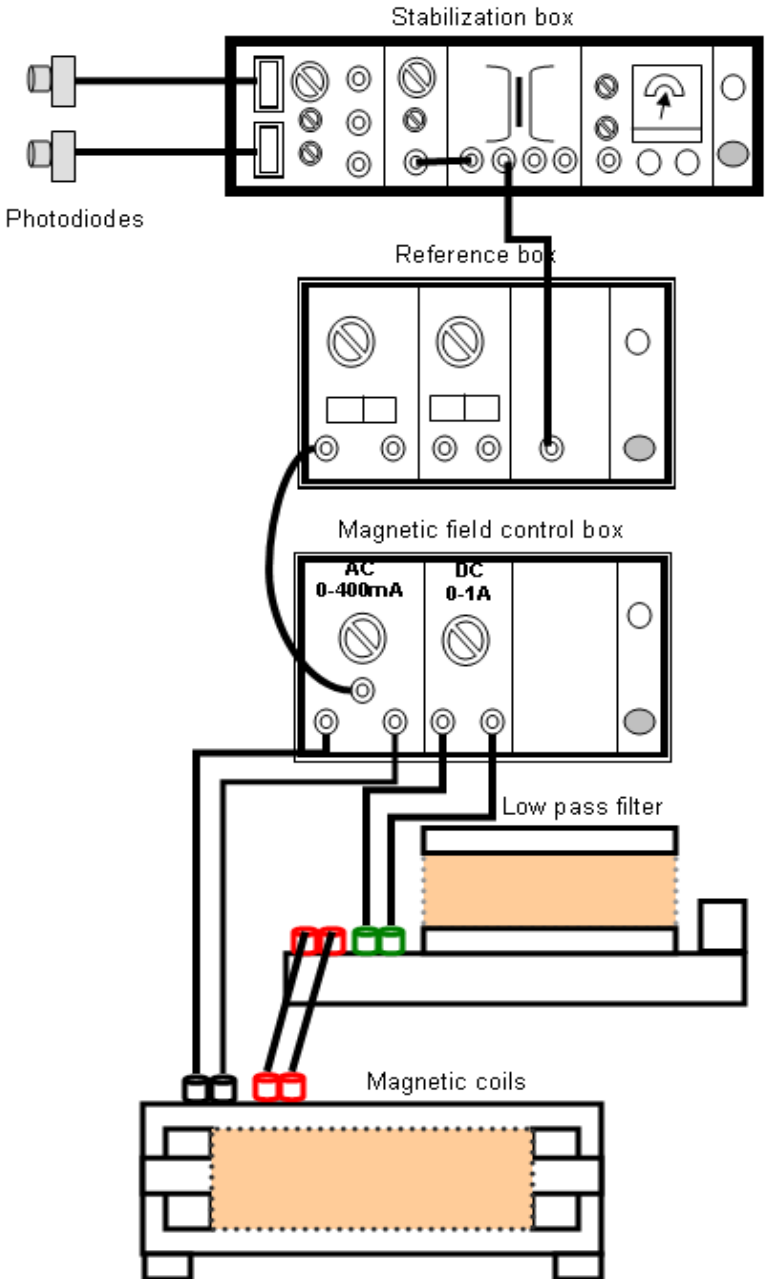

Figure 3.27: Electronic setup for stabilization of ^{87}Rb cooling laser. Set up consists of stabilization box, reference box, magnetic field control box, low pass filter and magnetic coils.

3.1.5 Repumping Laser

Cooling beam excites the atoms from $F=2 \rightarrow F'=3$ transition but one atom out of 1000 atom will decay into $F=1$ instead of $F=2$ state (Wieman *et al.*, 1994). So after some time the cooling laser is out of resonance with atomic resonance transition because all atoms decay into $F=1$ state. So for keeping the cooling cyclic process alive, we need an extra laser to pump the atom from $F=1 \rightarrow F'=2$. A Toptica DL 100 system is used for pumping the transition of $D_2(F=1 \rightarrow F'=2)$ of ^{87}Rb. The output power of diode laser is 20 mW at 780.019 nm wavelength. The hyperfine scheme is shown in the figure (3.28).

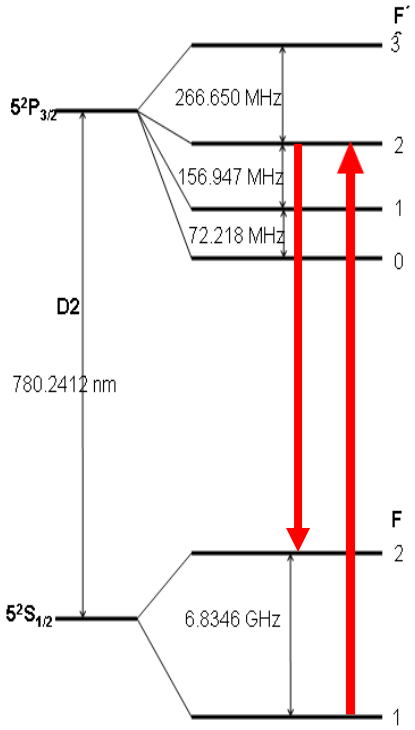

Figure 3.28: Hyperfine structure of ^{87}Rb.

3.1.6 Diode Laser

Diode laser in free run have a line width of more then 100 MHz. We are using the DL 100 diode laser system in which a littrow external cavity diode laser or grating stabilized diode laser is used (Wieman and Hollberg, 1991). The grating is used for two purposes, first is that the optical feed back is used for the stabilization which reduces the line width from 100 MHz to 1 MHz and second the grating is used to tune the laser to a particular wave length. The grating is mounted on a piezo-electrical ceramics which length is controlled electronically and capable to scan the frequency in particular range.

The cavity consists of the back facet of the diode laser and the surface of the diffraction grating as shown in figure (3.29). We used a Littrow configuration in which the grating angle is adjusted such as the first order diffraction light is coupled with the laser.

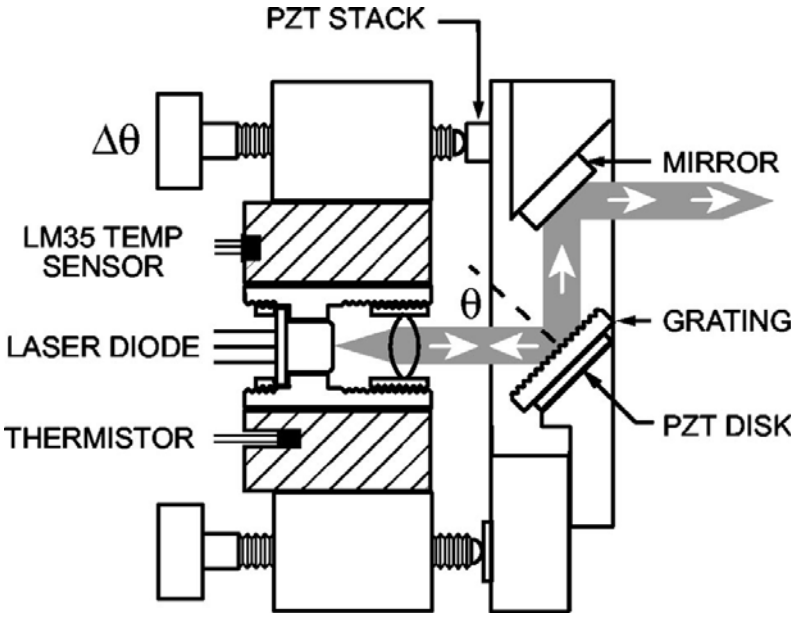

Figure 3.29: Design of external cavity diode laser. Diffraction grating in a Littrow configuration (Tuner *et al.*, 2002).

In Toptica DL 100 system, the laser frequency is control by temperature and current of laser diode. Module control box made by Toptica is consisted of following modules for control, scan and lock the frequency.

- Temperature control module

- Current control module
- Scan control module
- PID (Proportional Integral Differential) regulator

3.1.7 Stabilization System

An active stabilization system with polarization spectroscopy (Wieman and Hänsch, 1976) is used to generate an error signal. This signal is fed back into the laser tuning control box Cavity length and the ECDL (External Cavity Diffraction Grating) is controlled by the current (DCC 100) and piezo transducers (DTC 100). ^{87}Rb cell used for the polarization spectroscopy is heated at 70^{o}C by an external heating coil surrounding by the cell. This temperature keeps the optimum vapor pressure inside the cell so the hyperfine transitions have good amplitude and resolution for locking.

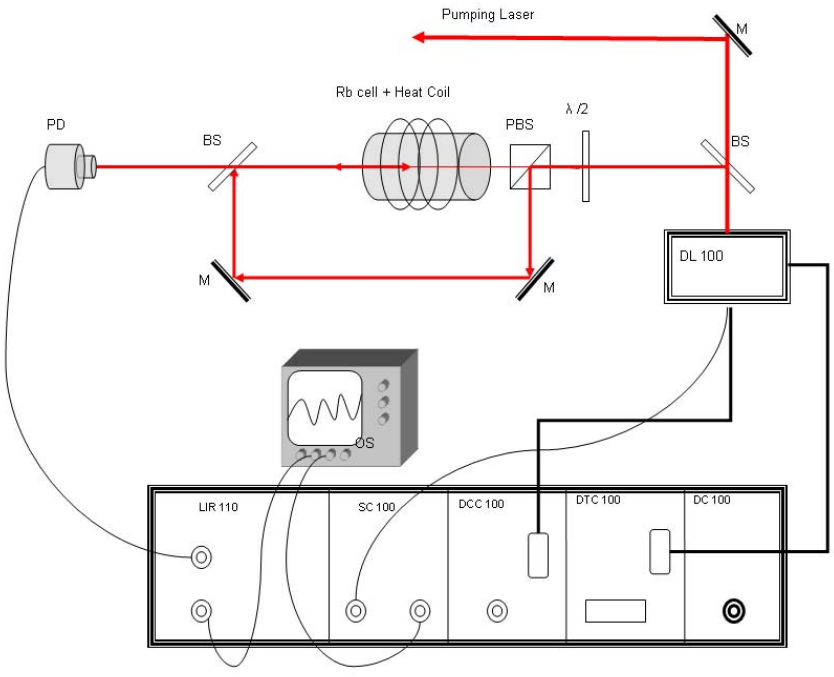

Figure3.30: Stabilization for Re-pumping beam for ^{87}Rb. Polarization Spectroscopy and DL 100 Diode Laser System. M…Mirror; PD…Photo diode; PBS…polarization beam splitter; OS…Oscilloscope; DC 100…DL 100 Controller; DTC 100….Temperature controller; DCC 100…Current controller; SC 100…Scan Controller; LIR 110…Lock in Regulator.

3.2 Sodium Magneto Optical Trap

The laser cooling system is consisting of Ar^+ laser, ring dye laser, lambda meter, spectrum analyzer.

3.2.1 Cooling Laser

^{23}Na has D_2 $(F=2 \rightarrow F'=3)$ transition in visible range at 589 nm. To excite this transition we used ring dye laser in which Rhodamine 6G dye is used. This dye is very stable and long life. Ring dye laser is pumped by Ar ion laser at power of 7 Watt. Output power of ring dye laser is 500-600 mW at cooling transition. The laser frequency is shifted away from the atomic transition frequency (see 3.2.3) and directly used for the cooling transition.

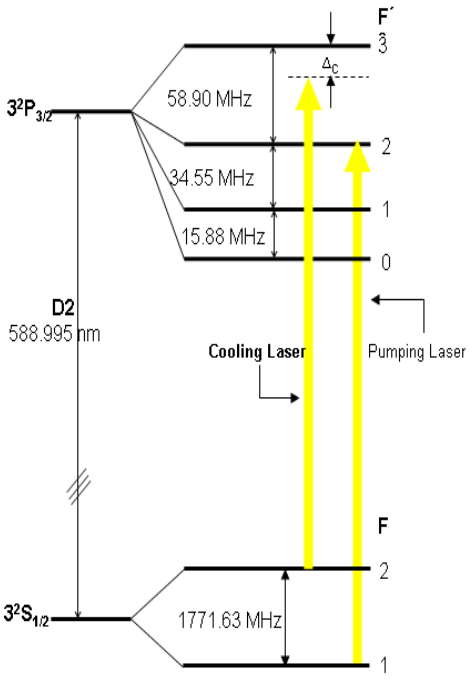

Figure 3.31: Hyperfine Structure of ^{23}Na where detuning Δ_c is 14 MHz.

3.2.2 Repumping Laser

The frequency splitting between ground state hyperfine energy level of sodium is 1771.63 MHz. An Acoustic Optical Modulator (AOM) is used to generate another frequency in order to pump the atom from $F=1$ to $F'=2$ state. In our experiment, by using the first order of AOM1 the frequency is shifted 1717 MHz. This frequency is used as repumper. A $(\lambda/2)$ plate before PBS is used to control the intensity ratio between the cooling and repumper laser. Laser beam is expanded by a pair of lenses.

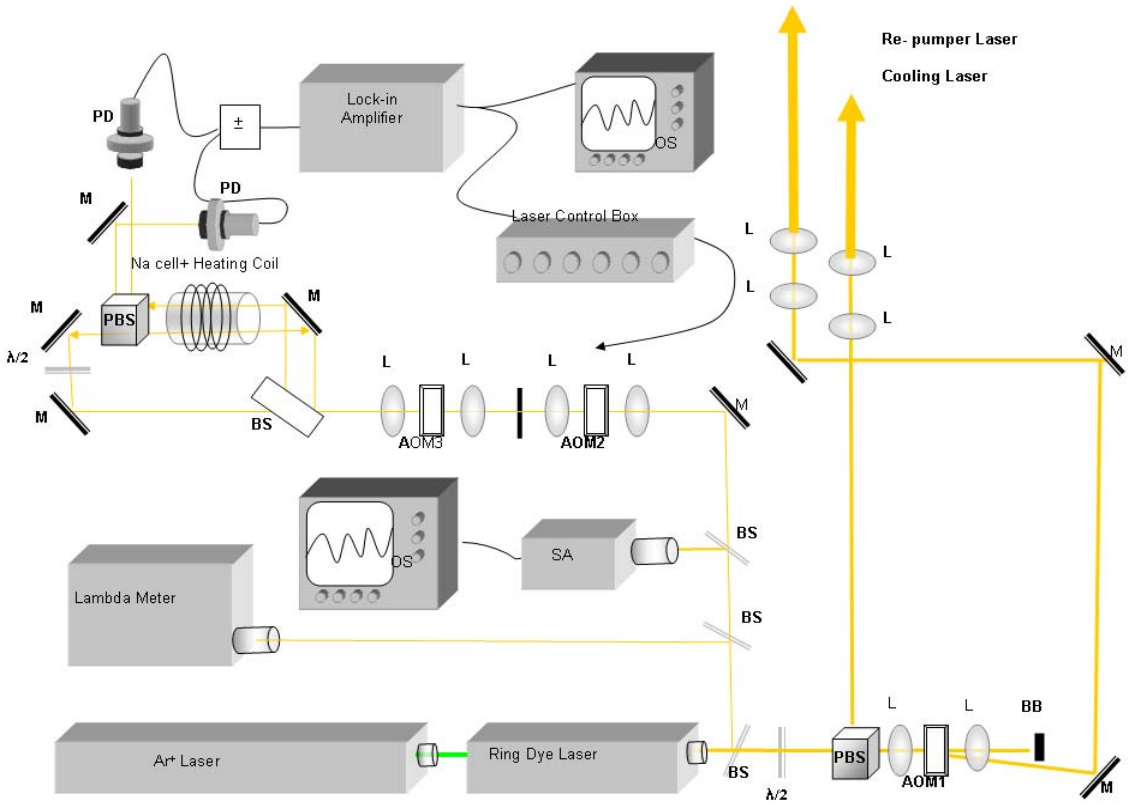

Figure 3.32: Schematic diagram of stabilization system for cooling Na atoms. Ar^{+}... Argon laser; PD... Photodiode; L...Lens; OS...Oscilloscope; AOM... Acoustic Optical Modulator; PBS...Polarization Beam Splitter; SA...Spectrum Analyzer. $\lambda/2$ ...Half wave plate.

3.2.3 Stabilization System

Stabilization due to reference cavity attached with dye laser system is not enough to control the long time stability of the laser frequency. Active stabilization system with saturation spectroscopy is used to keep the laser frequency stable. A small amount of laser light is splitted into three beams by using beam splitters; BS1, BS2 and BS3. After splitting, laser is used for lambda meter, spectrum analyzers and saturation spectroscopy. But before entering the heated ^{23}Na vapor cell, beam passed through AOM2 and AOM3 for red detuning. In our setup, AOM2 and AOM3 generate the frequency of 99MHz and 85MHz respectively such as to produce the red detuning (Δ_c) of 14 MHz for the cooling laser. AOM3 also modulated the frequency shift and creates the error signal for locking the laser frequency to an atomic transition. A crossover signal $F = 2 \rightarrow F' = 3$ and $F = 2 \rightarrow F' = 2$ transition of the sodium D_2 line (red detuned $\Delta_c \approx 14$ MHz). is used for locking the cooling beam.

3.3 Lithium Magneto Optical Trap

The laser cooling system is consisting of Ar^+ laser, ring dye laser, lambda meter, spectrum analyzer.

3.3.1 Cooling Laser

A single mode ring dye laser (coherent) is used to produce the laser light for D_2 transition $S_{1/2}(F = 2) \rightarrow P_{3/2}(F' = 3)$ for Lithium. Argon ion laser at 7.5 Watt is used to pump ring dye laser. For lithium, we are using DCM dye. The out put power of ring dye laser is 400-450 mW at wavelength 670.776 nm.

3.3.2 Repumping Laser

The energy difference of ground hyperfine levels $(F = 1 \rightarrow F = 2)$ is 803.5 MHz. Out put power from dye laser is passed through an electro optical modulator (EOM). EOM shifted the laser frequency into three main components as zero order, plus first and minus first order. Zero order is

taken as cooling beam where as plus first order side band is taken as the repumper beam which pumps the atoms from $S_{1/2}(F=1) \rightarrow P_{3/2}(F'=2)$.

Spectrum analyzer is used to look these sidebands and intensity ratio between the cooling and re-pumping laser can be adjusted accordingly.

3.3.3 Stabilization System

Active stabilization system is necessary to stabilize the laser frequency for a long time. Saturation spectroscopy with a heated lithium cell wounded by two coils is used. These coils are generating the static and the alternative magnetic field around the cell. Due to dc or ac magnetic fields the energy levels are shifted due to Zeeman splitting. The hyperfine levels of $P_{3/2}$ are not well resolved due to small energy differences. So the laser is locked at the cross over signal arising from the transition of $S_{1/2}(F=2) \rightarrow P_{3/2}$ as shown in figure (3.34)

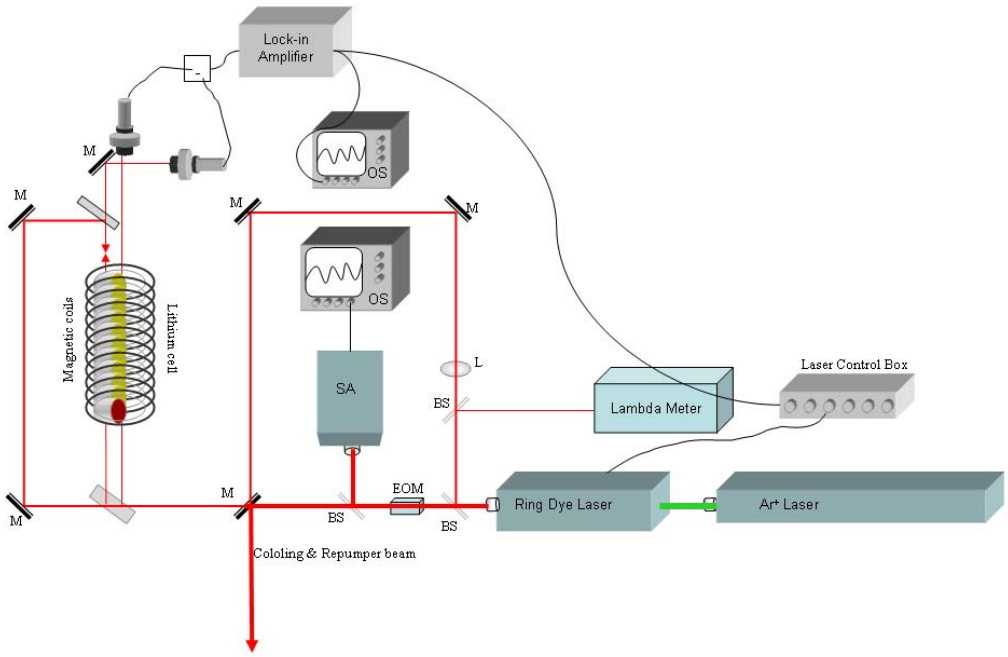

Figure 3.33: Stabilization system for lithium. M…Mirror, EOM…Electro optical modulator…BS…Beam Splitter, SA…Spectrum Analyzer, OS…Oscilloscope, L…Lens.

This lock point can be shifted by the strength of the homogenous magnetic field. In our setup, the locking point is adjusted at 25 MHz away from $F' = 2$ transition. Due to shifting of energy levels, the laser is red detuned (Δ_c) by 18 MHz (3Γ). By using ac and dc magnetic fields and the standard lock in technique, the laser is locked at 670.776 nm for a long time. More detail is in the diploma work (Fritz, 1999).

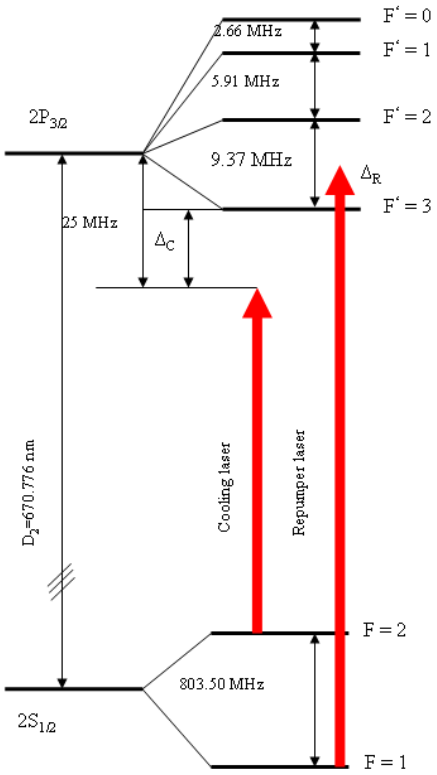

Figure3. 34: Hyperfine structure of ^{7}Li. Δ_R = 18MHz which is red detuning.

3.4 Optical Setup

Current MOT is able to cool and trap ^{23}Na, ^{87}Rb, ^{7}Li and ^{6}Li. MOT is placed on a separate optical table. Cooling and trapping beam enter the chamber from different directions of the optical table because each laser system for ^{87}Rb, ^{23}Na, ^{7}Li and ^{6}Li are also placed on separate optical tables surrounding the MOT table.

Each cooling beam of ^{87}Rb and ^{23}Na is expanded by a telescope. These beams enter from two different directions the MOT table and then the beams are splitted into three equal intensity beams by using beam splitters (BS). The repumper beams of ^{87}Rb and ^{23}Na are overlapped with cooling beams at the second BS. Repumper beam of each element is overlapped with the cooling beam only in two directions x and y. The vertical z-direction, the laser light of both elements are combined with dichroitic beam splitter specially made for ^{23}Na, ^{87}Rb and ^{7}Li frequency.

In three orthogonal directions the combined beams of cooling and pumping of each ^{23}Na and ^{87}Rb enter the chamber from separate view ports such as they intersect both beams in the center of the MOT and then are reflected back from the opposite side of the chamber. The orientation of the light is circularly polarized before and after the reflection in three–dimensions. So each beam of ^{23}Na and ^{87}Rb before entering and then reflecting from opposite direction of the MOT is passed twice through a special quarter wave plate of specification for Na and Rb frequency, respectively to keep defined polarization.

Similarly ^{7}Li have a single laser beam including cooling and pump frequencies. This beam is entering the optical table through aperture and overlapped by sodium cooling beam such that they enter the chamber in same view port. For simultaneously trapping of ^{23}Na and ^{7}Li, each splitting beam of ^{7}Li in x, y and z direction have to pass through the additional half wave plates to keep the polarization same before overlapping with the ^{23}Na light. Special dichroitic mirrors which have 99% reflection for sodium light and 99% transmission for lithium light are used for overlapping as shown in figure (3.35). Special quarter wave plates are used with retardation $\lambda/4$ for ^{7}Li and ^{23}Na resonance wave plates. The diameter of cooling and pumping beams of ^{23}Na, ^{87}Rb and ^{7}Li are 16 mm before entering the chamber.

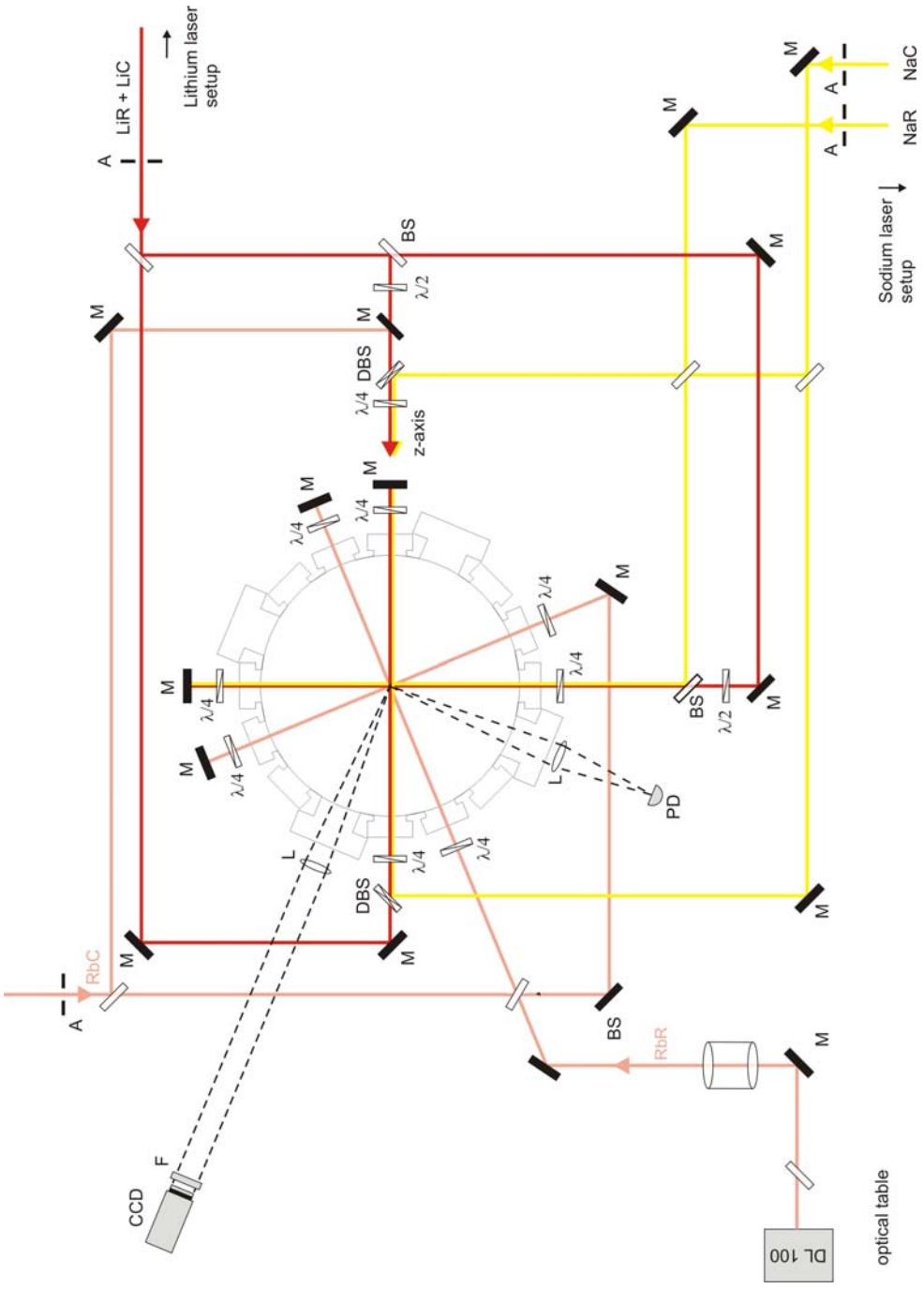

Figure 3.35: Optical setup for ^{23}Na, ^{87}Rb and ^{7}Li MOT; M...Mirror, A...Aperture, BS...Beam Splitter, DBS...Dichroitic Beam Splitter, PD...Photodiode, L...Lens, F...filter, λ/4...Quarter wave plate, λ/2...Half wave plate, NaC...Sodium cooling beam, NaR...Sodium re-pumper beam, RbC...Rubidium cooling beam...RbC, RbR...Rubidium re-pumper beam, LiR...Lithium re-pumper beam, LiC...Lithium cooling beam, DL 100...Diode Laser, CCD...CCD camera.

3.5 Vacuum System

3.5.1 Vacuum Chamber

Our vacuum chamber consists of main and old chamber. The old chamber used in the former experiments is now mounted in the upper part of our current chamber. Old chamber is magneto optical trap which was working well till 2007. This MOT has a certain limitation to cool the new elements. Our new setup which is combination of main and old chamber is able to cool and trap three alkali atoms simultaneously such as $^{23}Na, ^{87}Rb, ^{7}Li$ or ^{6}Li and also capable to expand for new future experiments. Our main vacuum chamber is designed by Prof. Windholz. This chamber has a lot of freedom to cool and trap different types of alkali atoms. It is made of high grade steel which has the magnetic susceptibility less then 0.01. The diameter of the chamber is 400 mm and height is 150 mm. There are 42 flanges of different sizes and there distribution in our experiment is listed in table 3.1.

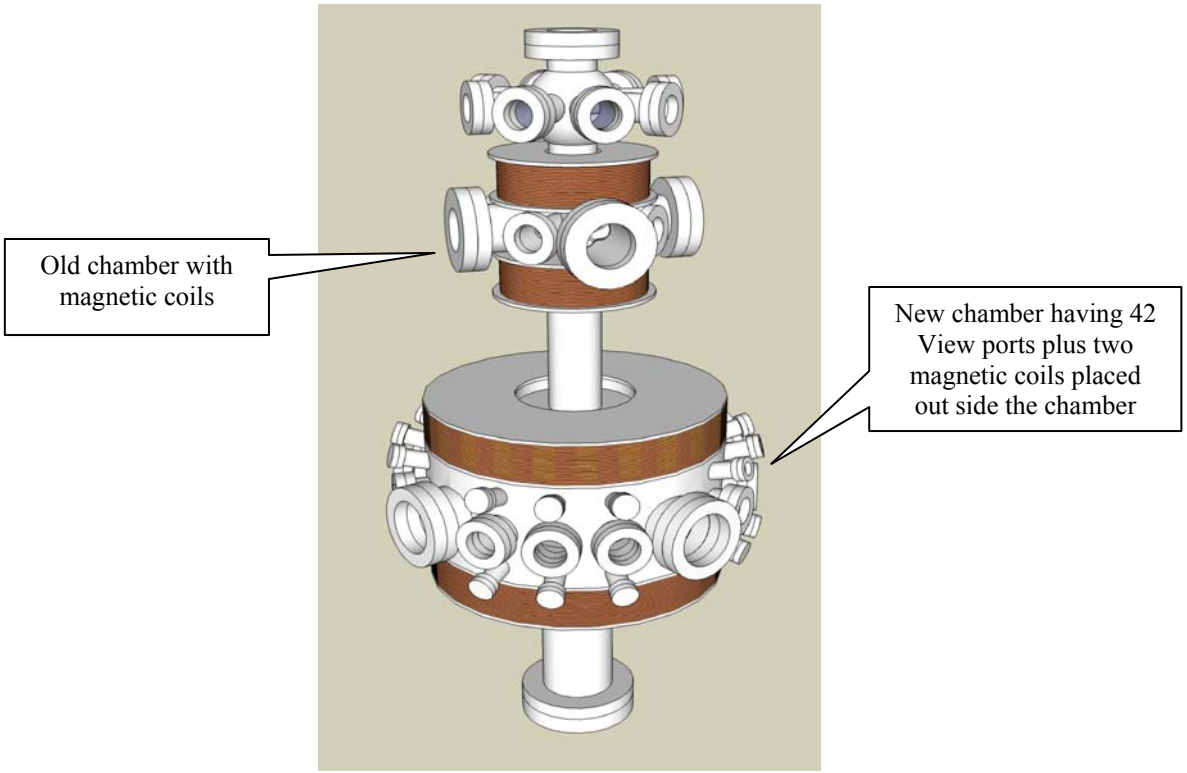

Figure 3.36: Sketch of Vacuum chamber which consist of main chamber with magnetic coils and old chamber with magnetic coils.

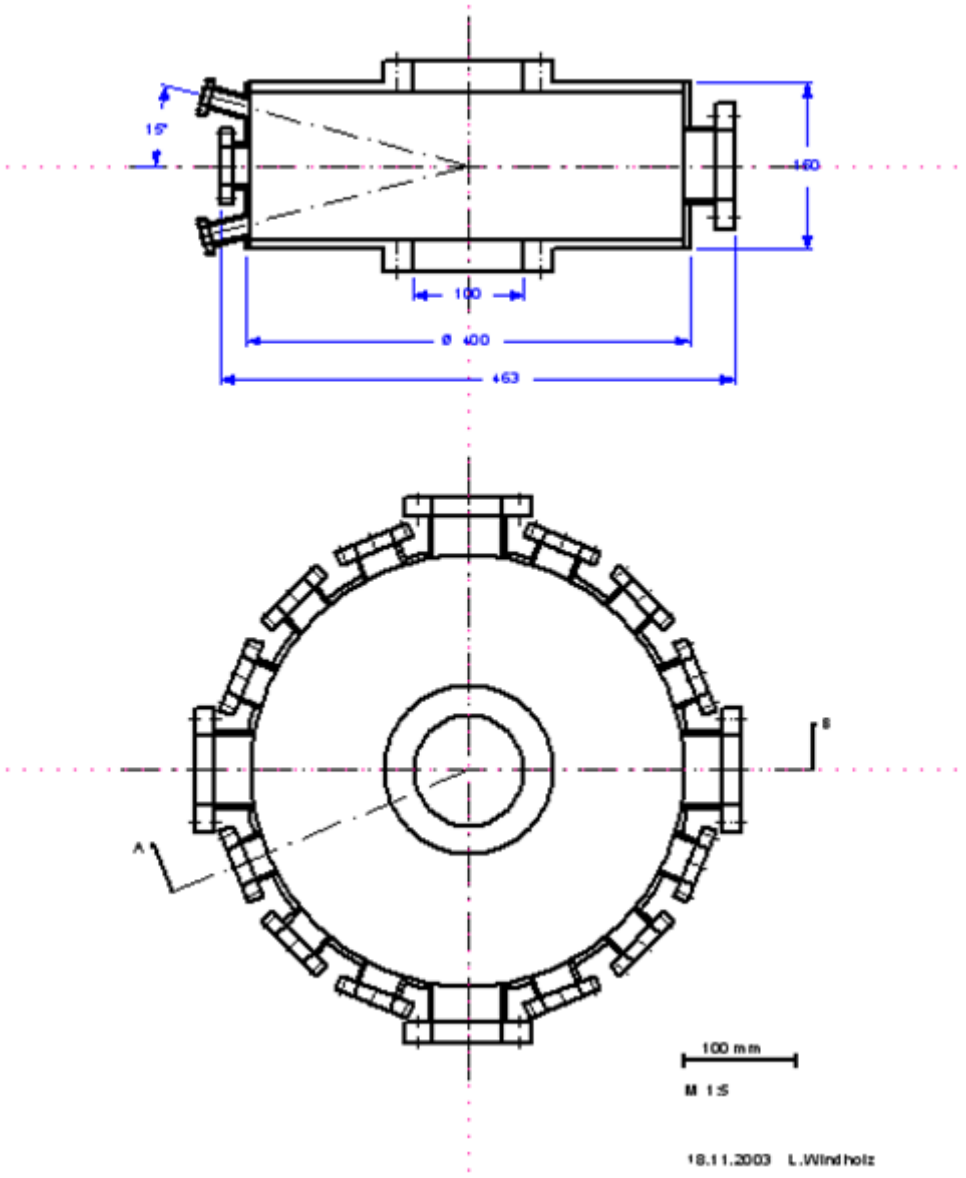

Figure 3. 37: Cross sectional side and top view of new chamber. Drawing is made by Prof. L. Windholz.

3.5.2 Vacuum

For the study of homonuclear and heteronuclear collision losses, ultra high vacuum has a great importance. To reach ultrahigh vacuum and less back ground pressure, the vacuum chamber and their accessories are well cleaned and backed before assembling. The vacuum system consists of different sizes and ranges of pumps and gauges used as shown in table 3.2. They all are connected with the chambers with CF connection.

For getting the vacuum in the range of 10^{-10} mbar, first we start the rotary pumps of main chamber and the oven section. This section can be isolated by the valves such as they can work independently

Table 3.1: Distribution of flanges and their uses

No	Types	Position	Uses
24	DN 16 CF	Horizontal	Three for ^{23}Na ,^{6}Li,^{7}Li ovens Three for view for naked eye.
12	DN 40 CF	Horizontal	Four for the cooling beam of ^{87}Rb, Four for cooling beam of ^{23}Na, Two for CO_2 laser, One for ^{87}Rb dispenser, One for TSP
4	DN 63 CF	Horizontal	One for fluorescence detection, two for two CCD cameras, one for viewing inside
2	DN 100 CF	Vertical	Connected with the old chamber Down flange is connected with T such as the horizontal side is connected with the Ion getter pump & other is view port

Table 3.2: List of vacuum pumps and vacuum gauges

No	Types	Company	Specification
2	Rotary pump	Pfeiffer vacuum	10^{-3}mbar
2	Turbo Molecular Pump(TMP)	Pfeiffer vacuum	60 l/s
1	Turbo Molecular Pump(TMP)	Pfeiffer vacuum	33 l/s
1	Ion Getter Pump(IGP)	Physical Electronics	100 l/s
1	Ion Getter Pump(IGP)	Physical Electronics	40 l/s
1	Titanium Sublimation Pump(TSP)	Balzers	3 titanium sublimation filaments
1	Pressure Display IGP 1	Physical Electronics	Display
1	Cold Cathode Manometer	Balzers	Reading
1	Hot Cathode Manometer	Phillips	Reading
1	Quadrupole Gas Analyzer	Hiden	Mass analyzer

After few minutes, three turbo molecular pumps, from which two are connected with main chamber section and one is connected with oven

section, are started. After few hours, the pressure in the main chamber as well as the oven section will reach at 10^{-8} mbar. After starting ion getter pumps which are attached only with the main chamber section, after few days vacuum pressure is reached at the range of 10^{-10} mbar in the main chamber but the oven section pressure remain in the range of 10^{-9} mbar. Before starting experiment, we can use the titanium sublimation pump for half hour at 40 ampere current to improve the vacuum.

During MOT operation, oven and the dispenser are producing the vapors then the pressure rises a little bit but after some time it stays at the optimum pressure of 3.10^{-9} mbar.

The hot cathode gauge which is attached with old chamber is used to measure the vacuum.

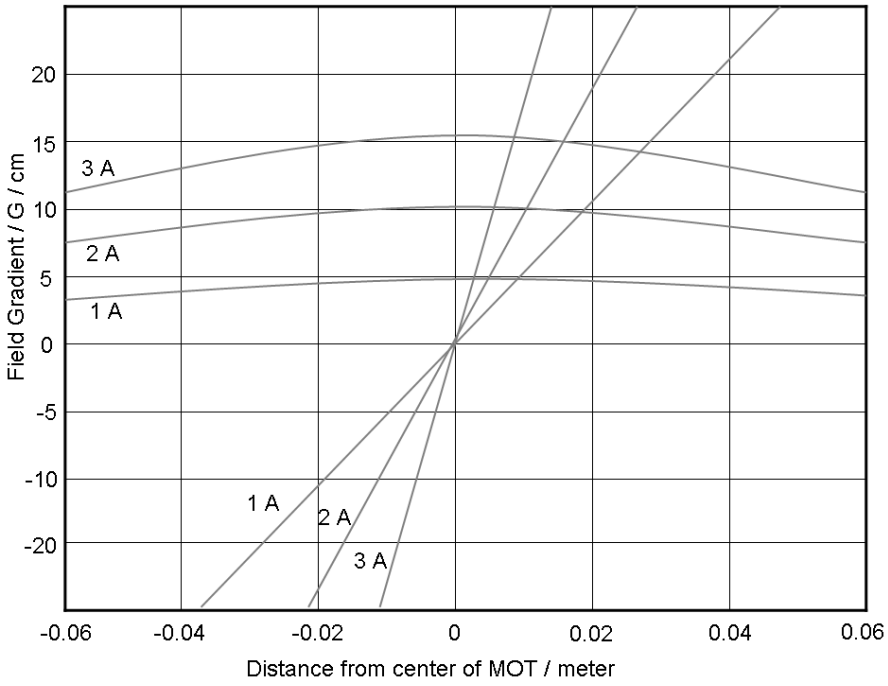

Figure 3. 38: Magnetic field gradient from center of MOT (Weiler, 2007)

3.5.3 Magnetic Field Coil for Trapping

For trapping the alkali atoms, magnetic field gradient is used to hold and push the atoms towards the center. In our setup, this magnetic field gradient is generated by a pair of coils in anti-Helmholtz configuration. These coils are placed outside the vacuum main chamber. The distance between the two coils is 160 mm. The diameter of each coil is 340-390

mm and thickness is 55 mm. Winding of wire is made of pure copper and its diameter is 1.5 mm. This wire is specially coated and can be heated up to 210°C. Each coil has 2520 winding and produced I.(0.58) mT./cm in axial direction where 'I' is current in ampere as shown in figure (3.38). Two separate power supplies, model QPX 1200 made by TTi UK are used.

3.6 Atom Sources

3.6.1 Rubidium Dispenser

For loading our MOT, atomic oven for ^{23}Na and alkali metal dispenser for ^{87}Rb is used. ^{87}Rb dispenser is from SAES getter, Italy. ^{87}Rb dispenser can easily handled at room temperature and in air without any oxidation. The dispenser is placed in the chamber mounted with feed through. During the initial vacuum and heating process, the dispenser is degassed for one day at current of about 1 Ampere and then slowly increased the current by factor of 0.2A after one hour until it reached 3A current. In this way we are able to get the good flux of ^{87}Rb atom at minimum time. This flux of rubidium atoms can be shut down when the current is suddenly switched off.

3.6.2 Sodium Oven

Sodium oven is made of glass and attached with main chamber. To produce the atomic beam, a heating coil is used to heat the ^{23}Na reservoir. In our experiment, the atomic beam of Na at temperature 120^0C is used. Maximum bear temperature of this glass is 180^0C. A magnetic shutter is used to open and block the atomic beam.

3.6.3 Lithium Oven

Lithium oven is made of high grade steel and filled with natural lithium (93% ^{7}Li and 7% ^{6}Li). Lithium has the melting point at 180.54°C.The oven is surrounded by a heating coil which can produce maximum temperature up to 450°C. In our set up, we operate the oven at 375°C to get the atomic beam at optimum vapor pressure as shown in figure

(3.39). This is a high temperature environment so water cooling is required for cooling the section between oven and chamber. This oven can be separated from the trap by valve. Electromagnetic shutter is used to control the atomic beam.

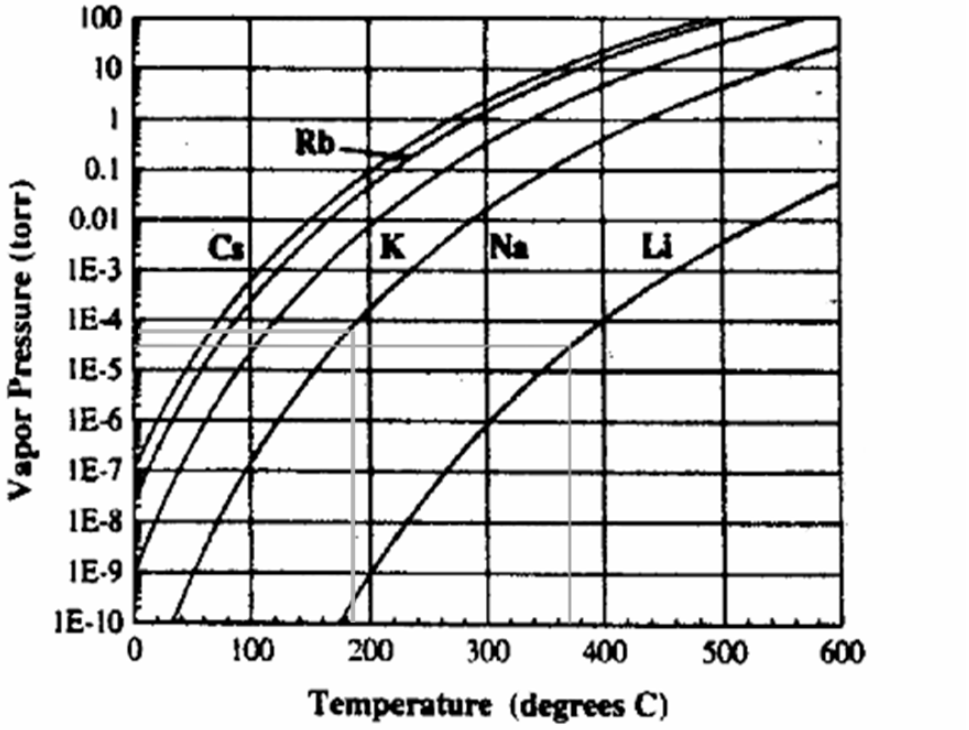

Figure 3.39: Vapor pressure of alkali atoms as a function of temperature (Weast, 1972)

3.7 The Detection System

A calibrated photodiode is used to measure the fluorescence intensity of cloud. This fluorescence signal is then amplified and send to a computer which converts the signal by National Instrument measuring card (12-bit analog-digital(A/D) and digital-analog(D/A) converter) controlled by Lab View program. The schematic scheme for detection system is shown in figure (3.40)

For recording of load and decay process, the atomic beam is controlled by magnetic shutters which are connected with a programmable controlled power supply.

For measuring the density distribution of the cloud, CCD camera is used which is coupled with an amplifier and an oscilloscope. The picture of the cloud can also be seen directly on a TV screen.

Two CCD cameras are used to check the overlapping of both clouds in two orthogonal directions.

3.7.1 Determination of Atom Number

Atom number is measured by the fluorescence light coming from the cloud and detected by the photodiode out side of the chamber. A lens of diameter of 63 mm and focal length of 126 mm is used to focus the cloud image on the aperture of photodiode at distance 133.25 mm. The distance between the lens and cloud is 231.5 mm. The signal of cloud is very weak as compare to the background light. An amplifier is used to amplify the cloud signal. The edge filter is used to filter the required fluorescence of the cloud. During the simultaneous trapping of the atoms, special edge filters are used to detect the fluorescence light of the required atom and to quench the fluorescence of other atom and background. It is necessary that during the detection of fluorescence, the back ground should be low and photodiode with amplifier is well calibrated.

Out side the chamber, a calibration system is made in such a way that the distance of lens from cloud and the photodiode and the amplified factors on the amplifier remain constant. By using this calibration system, at different fluorescence light intensities then corresponding voltages are measured with and without of the edge filter.

By using equation (3.1), the number of atoms N of the cloud can be calculated

$$N = \frac{L}{\eta \rho^{(e)} \hbar \omega_L \Gamma} \qquad (3.1)$$

With

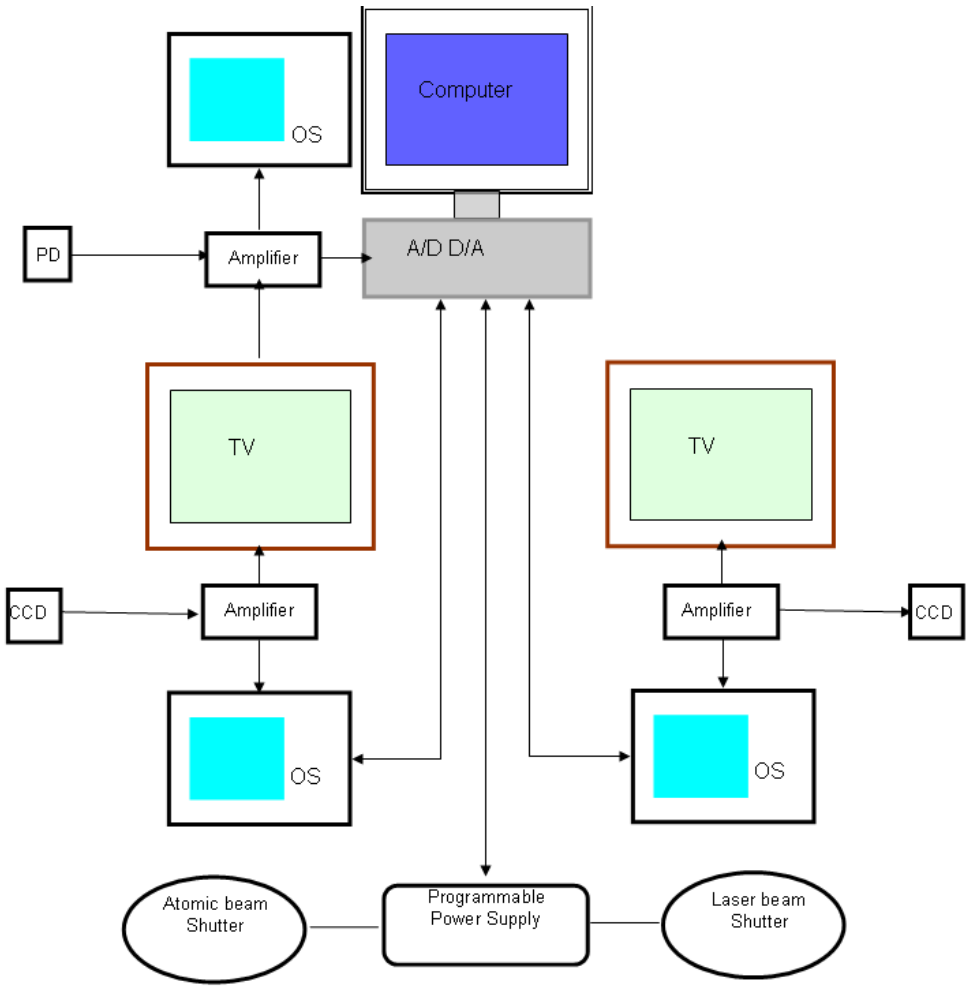

Figure 3. 40: Schematic diagram of detection system.

- L is detecting light power.
- Γ is life time of excited atom.
- η is the detection efficiency of total fluorescence and can be determined as

$$\eta = \frac{\pi (d/2)^2}{4\pi a^2}. \qquad (3.2)$$

Where *d* is diameter and *a* is the distance between the lens and cloud.

In our set up, $\eta = 0.0023$

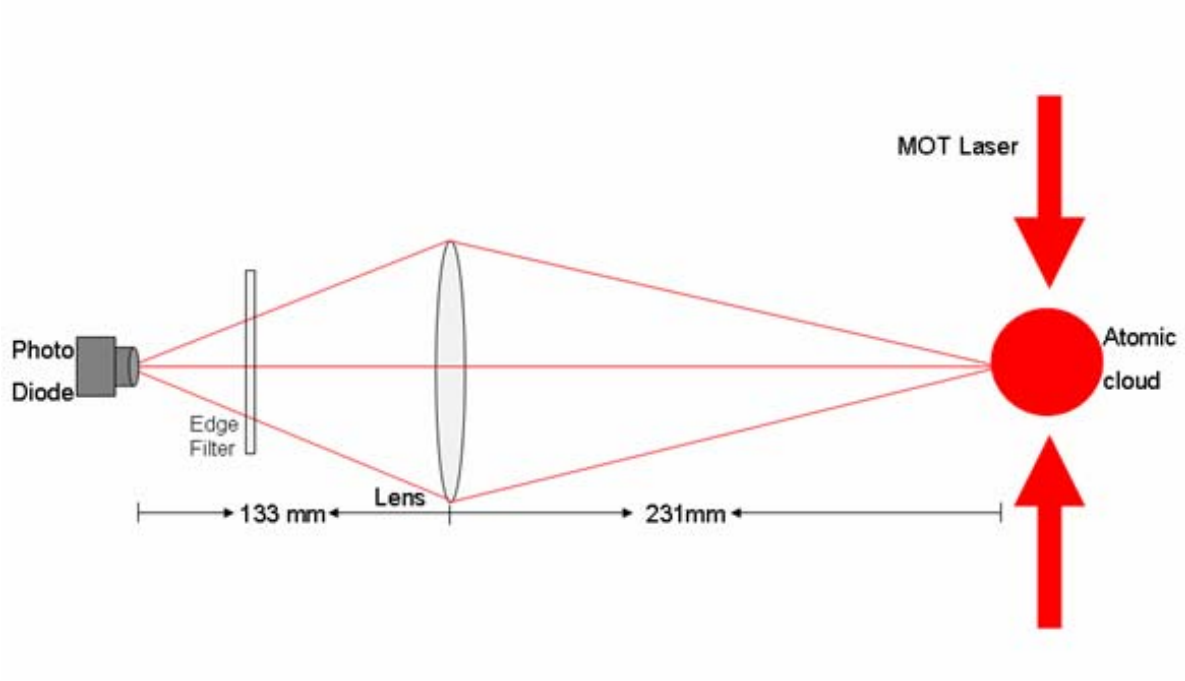

Figure 3.41: Florescence detection system

- $\rho^{(e)}$ is fraction of excited atoms and determined by the steady state solution of the rate equation for atoms in trap (Shore,1990) and calculated as

$$\rho^{e} = \frac{\Gamma}{2}\frac{I/I_o}{1+I/I_o+(2\Delta/\Gamma)^2} \qquad (3.3)$$

Where Δ is detuning, I is the total intensity of all six beams and I_0 is the saturation intensity. ^{87}Rb, ^{23}Na and ^{7}Li have the saturation intensity $1.6\ mW.cm^{-2}$, $6.26\ mW.cm^{-2}$ and $2.56\ mW.cm^{-2}$, respectively.

3.7.2 Determination of Density Distribution

A CCD camera model CV-M300 is used to measure the spatial distribution of the cloud. A lens of focal length of 200 mm is used to enlarge the image of cloud on the chip of CCD. The image is a two dimensional projection of the cloud and is viewed online via TV. For determination of the exact size of the atomic cloud, the CCD camera is well calibrated. Using an optical grid of size 4 lines per mm instead of cloud, keeping the same distances between lens and CCD camera, the calibration is made outside the chamber. In our experiment, 1mm

corresponds to 76.8 pixels of CCD. The image of cloud is nearly Gaussian profile and the Gaussian radius r_e is calculated in computer software program Origin 8.1 by using equation 3.4.

$$y = y_o + Ae^{\frac{(x-x_c)^2}{2w}} \qquad (3.4)$$

Where $r_e = \frac{w}{\sqrt{2}}$ with ' w ' is fitting parameter.

Volume of cloud can be determined by

$$V = \pi^{\frac{3}{2}} r_e^3 \qquad (3.5)$$

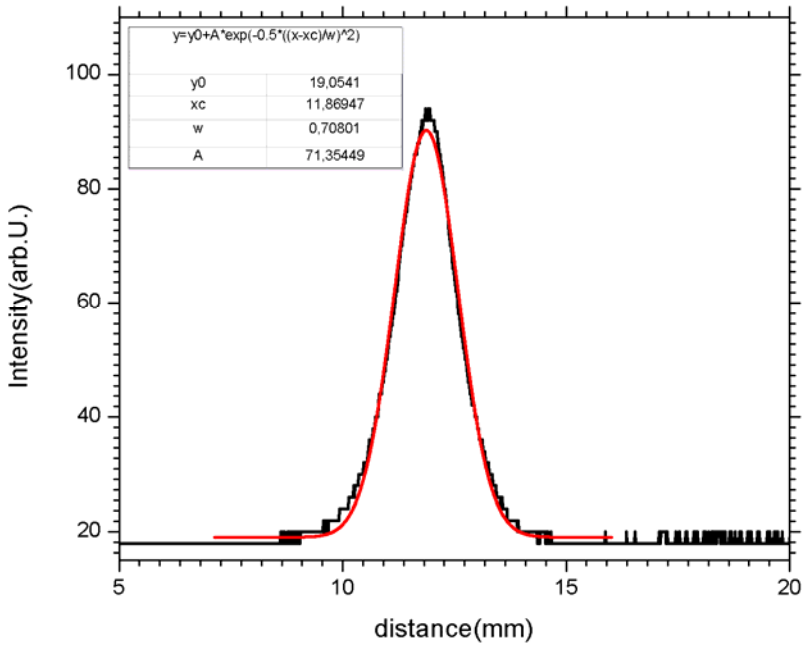

Figure 3.42: Gaussian density distribution profile of ^{87}Rb cloud, red line is best fit of data using temperature limited model

4. Measurements & Results

4.1 Data Evaluation Procedures

Magneto optical trap (MOT) is a very effective tool to trap cold atoms. The decay or load curves are used to measure the steady state numbers of atoms, their density and the homo- or heteronuclear collisional losses in MOT. The number of trapped atoms in MOT depends upon different parameters and conditions. The laser light stability, intensity, detuning, magnetic field gradient, diameter of cooling beam, intensity ratio of cooling beam & repumping beam, alignment of all laser beams, vacuum of chamber and vapor pressure of the alkali atoms are the major parameters. These parameters have a great influence on the shape of the load or decay curves and thus on the number of trapped atoms. In this work, decay curves are used to measure the trap losses which are more accurate and reliable compared to load curves. In decay curves, the uncertainty due to influence of the atomic vapor and fluctuations in trapped atoms are reduced because the atomic beam is closed.

The decay curve is recorded by detecting the fluorescence intensity of the cold atoms while closing the magnetic shutter in front of the ovens via time. The behavior of curve is nearly exponential as shown in figure (4.43). The starting position of the curve represents the stationary state number of N_∞ where at that time the maximum atoms are captured.

The comprehensive procedures to record the decay curve for homo- and heteronuclear cold collision losses are described in section 4.1.1 and 4.1.2.

4.1.1 Measurement Technique for Homonuclear Trap Losses

The following procedure is adopted to record decay curves for measuring homonuclear trap losses (β).

1. Heat the ovens of ^{23}Na and ^{7}Li up to $120^{o}C$ and $370^{0}C$, respectively, or, in case of ^{87}Rb, a dispenser is used at 2.7 A current.

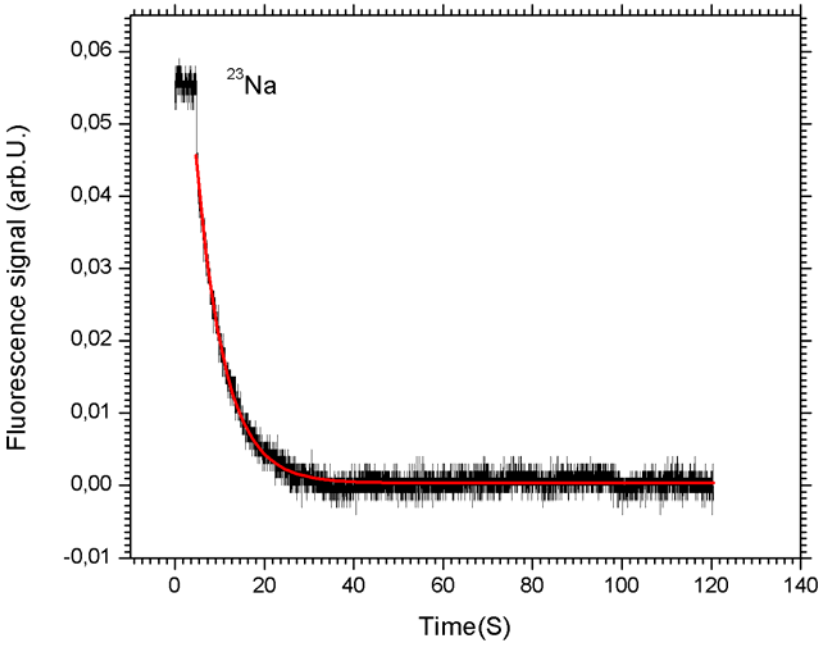

Figure 4.43: Na decay curve, type II trap (see 4.2.2) with laser is locked 14 MHz to the red of transition $(F = 2 \rightarrow F' = 3)$, fitted with temperature limited model.

2. Check the beam profile of the cooling beam. It should be a Gaussian profile.

3. Measure total power P_{Total} of the cooling beam by using a calibrated power meter.

4. Measure center intensity I_C of the cooling beam. I_C is used to calculate the fraction of excited atoms in equation (3.3).

5. Detect the background light intensity by using the photo diode (PD) such that

   - Opposite window across the PD is covered.
   - Set magnetic coils current to zero Ampere (no magnetic field).
   - Open oven (note: background including fluorescence but without cloud)

6. Load the trap by opening the magnetic shutter. Magnetic field is switched on (wait till optimize fluorescence power is achieved).

7. Close the magnetic shutter and record the fluorescence light until decay curve reached at the ground level.

8. Record the signal of spatial intensity distribution of atomic cloud in two dimensions by using a CCD camera (no background signal measurement is necessary). This Gaussian distribution profile is used to calculate the volume of the cloud in equations (3.4) and (3.5)

9. Recheck laser total power and center intensity of cooling beam.

4.1.2 Measurement Technique for Heteronuclear Trap Losses

For measuring heteronuclear cold collisions between two elements A and B, two decay curves are recorded with and without second element trapped.

- *Decay curve of A=lithium/sodium/rubidium element in presence of cloud of B = lithium/sodium/rubidium element*

1. Heat oven of ^{23}Na and ^{7}Li up to 120°C and 370^{0}C respectively, or, in case of ^{87}Rb, use a rubidium dispenser is operated at 2.7 A current.

2. Check the beam profile of the cooling beam. It should be a Gaussian profile.
3. Measure total power P_{Total} of the cooling beams of A and B elements by using the calibrated power meter.

4. Measure center Intensity I_C of the cooling beams.

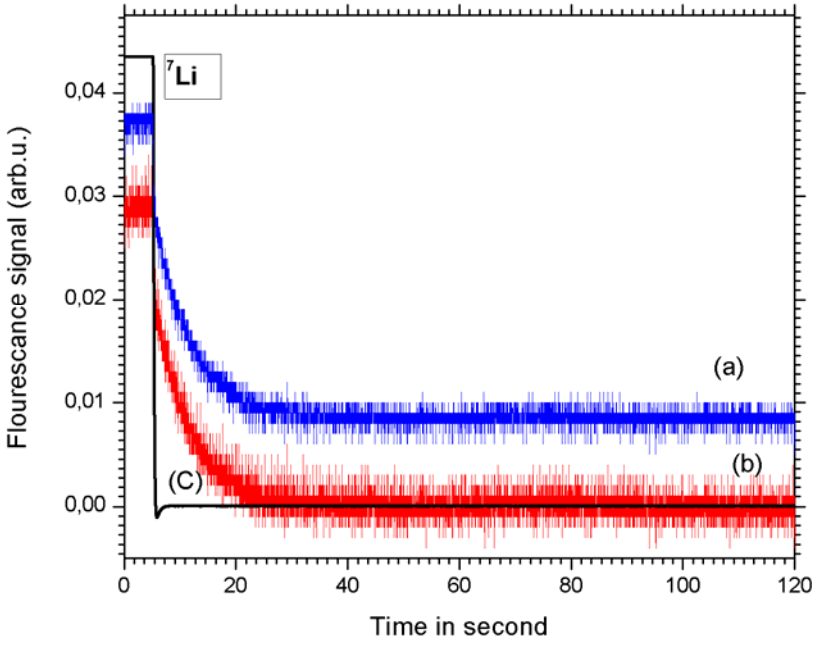

Figure 4.44: Lithium decay curves. (a) with background light (b) without background light. (c) voltage signal, used as marker for starting point of decay curve.

5. Optimize the cloud fluorescence (temperature limited regime) of both trapped elements.

6. Check overlapping of both clouds, two CCD cameras are used in x and y directions.

7. Measure spatial intensity distribution signal of each element separately by using the CCD camera.

8. For measuring the stationary atom number for B element, the laser light for trapping of element A is blocked and record the fluorescence of cloud B without using an edge filter.

9. For measuring background B element as above, just block the retro laser light of element B.

10. Insert the appropriate edge filter. These edge filters are depended upon wavelength. In our case for Na and Rb, We are using two

different edge filters which are made by Semrock. An edge filter (inv. no. V/1289) has a 99 % transmission for sodium atoms where as edge filter (inv. no. V/1292) has a transmission 99 % for rubidium atoms

11. Measure the background light for element A in the presence of cloud of element B by closing the magnetic shutter of element A.

12. Record the decay curve of element A in the presence of cloud of element B.

- *Decay curve of A=lithium/sodium/rubidium element in presence of cloud of B = lithium/sodium/rubidium element*

13. Measure the spatial intensity distribution of element A for calculating the cloud volume (the laser light for trapping element B is blocked).

14. Measure the background for the element A by closing the shutter of element A.

15. Record the decay curve of element A.

It is important that all parameters related to the MOT and detection system remain the same and stable during recording the data. For calculation of homonuclear loss rate coefficient β_A^A, subtract the background from the decay curve and calculate the atomic numbers by using equation (3.1). The decay curves are evaluated by computer software Origin vol.8 or the computer program in appendix A to find the fitting parameters ξ, τ_d and N_0 (where τ_d the is decay time and N_0 is stead state atoms). These fitting parameters are used in equation (2.64).

Central density 'n' of the cloud is

$$n = \frac{N_0}{(4\pi)^{\frac{3}{2}} a^3} \qquad (4.1)$$

where ‘a’ is its Gaussian radius.

By using central density 'n', fitting parameter 'ξ' and $\alpha = \frac{1}{\tau_d}$, homonuclear loss rate coefficient can be calculated as

$$\beta_A^A = \frac{\xi\sqrt{8}\alpha}{(1-\xi)n_0} \qquad (4.2)$$

Similarly heteronuclear loss rate β_B^A can be calculated by using equation (2.85). Decay curves in the presence of second elements have a shorter time due to extra losses as shown in figure (4.45). The linear loss rate 'α' is directly related to the background pressure, so, for better measurements of heteronuclear losses β_B^A, the background pressure should be as low as possible.

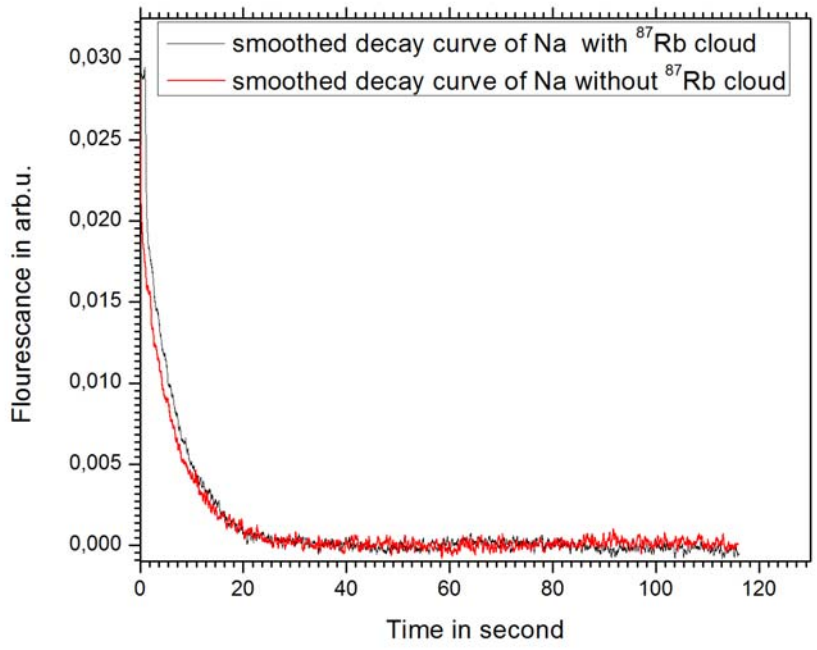

Figure 4.45: Decay curves of ^{23}Na with and without presence of ^{87}Rb.

4.2 Measurements for Homonuclear Cold Collisions

The measurements for homonuclear cold collision of ^{87}Rb, ^{23}Na and ^{7}Li are discussed in sections 4.2.1, 4.2.2 and 4.2.3, respectively. Atom numbers, volume and density of the cloud are also measured by evaluating decay curves in the temperature limited range. In our trap, error bars have the value of 50% . The total errors are depended upon systematic errors as well uncertainty to measure the volume of cloud in a magneto optical trap.

4.2.1 87Rb MOT Characteristics

Rubidium atoms are trapped according to the parameters in table 4. The red detununing of cooling laser is performed by a dc magnetic field. In rubidium saturation cell, the absorption frequency is shifted with different magnetic field at constant intensity. In our setup, 0.5 A current produced approximately 20 gauss magnetic field which shifted the transition $F = 2 \rightarrow F' = 3$ such that laser light is red tune at 18 MHz ($\approx -3\Gamma$).

Rubidium dispenser current is set to 2.7 A. By increasing the current, the trapped atom increases as shown in figure (4.46) at 40 $mW.cm^{-2}$ laser power. If the current is off the emission is stopped and fluorescence decay exponentially. For each decay curve of ^{87}Rb atoms, it is important to wait for ten minutes until rubidium atoms are reached at the equilibrium value in the MOT.

By recording the decay curves according to procedure above, steady state atoms (N_∞), density (n), fraction of excited atoms (ρ), linear loss rate coefficient (α) and collisional loss rate coefficient (β) are measured as shown in the figures (4.47, 4.48, 4.49, 4.50 and 4.51). The summery of the measured data is given in table.3.

Table 3: Measured results at different ^{87}Rb intensity. Each result is evaluation of the ^{87}Rb decay curve and density distribution.

$I(mW/cm^2)$	N	$\tau(s)$	ξ	$\omega(mm)$	$n(cm^{-3})$	$\alpha(s^{-1})$	$\beta(cm^3/s)$
109	87410	13.52	0.35284	0.1534	1.2e10	0.740	9.2e-12
94	108163	9.912	0.06005	0.17149	1.0e10	0.100	1.67e-12
77	74496	9.06	0.11429	0.1548	1.0e10	0.110	3.9e-12
62	114200	12.19	0.49226	0.14605	1.8e10	0.082	1.2e-11
55	70482	9.2	0.11113	0.12602	1.7e10	0.108	2.1e-12
35	40363	9.27	0.4172	0.09515	2.3e10	0.107	9.1e-12
24	47425	9.5133	0.13943	0.14349	8.1e9	0.105	5.9e-12
22	30658	6.21	-0.8034	0.09534	1.7e10	0.161	-

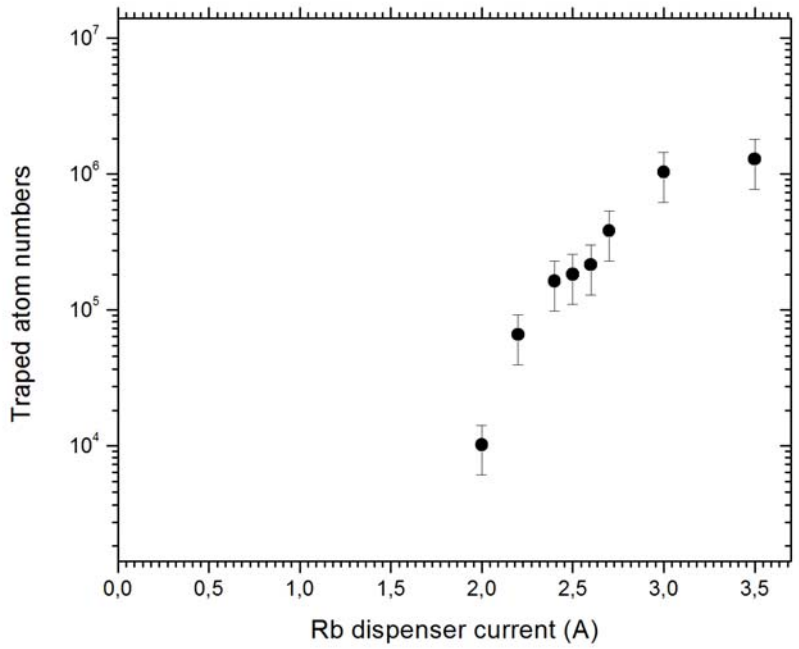

Figure 4.46: Number of trapped atoms at different rubidium dispenser current.

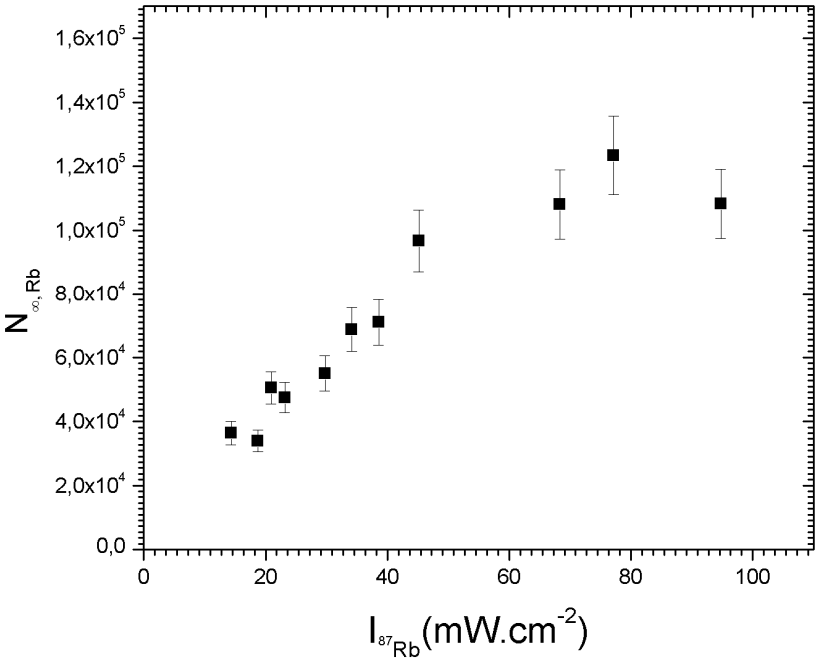

Figure 4.47: Measured stationary atom numbers of ^{87}Rb versus different cooling laser intensities I_{Rb} at 2.7 A dispenser current.

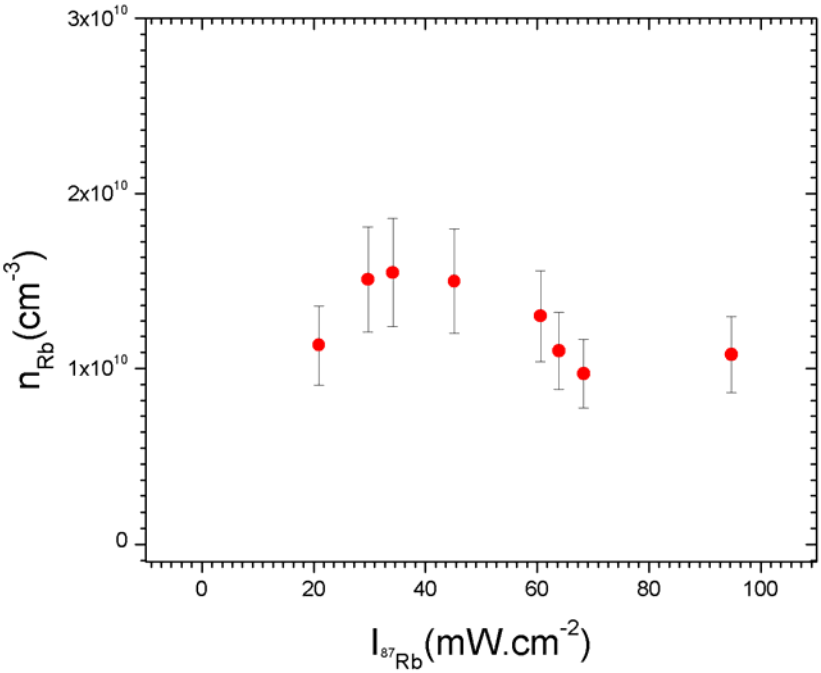

Figure 4. 48: Measured rubidium density (n_{Rb}) as a function of laser intensity (I_{Rb}).

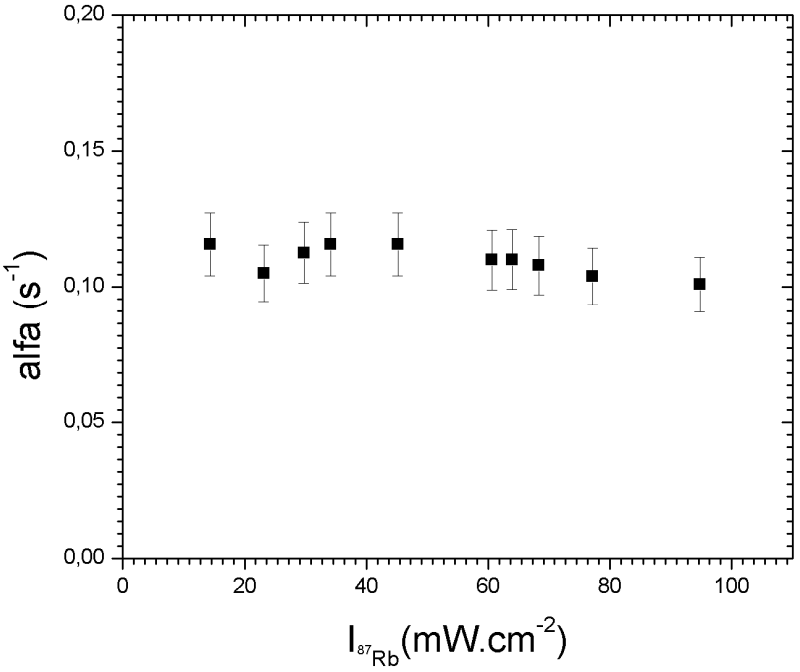

Figure 4.49: Measurements of linear loss rate coefficient (α) versus laser intensity (I_{Rb}) at 2.7 A.

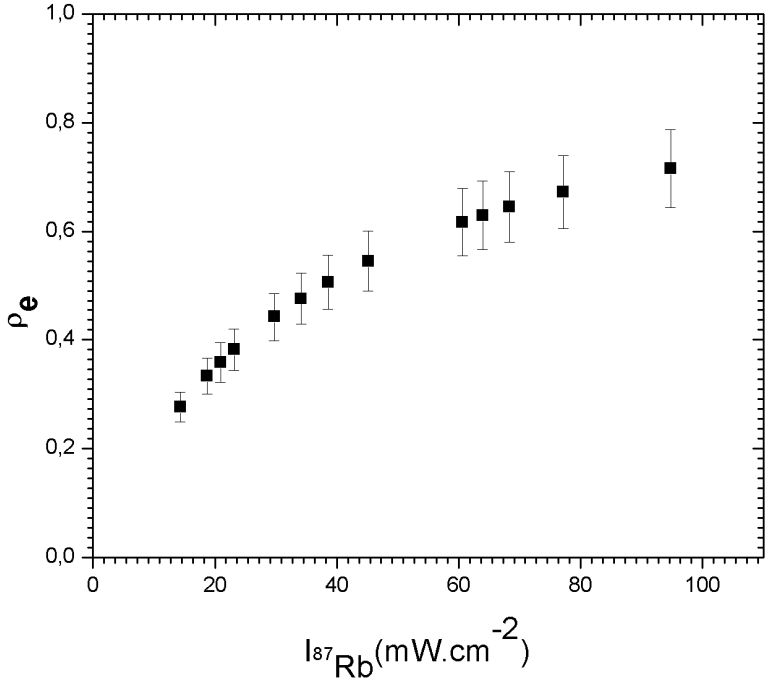

Figure 4.50: Fraction of excited state atoms (ρ_e) of rubidium as a function of laser intensity (I_{Rb}).

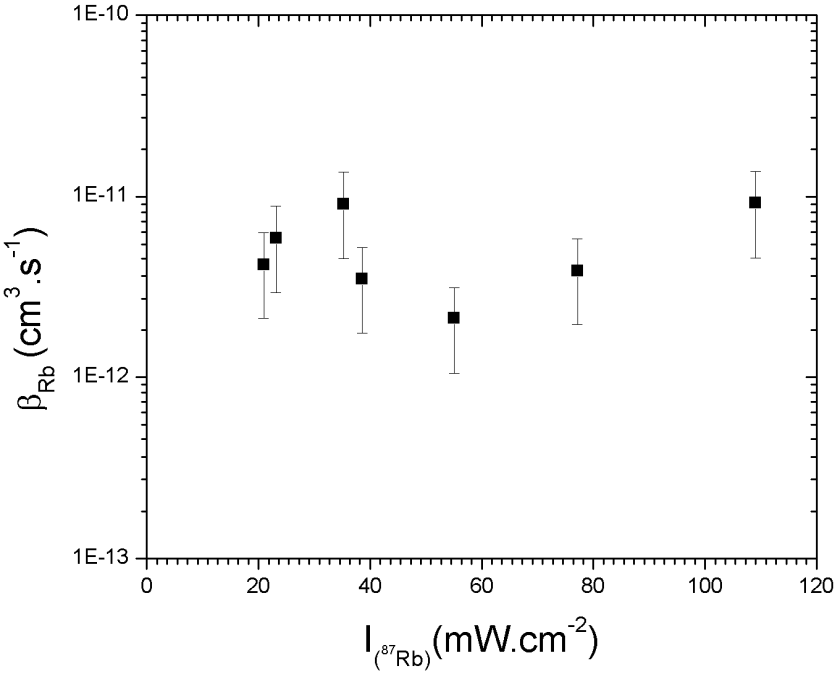

Figure 4.51: Measurements of collisional loss rate coefficient (β) versus laser intensity (I_{Rb}).

4.2.2 ^{23}Na MOT Characteristics

Sodium can be trapped at two different transitions called "type I" and "type II" traps. In "type I" trap, cooling laser is locked near the transition $F=2 \rightarrow F'=3$ and repumper laser is locked at the transition $F=1 \rightarrow F'=2$ where as in "type II" trap the cooling laser is locked near transition $F=2 \rightarrow F'=2$ and repumper laser is locked at $F=1 \rightarrow F'=2$. The cooling laser is red detuned in both cases. The "type I" trap is more compact and colder then "type II" trap (Atutov *et al.*, 2001). The intensity and size of "type I" is comparatively larger than the "type II" trap. In our experiment, "type I" trap is used and we measured the atom number, density and trap losses for homo and heteronuclear cold collisions.

In sodium MOT, steady state number of trapped N_∞, excited state atom 'ρ', density 'n', linear losses rate coefficient 'α' and finally the collision loss rate coefficient 'β' are measured with different cooling laser intensities as shown in figures (4.52, 4.53, 4.54, 4.55 and 4.56). Neutral density filters are used to change the intensity of the cooling beam. The decay curve is recorded according to procedure in section

4.1.1. A magnetic shutter is used to close and open the Na atomic beam. The measured results are summarized in table 5.

Table 4: Measured values at different ^{23}Na intensity. Each result is evaluation of the ^{23}Na decay curve and density distribution.

$I(mW.cm^{-2})$	N	$\tau(s)$	ξ	$\omega(mm)$	$n(cm^{-3})$	$\alpha(s^{-1})$	$\beta(cm^3/s)$
114	182896	9.12	0.3508	0.247	6.13e9	0.1096	2.7e-11
108	203395	9.61	0.4418	0.246	6.91e9	0.1040	3.3e-11
97	176286	11.3	0.5314	0.223	8.02e9	0.0884	3.5e-11
87	144551	9.78	0.3894	0.213	7.51e9	0.1022	2.4e-11
60	112315	15.9	0.6934	0.192	7.98e9	0.0629	5.0e-11
53	115980	20.3	0.8319	0.151	1.7e10	0.049	4.0e-11
49	86861	12.4	0.4608	0.189	6.47e9	0.0802	2.9e-11
38	99744	9.96	0.41152	0.188	7.61e9	0.1004	2.6e-11
34	98673	7.25	0.14109	0.200	6.22e9	0.1379	1.0e-11

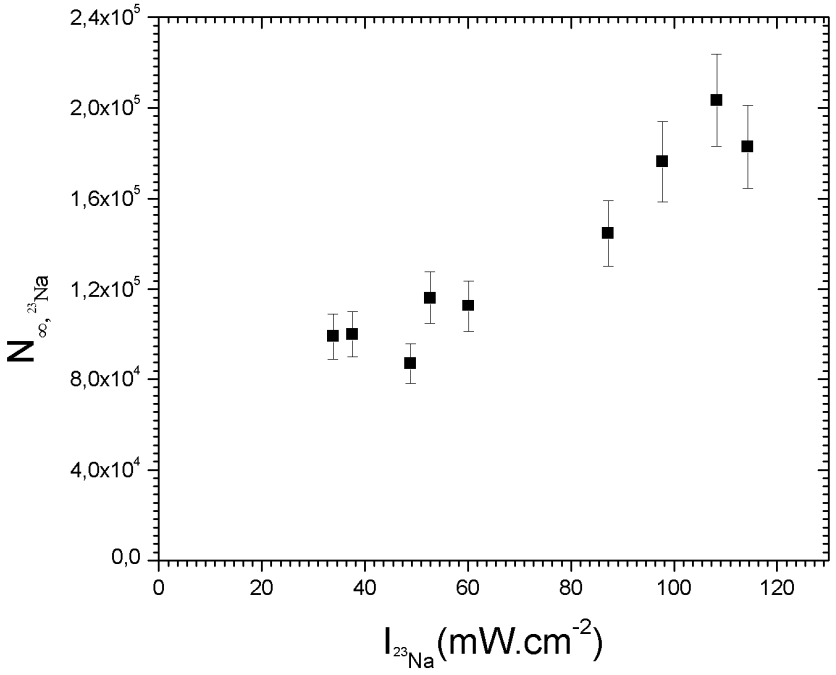

Figure 4.52: Measured stationary number of trapped atoms $N_{\infty,Na}$ as a function of laser intensity I_{Na} at Na oven temperature is $120\,^{o}C$.

Table 5: $\lambda(nm)$....wavelength, $LB_D(mm)$....Laser beam, $O_T(^oC)$....oven temperature, diameter. $I_0\ (mW.cm^{-2})$....Saturation Intensity, $\tau(ns)$....decay time, $\Gamma(MHz)$....life time of excited state, I....Nuclear spin, $T_D(\mu K)$....Doppler temperature, $T_R(\mu K)$....Recoil temperature, C_{Tran}....cooling transition, R_{Tran}....repumping transition, Δ_C.... Detuning of cooling beam, L_C/L_R.....ratio of cooling beam and repumping beam, $H_I(A)$....Heating current of oven and dispenser, $MC_I(A)$.....Magnetic coil current, $T_M(^0C)$....Melting point.

Parameters	^{87}Rb	^{7}Li	^{23}Na
$\lambda(nm)$	780.023	670.776	588.995
$\tau(ns)$	26.23	27.2	16.23
$\Gamma(MHz)$	$2\pi(6.0666)$	$2\pi(5.9)$	$2\pi(9.8)$
I	3/2	3/2	3/2
$I_0\ (mW.cm^{-2})$	1.699	2.56	6.26
$T_D(\mu K)$	145.57	142.11	240.18
$T_R(\mu K)$	0.36196	6.061	2.399
C_{Tran}	$F=2\rightarrow F'=3$	$F=2\rightarrow F'=3$	$F=2\rightarrow F'=3$
R_{Tran}	$F=1\rightarrow F'=2$	$F=1\rightarrow F'=2$	$F=1\rightarrow F'=2$
Δ_C	-3Γ	-3Γ	-1.6Γ
L_C/L_R	$\approx 3/1$	$\approx 3/1$	$\approx 10/1$
$H_I(A)$	2.7	1.7	1.1
$MC_I(A)$	1.69	1.69	1.69
$T_M(^0C)$	39.30	180.54(^0C)	97.8(^0C)
$O_T(^oC)$	-	370	120
$LB_D(mm)$	16	16	16

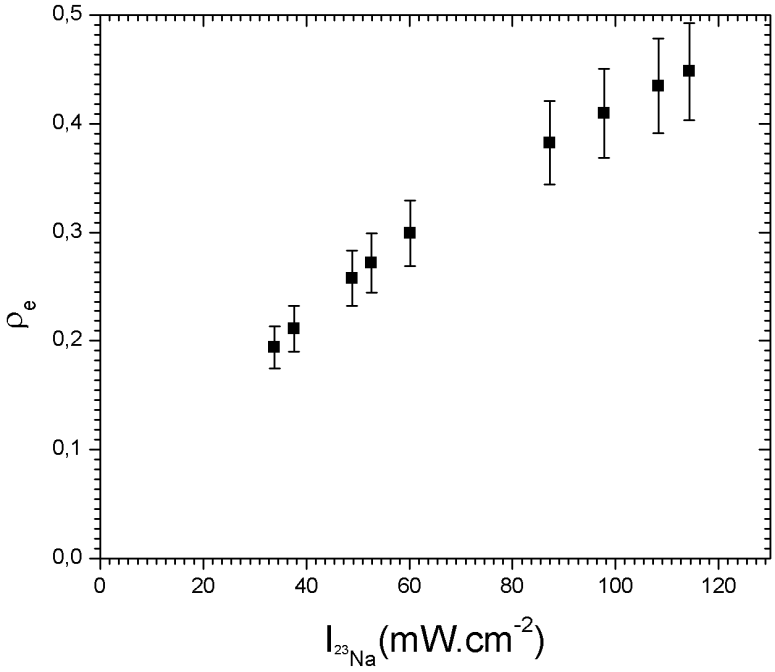

Figure 4.53: Fraction of excited state atoms ρ_e of ^{23}Na as function of laser intensity (I_{Na}). The oven Temperature of Na is $120\,^{o}C$.

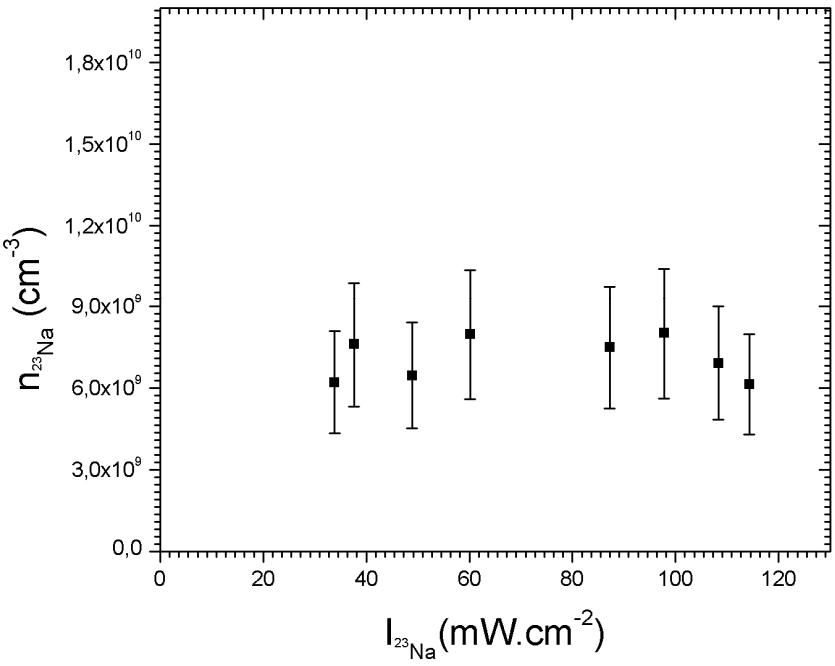

Figure 4.54: Measured density n_{Na} of ^{23}Na versus laser intensity (I_{Na}).

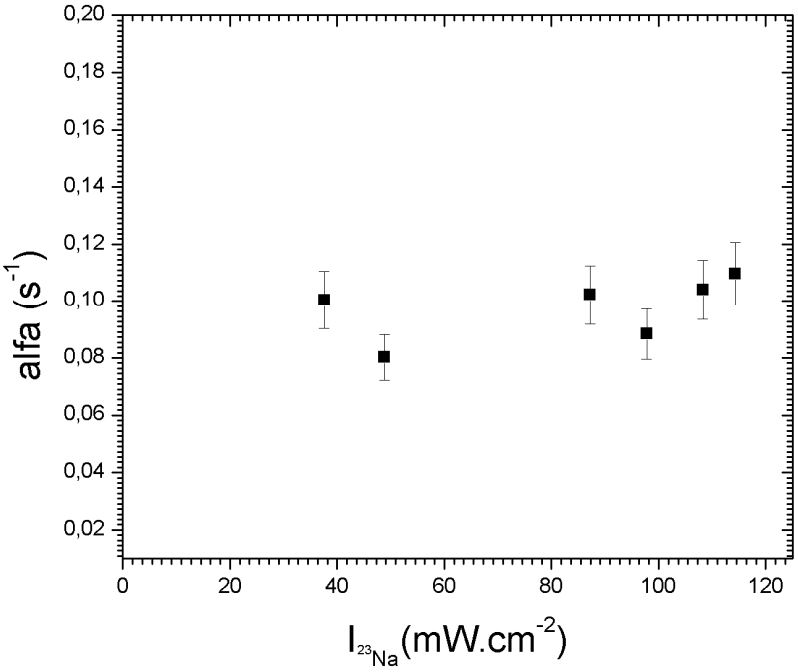

Figure 4.55 Measured linear loss rate coefficient (α) of ^{23}Na versus laser intensity (I_{Na}).

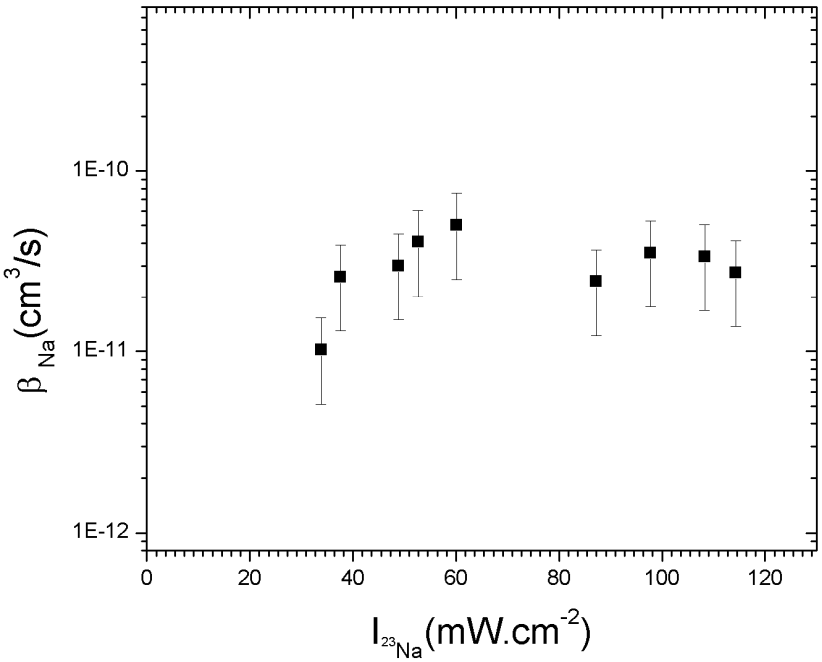

Figure 4.56: Measured values of collisional loss rate coefficient (β_{Na}) due to laser Intensity (I_{Na}).

4.2.3 ^{7}Li MOT Characteristics

Collision loss rate is dependent upon the different MOT parameters .In this experiment, detuning of cooling beam (Δ_c), detuning of the repumper beam (Δ_c), ratio of cooling beam and repumper beam (I_C/I_R), temperature of lithium oven (T_0) is kept to the same values as stated in (Auböck *et al.*, 2006) and mentioned in table 4.

By using these parameters, steady state atom N_∞, fraction of excited state atoms ρ, density n, linear loss rate α and collision loss rate coefficient β are measured as shown in figures (4.57, 4.58, 4.59, 4.60 and 4.61).

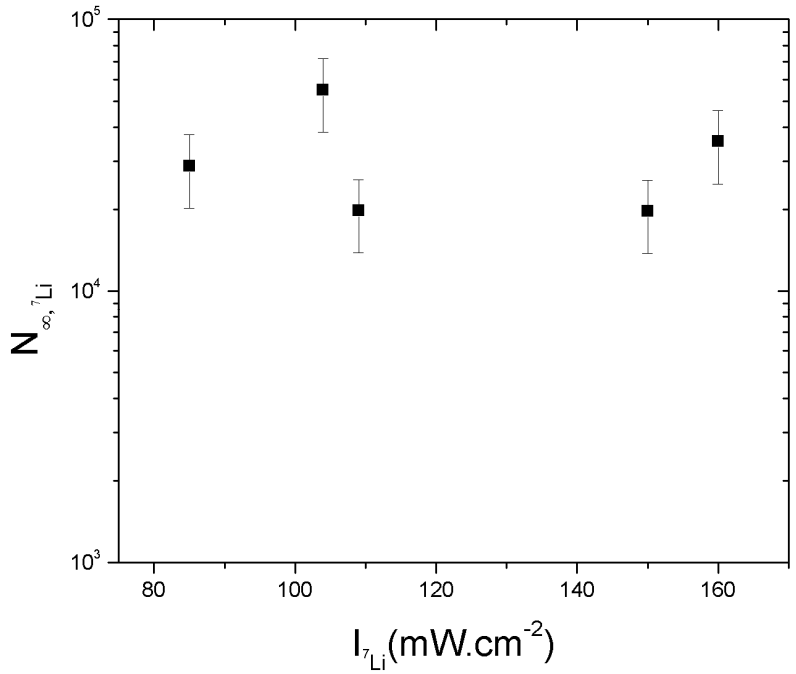

Figure 4.57 Measured number of ground state atoms of lithium as a function of laser intensity (I_{Li}). The oven temperature of ^{7}Li is 375 ^oC.

Table 6: Measured results at different ^{7}Li intensity. Each result is evaluation of the ^{7}Li decay curve and density distribution.

$I(mW/cm^2)$	N	$\tau(s)$	ξ	ρ	$n(cm^{-3})$	$\alpha(s^{-1})$
160	35470	22.86	0.696	0.70694	4.15e9	0.04373
104	55000	17.024	0.6625	0.61115	1.129e10	0.05874
124	70660	16.3	0.4129	0.65084	1.018e10	0.06133
97	38160	8.48	-	0.5938	8.53e9	0.1181
85	28900	10.64	0.4825	0.56126	1.077e10	0.0939
109	19750	13.54	0.4329	0.6018	1.19e10	0.07383

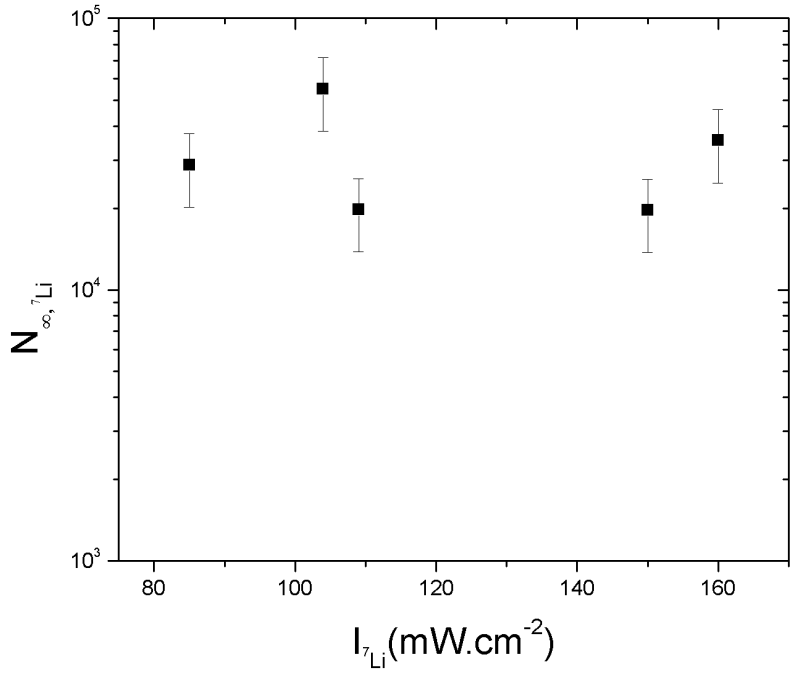

Figure 4.58 Measured number of ground state atoms of lithium as a function of laser intensity (I_{Li}). The oven temperature of ^{7}Li is 375 ^{o}C.

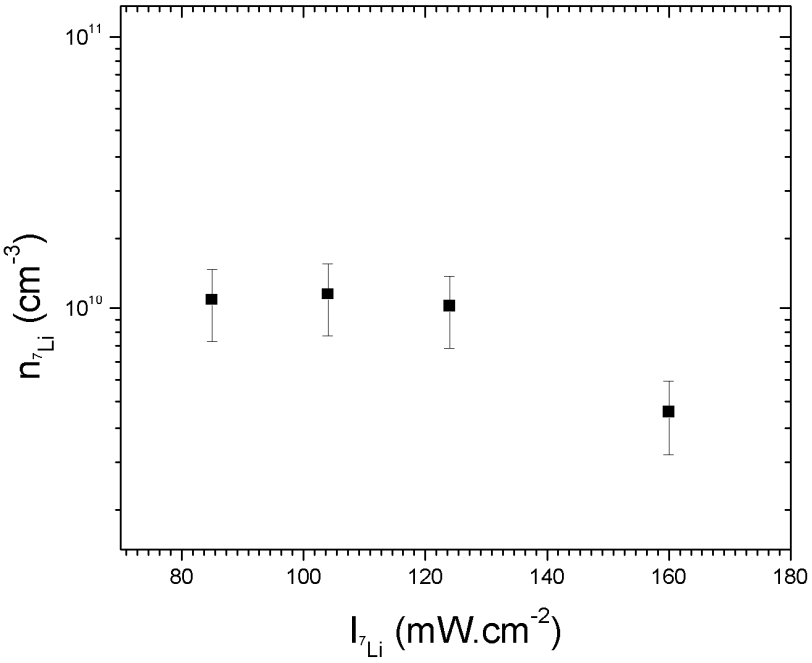

Figure 4.59: Measured value of density (n_{Li}) versus laser intensity (I_{Li}).

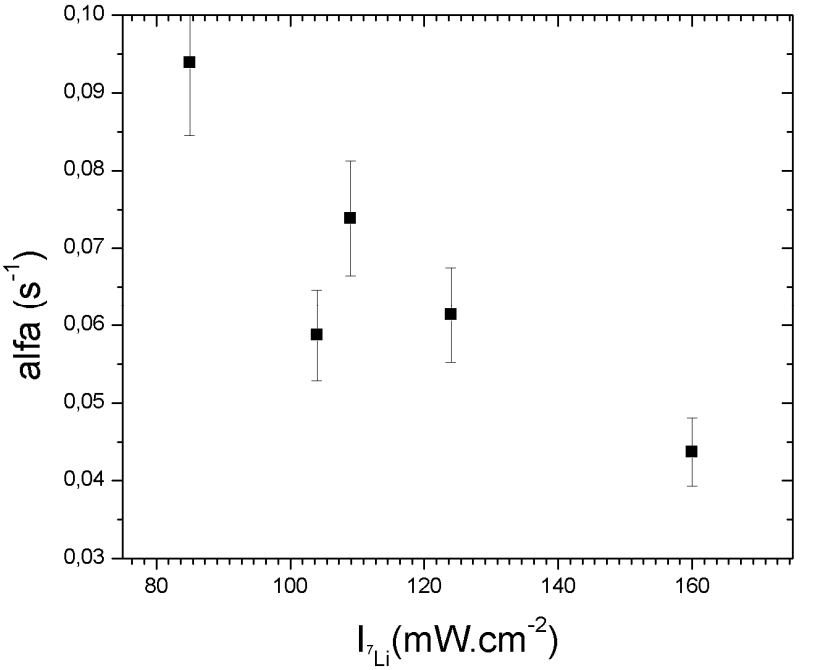

Figure 4.60: Measured linear loss rate coefficient (α) of lithium versus laser intensity (I_{Li}).

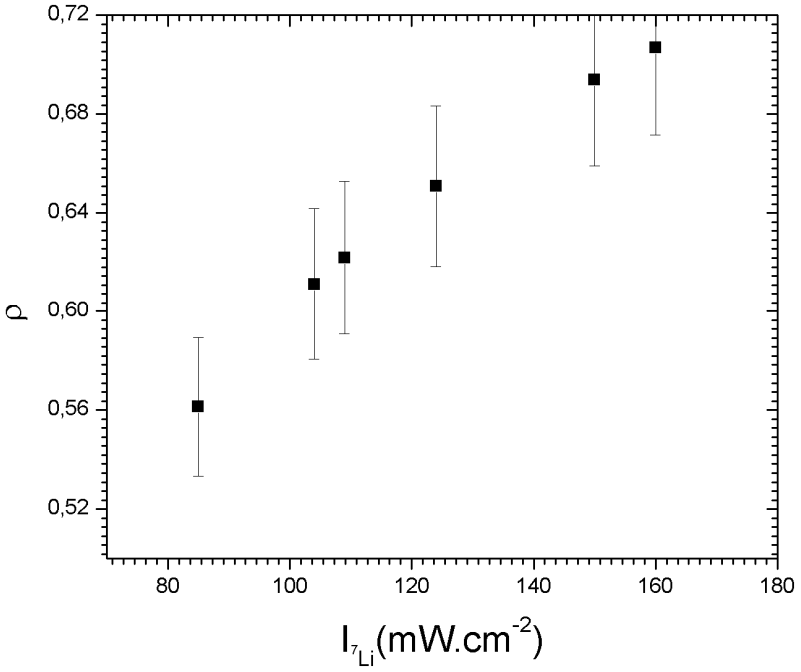

Figure 4.61: Fraction of excited state atom of ^{7}Li versus laser intensity (I_{Li}). The oven temperature of ^{7}Li is 375 ^{o}C.

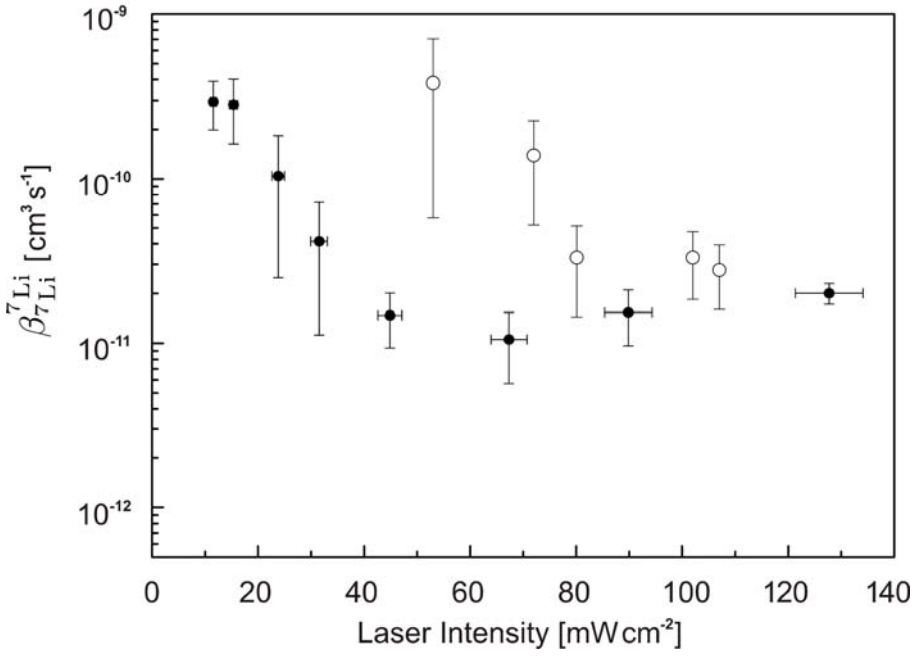

Figure 4.62: Measured values of collisional loss rate coefficient (β_{Li}) due to laser intensity (I_{Li}). Open and closed circles refer to new results and those from (Auböck *et al.*, 2006).

4.3 Measurements of Heteronuclear Cold Collisions

Inelastic cold collision losses are measured between ^{23}Na and ^{7}Li as well as ^{23}Na and ^{87}Rb in a two-species magneto optical trap. ^{23}Na, ^{87}Rb and ^{7}Li atoms are loaded independently. ^{7}Li and ^{23}Na atoms are produced by oven reservoirs controlled by temperature (using heating coils). ^{87}Rb atoms are produced by dispenser. Each element has a different vapor pressure at different temperature. In heteronuclear cold collision experiment, the partial pressure of the one element on the other element has to be considered. In our experiment, temperature of ^{23}Na and ^{7}Li ovens are 120 ^{0}C and 375 ^{0}C, respectively, where as current of the ^{87}Rb dispenser is 2.7 ampere.

4.3.1 Li-Na Combined MOT

Collision losses are measured between ^{7}Li and ^{23}Na in a magneto optical trap at different laser intensities according to the parameters in table 4 and the technique said in section 4.1.2. By taking the difference of the linear lose rate (α) of lithium with out and linear loss (α') with presence of sodium atoms, heteronuclear collisional loss rate coefficients $\beta_{^{7}\mathrm{Li}}^{^{23}\mathrm{Na}}$ are measured. The density of the ^{7}Li is 1.1×10^{10} atoms/cm^3 at intensity 124 mW/cm^2 where as the density of the Na is 6.9×10^{9} atoms/cm^3 at constant intensity 100 mW/cm^2. Vacuum in chamber during the experiment is $(2-5)\times10^{-9}$ mbar. The measured data are compared with published results (Auböck *et al.*, 2006) as shown in the figure (4.62).

4.3.2 Na-Rb Combined MOT

^{23}Na and ^{87}Rb atoms are trapped simultaneously in a combined magneto optical trap. We have measured the collisional losses of ^{23}Na trap in the presence and absence of ^{87}Rb atoms by using the rate equation (2.67). We measured the collisional trap losses as function of different intensities as described in section 4.1.2 and plotted in figure (4.63).

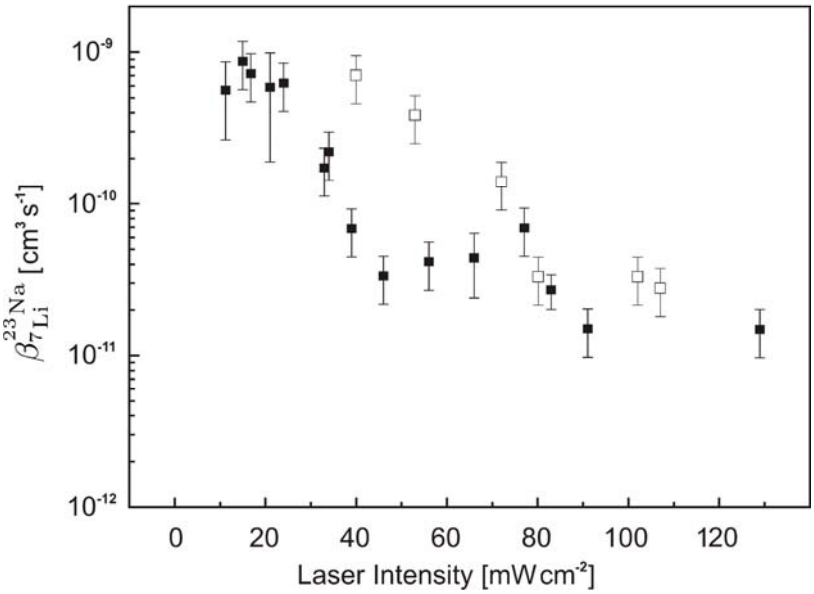

Figure 4.63: Heteronuclear loss rate coefficient ($\beta_{^7Li}^{^{23}Na}$) versus lithium MOT intensity. Open and closed square refer to new results and those from (Auböck *et al.*, 2006).

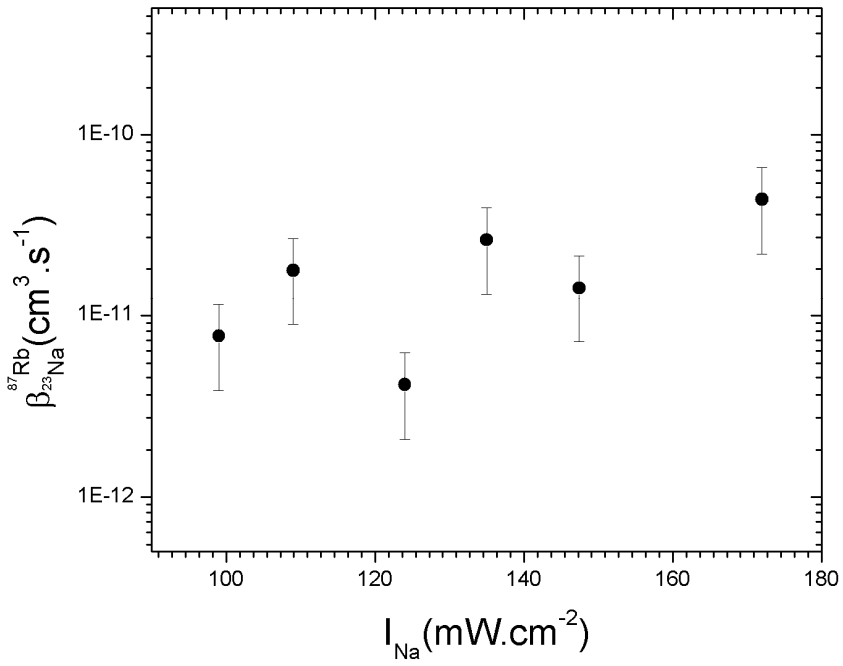

Figure 4.64: Heteronuclear trap losses of Na due to cold collision of rubidium in a combined ^{23}Na–^{87}Rb Magneto Optical Trap versus ^{23}Na cooling laser beam intensity. (Young et al., 2000) measured the heteronuclear trap loss rate coefficient $\beta_{^{23}Na}^{^{87}Rb}$ in range of $1\times10^{-11}-6\times10^{-11}$.

The back ground pressure and magnetic field gradient in axial direction in the vacuum chamber is 3×10^{-9} mbar and 0.58 mT.cm^{-1} respectively. Size of ^{23}Na cloud is small as compared to size of ^{87}Rb cloud. We measured the density $(1.2-1.7)\times10^{10}$ atoms/cm^3 for ^{87}Rb and $(6.1-6.8)\times10^{9}$ atoms/cm^3 for ^{23}Na. The trapping intensity of the ^{23}Na cooling laser beams ranges from 34 mW.cm^{-2} to 114 mW.cm^{-2}, where as the ^{87}Rb cooling laser beam has a fixed intensity value i.e. 30 mW.cm^{-2} during the measurement. By using the parameters of table 4, we measured the decay curves according to the technique in section 4.1.2.

4.4 Results and Discussions

Rubidium atoms are trapped with our newly built MOT. We used two independent laser systems for generating cooling and repumping frequencies. The diode laser (see 3.1.5) is used as a repumper beam and it is stabilized by polarization spectroscopy. The cooling laser beam is locked and stabilized by saturation spectroscopy. For locking the cooling laser frequency, ac and dc magnetic fields are used. By using this technique, we measured the steady state ^{87}Rb atom numbers, volume, density, linear loss rate coefficient (α), collisional loss rate coefficient (β) and hetero nuclear loss rate coefficient ($\hat{\beta}$) as described in sections (4.2.1, 4.2.2 and 4.2.3).

We also measured the collisional trap losses $\beta_{^{87}Rb}$, $\beta_{^{23}Na}$ and $\beta_{^{7}Li}$ as a function of the laser intensity (I) by using the technique in section 4.1.1 and observed the following behavior which is according to theory in section 2.3.

- If the density of the cloud is increased then the collisional loss rate (β) are also increased.
- Toward high intensity region

    1. Change in collisional losses are small.
    2. Atoms are going to be excited so the collisions started between ground- excited atoms or excited- excited atoms. Due to these collisions, homonuclear losses are increased.
    3. Trap is deep so losses are less as compare to low intensity region.

- Towards low intensity region

    1. Linear loss rate (α) is increased.
    2. Collisional losses are (β) also increased.
    3. Back ground gas has more influence on trapped atoms.
    4. Shape of cloud is expanded.

Measured collision loss rate (β) according to the parameters in table 4 and shown in the figures (4.51, 4.56 and 4.61) are

$(1.2\times10^{-11}$ to $9.2\times10^{-12})$ cm^3/s for ^{87}Rb @ (24 to 109) $mW.cm^{-2}$

$(1.02\times10^{-11}$ to $2.73\times10^{-11})$ cm^3/s for ^{23}Na @ (34 to 114) $mW.cm^{-2}$

$(3.82\times10^{-10}$ to $2.77\times10^{-11})$ cm^3/s for ^{7}Li @ (53 to 107) $mW.cm^{-2}$

^{7}Li has a special feature that fine structure splitting (ΔE_{FS}) is approximately equal to the trap depth $0.34\,cm^{-1}$(0.48K). If the trap depth is smaller the half of the ΔE_{FS} then both FSCC and RE are responsible for the trap loss but when the trap depth is exceed this value then only FSCC is the dominate loss channel which is shown in the figure (4.61).

My results are also reconfirmed (Auböck *et al.*, 2006) as shown in figures (4.61 and 4.62). The results show that losses due to fine structure changing collisions (FSCC) are larger as compared to radiative escape (RE).

^{23}Na and ^{87}Rb atoms have large masses as compared to the ^{7}Li atom. The probability of homonuclear collision losses due to FSCC is much larger. The FSCC mechanism is also independent of the trap depth for ^{23}Na and ^{87}Rb. The ratio of the probability for FSCC and the probability to RE for the sodium trap atoms is approximately 20. The measured values of collision losses (β) ^{23}Na in a figure (4.56) and ^{87}Rb in the figure (4.51) shows that collisions between ^{23}Na-^{23}Na & ^{87}Rb-^{87}Rb pairs are excited and FSCC mechanism occur according to the Gallagher-Pritchard model (section 2.3.1).

For low intensity region, hyperfine structure changing collision (HFSCC) is main source of losses which released a energy equal to splitting of the ground Hyper Fine Structure.

In case of heteronuclear cold collisions, we measured the trap losses for Li with and without presence of ^{23}Na atom as shown in the figure (4.62) and observed the following behavior.

- Heteronuclear loss rate is increasing towards the lower intensity.
- Li atom has greater velocity than Na atoms due to their mass ratio $m_{^7\mathrm{Li}}/m_{^{23}\mathrm{Na}} \approx 0.3051$.
- Hyperfine splitting of ^{23}Na atom is 1771 MHz = 85 mK.
- Hyperfine splitting of ^{7}Li atom is 803.5 MHz = 38.5 mK.
- Towards higher intensity, the heteronuclear loss rates are decreasing compared to the heteronuclear loss rates at lower intensity.

In our measured data, collisional loss rate coefficient 'β' is $7\times10^{-10}\ \mathrm{cm^3.s^{-1}}$ at $40\ \mathrm{mW.cm^{-2}}$.

Towards lower trapping laser intensity, fine structure changing collision (FSCC) is also occur due to the ^{23}Na atom (independent of trap depth due to heavy mass), additionally collision with each other, energy is transferred to ^{7}Li atom due to mass ratio and they escape quickly from magneto optical trap.

Towards higher intensity, RE as well as FSCC mechanism is the main cause of losses in heteronuclear collisions according the section 2.2.2 (Szczepkowski *et al.*, 2007). Similarly, for heteronuclear cold collision between ^{23}Na and ^{87}Rb element, from the measured data and figure (4.63), we observed

- For higher intensity the change in heteronuclear trap losses are small.
- The trap losses are measured in range of 100 $\mathrm{mW.cm^{-2}}$ to 160 $\mathrm{mW.cm^{-2}}$ and the corresponding heteronuclear trap loss rates are $1.7\times10^{-11}\ \mathrm{cm^3.s^{-1}}$ to $4.4\times10^{-11}\ \mathrm{cm^3.s^{-1}}$ respectively.
- ^{23}Na atoms have greater velocity than ^{87}Rb atoms due their mass ratio $m_{^{23}\mathrm{Na}}/m_{^{87}\mathrm{Rb}} \approx 0.2645$.
- Hyperfine splitting of ^{23}Na atom is 1771 MHz = 85 mK.
- Hyperfine splitting of ^{87}Rb is 6834 MHz = 328.36 mK.

Rubidium atoms are heavier than the ^{23}Na atoms. ^{23}Na has a great probability to escape from the MOT for all values of laser intensity.

According to GP model, there are two possibilities for FSCC, either ^{23}Na atom is excited and makes a quasi molecule with the ground stable rubidium atom ($Na^{*}Rb$) or ^{87}Rb atom is excited and make the molecule with the ground state ^{23}Na atom ($NaRb^{*}$), but in both cases FSCC mechanism is involved. So FSCC is main mechanism for atoms to escape from the trap.

According to (Young et *al.,* 2000), radiative escape (RE) has very less contribution in the heteronuclear losses of NaRb in MOT. Toward the low intensity, hyperfine changing collisions are the dominate mechanism for trap losses.

The heteronuclear loss rate coefficients $\beta_{^{7}Li^{23}Na}$ and $\beta_{^{23}Na^{7}Rb}$ are also measured by other groups as shown in the table 7 and our results are in good agreement with their results.

Table7: Published measurements of heteronuclear cold collisional loss rates $\beta_{^{7}Li^{23}Na}$ and $\beta_{^{23}Na^{7}Rb}$.

Heteronuclear loss rates	$\hat{\beta}(cm^{3}.s^{-1})$	References
$\beta_{^{7}Li^{23}Na}$	$10^{-11}-10^{-10}$	Auböck *et al.*, 2006
$\beta_{^{23}Na^{7}Rb}$	$1\times10^{-11}-6\times10^{-11}$	Young *et al.*, 2000

5. Conclusions

Experimental setup for the study of homo-heteronuclear losses in a combined magneto optical trap is consisting of many complicated and delicate sub systems. In order to use these systems a thorough understanding is required. Especially during cooling of alkali atoms with ring dye laser systems, one needs high proficiency to handle these ring dye laser systems to produce a stable laser light in terms of frequency and intensity for long period of time. Furthermore, It needs more effort to keep all the systems work properly during the measurements.

In this work, a magneto optical trap (MOT) of rubidium is built. The MOT is loaded with rubidium dispenser vapors and laser light is generated by a ring dye laser pumped by a Kr ion laser. This is first time according to my knowledge that the collision losses of rubidium are measured such that cooling laser is stabilized on a saturation spectroscopy signal which is shifted and modulated by static and oscillating magnetic fields. We have achieved ^{87}Rb density and homonuclear losses β, $(1-9)\times10^{10}\ atoms/cm^3$ and $(1.2-3.82)\times10^{-11}\ cm^3.s^{-1}$, respectively.

The elements ^{87}Rb-^{23}Na or ^{7}Li-^{23}Na can be trapped simultaneously or independently in current combined magneto optical trap (MOT). The atom number, density and position of the clouds can be selected separately.

^{23}Na, ^{7}Li and ^{87}Rb MOTs are characterized by measuring the maximum number of trapped atoms, density and alternatively the homonuclear losses. The measured homonuclear trap loss rates for ^{23}Na and ^{7}Li are $(1.02-2.73)\times10^{-11}\ cm^3.s^{-1}$ and $(2.77\times10^{-11}-3.82\times10^{-10})\ cm^3.s^{-1}$, respectively as shown in figures (4.56, 4.61).

Heteronuclear losses $\beta_{^{23}Na}^{^{87}Rb}$ and $\beta_{^{7}Li}^{^{23}Na}$ are also measured in the combined magneto optical trap. The measured values for heteronuclear losses $\beta_{^{23}Na}^{^{87}Rb}$ and $\beta_{^{7}Li}^{^{23}Na}$ are $(1.7\pm50)\times10^{-11}\ cm^3.s^{-1}$ and $(1.39\pm40)\times10^{-10}\ cm^3.s^{-1}$, respectively.

Appendix A

MATLAB Code to Calculate Homonuclear and Heteronuclear Trap Losses.

```
clear all;
close all;
warning off;


% 1 CONSTANTS
% ------------------------

c = 2.997924E8;              % Speed of light [m/s]

h = 6.62606896E-34;          % Planck's Constant [Js]
gamma = 2*pi*5.9E6;          % Natural line width of transition [Hz]
gammaNa = 2*pi*9.8E6;

lambda = 670.776E-9;         % Li D2 Wavelength [m]
lambdaNa = 588.995E-9;       % Na D2 Wavelength [m]

delta = 17.7E6;              % Detuning [Hz]
deltaNa = 15.68E6;

%Plas = 0.023;               % Total Laser Power [W]
Plas=input('Total Laser Power [mW],  P = ')/1000;
Plas_c = 0.002;              % Power of Laser Beam Center through 1mm pinhole [W]
PlasNa=0.1;

rlas = 0.00389;              % Laser Beam Radius [m]
rlasNa = 0.0046;

Itot = Plas/(pi*rlas^2);     % Total Laser Intensity [W/m²]
ItotNa = PlasNa/(pi*rlasNa^2);

I = Itot/(1-exp(-2));        % Laser Center Intensity (through 1mm pinhole)
fprintf('\nLaser center intensity [mW/cm²], I = %.4f\n',I/10);
INa = ItotNa/(1-exp(-2));

% Saturation Intensity
I0 = (h/(2*pi)*(2*pi*c/lambda)^3*gamma)/(12*pi*c^2);
%I0=25.33;
```

```
%eta = 1/105;                % Detection efficiency
eta=((0.055/0.2815)^2)/16;

%rho = 0.14448;              % Fraction of excited atoms
rho=input('\nFraction of excited atoms, rho = ');
%rho = (I/I0)./(1+2*I./I0+(2*delta/gamma)^2);
rhoNa = 0.22478;

% 2 DATA IMPORTING
% ------------------------
fprintf('\nImporting data ...\n');
% grdfileA=input('data file 1 (shutter closed, A)   ', 's');
% sigfileA=input('data file 2 (shutter open, A)   ', 's');
% decfileA=input('data file 3 (decay, A)   ', 's');
%
% grdfileAB=input('data file 4 (shutter closed, A+B)   ', 's');
% sigfileAB=input('data file 5 (shutter open, A+B)   ', 's');
% decfileAB=input('data file 6 (decay, A+B)   ', 's');
%
% grdfileB=input('data file 7 (shutter closed, B)   ', 's');
% sigfileB=input('data file 8 (shutter open, B)   ', 's');
pps=10;

[gTime,ground,gshut,ndata1]=getdata('ligr11.tab');
[sTime,signal,sshut,ndata2]=getdata('ligr11.tab');
[dTime,decay,dshut,ndata]=getdata('licur.tab');
dTime=(1:ndata)'./pps-1/pps;

[gTimeAB,groundAB,gshutAB,ndata1AB]=getdata('ligr01.tab');
[sTimeAB,signalAB,sshutAB,ndata2AB]=getdata('ligr01.tab');
[dTimeAB,decayAB,dshutAB,ndataAB]=getdata('linacur.tab');
dTimeAB=(1:ndataAB)'./pps-1/pps;

[gTimeB,groundB,gshutB,ndata1B]=getdata('na02.tab');
[sTimeB,signalB,sshutB,ndata2B]=getdata('na01.tab');
dTimeB=(1:ndata2B)'./pps-1/pps;

mground=ones(length(ground),1)*mean(ground(10:length(ground)));
mgroundAB=ones(length(groundAB),1)*mean(groundAB(10:length(groundAB)));
mgroundB=ones(length(groundB),1)*mean(groundB(10:length(groundB)));

%figure
%plot(gTime,ground,gTime,mground,'r')

%figure
%plot(sTime,signal)
```

```
% 3 DATA EVALUATION (Fluorescence, Number of atoms)
% ------------------------------------------------
fprintf('\nCalculating atom numbers ...\n');
F=((signal).*33.3+0.2)./10^9;          % Fluorescence Power und PD calibration function
[W]
Fg=((ground).*33.3+0.2)./10^9;         % only A
Fd=((decay).*33.3+0.2)./10^9;

FAB=((signalAB).*33.3+0.2)./10^9;      % Fluorescence Power und PD calibration
function [W]
FgAB=((groundAB).*33.3+0.2)./10^9;     % A+B
FdAB=((decayAB).*33.3+0.2)./10^9;

FB=((signalB).*30.7+0.6)./10^9;        % Fluorescence Power und PD calibration
function [W]
FgB=((groundB).*30.7+0.6)./10^9;       % only B (without filter)

%********

Ng=Fg/(eta * (h*c/lambda) * rho * gamma);          % Number of Atoms (ground signal)
mNg=mean(Ng(10:length(Ng)));                       % only A
sNg=std(Ng(10:length(Ng)));

NgAB=FgAB/(eta * (h*c/lambda) * rho * gamma);      % Number of Atoms (ground
signal)
mNgAB=mean(NgAB(10:length(NgAB)));                 % A+B
sNgAB=std(NgAB(10:length(NgAB)));

NgB=FgB/(eta * (h*c/lambdaNa) * rhoNa * gammaNa);        % Number of Atoms
(ground signal)
mNgB=mean(NgB(10:length(NgB)));                    % only B
sNgB=std(NgB(10:length(NgB)));

%********

N=F/(eta * (h*c/lambda) * rho * gamma);            % Number of Atoms
mN=mean(N(10:length(N)));                          % only A
sN=std(N(10:length(N)));

NAB=FAB/(eta * (h*c/lambda) * rho * gamma);        % Number of Atoms
mNAB=mean(NAB(10:length(NAB)));                    % A+B
sNAB=std(NAB(10:length(NAB)));

NB=FB/(eta * (h*c/lambdaNa) * rhoNa * gammaNa)-mNgB;          % Number of
Atoms
mNB=mean(NB(10:length(NB)));                       % only B
```

```
sNB=std(NB(10:length(NB)));

%********

Nd=Fd/(eta * (h*c/lambda) * rho * gamma)-mNg;          % Decay curve
%Nd=smooth(Nd,20);                                    % only A
%Nd=Nd;


NdAB=FdAB/(eta * (h*c/lambda) * rho * gamma)-mNgAB;    % Decay curve
%NdAB=smooth(NdAB,10);                                % A+B
%Nd=Nd;

figure;
plot(Nd);
hold on;
plot(dshut*1000,'r');
plot(NdAB,'g');
plot(dshutAB*1000,'r');
xlabel('Data point number');
legend({'number of atoms','shutter signal'},'location','NorthWest');
hold off;

pause;

% 4 STATISTICS
%---------------------
onoffs=2;
points=find(abs(diff(dshut))>1);              % Find Starting Points t0 (A)
if points(1)==1 points=points(2:end); end
k=1;
ii=1;
j=1;
while k<=onoffs && ii<=length(points)
   v(j)=points(ii);
   if ii<length(points) ii=ii+1; end
   if(points(ii)-points(ii-1))<10 && ii<length(points)
      j=j+1;
      v(j)=points(ii);
   else
      t0v(k)=v(1);
      k=k+1;
      j=1;
   end
end

clear points;
```

```
points=find(abs(diff(dshutAB))>1);            % Find Starting Points t0 (AB)
if points(1)==1 points=points(2:end); end
k=1;
ii=1;
j=1;
while k<=onoffs && ii<=length(points)
   v(j)=points(ii);
   if ii<length(points) ii=ii+1; end
   if(points(ii)-points(ii-1))<10 && ii<length(points)
      j=j+1;
      v(j)=points(ii);
   else
      t0vAB(k)=v(1);
      k=k+1;
      j=1;
   end
end

if dshut(t0v(1)+1)-dshut(t0v(1)) < 0
end


smoothing=1;
step=1;
%maximum=ceil(35500/step);

lo=smooth(Nd(end-500:step:end),smoothing);
hi=smooth(Nd(t0v(2)-500:step:t0v(2)),smoothing);
mlo=mean(lo);
mhi=mean(hi);
stdlo=std(lo);
stdhi=std(hi);

loAB=smooth(NdAB(end-500:step:end),smoothing);
hiAB=smooth(NdAB(t0vAB(2)-500:step:t0vAB(2)),smoothing);
mloAB=mean(loAB);
mhiAB=mean(hiAB);
stdloAB=std(loAB);
stdhiAB=std(hiAB);

c_fac=1/mean(hi)*sqrt(stdhi*stdhi-stdlo*stdlo);

bins=40;
y1=lo-mean(lo);
y2=hi-mean(hi);
xh=linspace(-3*stdhi,3*stdhi,bins);
```

```
H1=hist(y1,xh);
H2=hist(y2,xh);

y1f=max(H1)*exp(-xh.^2/(2*stdlo.^2));
y2f=max(H2)*exp(-xh.^2/(2*stdhi.^2));

figure
hold on;
bar(xh,H2,1);
H = findobj(gcf,'Type','patch');
set(H,'FaceColor','r','FaceAlpha',0.5)
plot(xh,y2f,'r');
bar(xh,H1,1);
H = findobj(gcf,'Type','patch');
set(H,'FaceAlpha',0.5)
plot(xh,y1f,'b');
xlabel('N - mean(N)'); ylabel('Number of Data Points');
legend({'','trap loaded','','trap empty'},'location','NorthWest');
hold off;

% figure(12)
% plot(dTime,Nd,'-b',dTimeAB,NdAB,'-r');
% xlabel('Time'); ylabel('Number of Atoms');
% legend({'only Li7','Li7 + Na'},'location','SouthWest');

% 5 DATA FITTING
% ------------------------

% 5.1 HOMONUCLEAR COLLISIONS
%*******************************

nfit=500;
ii=2;

if ii<length(t0v)
   int=t0v(ii):step:t0v(ii+1);
else
   int=t0v(ii):step:t0v(ii)+nfit;
end

x=dTime(int)-dTime(t0v(ii));
%data=log(abs(smooth(Nd(int),smoothing)));
data=smooth(Nd(int),smoothing);

tau=5;
xi=0.4;
N0=mhi;
```

```
y0=0;
t0=0;

partxt = {'tau','xi','N0','y0','t0'};
par0   = [tau xi  N0  y0  t0];
parfix = [0   0   1   0   1];

sigN=sqrt(stdlo^2 + c_fac^2.*data.^2);
w=1./(sigN.^2);

loadfuntxt=('modelfun = @(par,x) w.* (par(4) + par(3).*(1-(1+abs(par(2))).*exp(-(x-
par(5))./par(1))./(1+abs(par(2)).*exp(-(x-par(5))./par(1)))));');
lossfuntxt=('modelfun = @(par,x) w.* (par(4) + par(3).*(1-abs(par(2))).*exp(-(x-
par(5))./par(1))./(1-abs(par(2)).*exp(-(x-par(5))./par(1))));');

for i=1:5
   if parfix(i)==1
      loadfuntxt = strrep(loadfuntxt,['par(',num2str(i),')'],partxt(i));
      lossfuntxt = strrep(lossfuntxt,['par(',num2str(i),')'],partxt(i));
   end
end

if (data(1)-data(end))>0
   eval(char(lossfuntxt));
else
   eval(char(loadfuntxt));
end

%options=statset('TolX',[eps],'TolFun',[eps],'MaxIter',1e4,'DerivStep',[]);%,'Display','ite
r');
%[par,r,J,Sigma,MSE]=nlinfit(x,data,modelfun,par,options);
[par,r,J]=nlinfit(x,w.*data,modelfun,par0);%,options);
%nlintool(x,w.*data,modelfun,par0);

%ci = nlparci(par,r,'covar',Sigma);
ci = nlparci(par,r,J);
err=(ci(:,2)-ci(:,1))/2;

fitvec=modelfun(par,x)./w;
res=fitvec-data;

chisq=sum(1./(sigN.^2).*(r./w).^2);
DoF=length(data)-length(par);
Var=chisq/DoF;

fitvec=modelfun(par,x)./w;
```

```
intneg=t0v(ii)-50:step:t0v(ii);
xneg=dTime(intneg)-dTime(t0v(ii));

figure(2)
plot([xneg;x],[Nd(intneg);data],'b',[xneg;x],[mhi.*xneg./xneg;fitvec],'r');
xlabel('Time'); ylabel('Number of Atoms');
legend({'Li-7', 'Fit'},'location','NorthEast');

figure
plot(x,data,'b',x,fitvec,'r-',xneg,Nd(intneg),'b',xneg,mhi,'r-');
xlabel('Time'); ylabel('Number of Atoms');
legend({'Li-7', 'Fit'},'location','NorthEast');

% 5.1.1 LOSS RATE COEFFICIENTS

n0txt=('n0 = par(3)/abs(VolA);');
alphatxt1=('alpha = 1/par(1);');                                    % decay
alphatxt2=('alpha = (1-par(2))/(1+par(2)) * (1/par(1));');          % loading
betatxt1=('beta = abs(par(2))*sqrt(8)/((1-abs(par(2)))*n0*par(1));');   % decay
betatxt2=('beta = abs(par(2))*sqrt(8)/((1+abs(par(2)))*n0*par(1));');   % loading

for i=1:3
   if parfix(i)==1
      n0txt = strrep(n0txt,['par(',num2str(i),')'],partxt(i));
      alphatxt1 = strrep(alphatxt1,['par(',num2str(i),')'],partxt(i));
      alphatxt2 = strrep(alphatxt2,['par(',num2str(i),')'],partxt(i));
      betatxt1 = strrep(betatxt1,['par(',num2str(i),')'],partxt(i));
      betatxt2 = strrep(betatxt2,['par(',num2str(i),')'],partxt(i));
   end
end

[VolA,radA]=volume('liv11.tab');        % cloud volume [cm³], cloud gauss radius [cm]
eval(char(n0txt));                      % cloud center density [1/cm³]


if (data(1)-data(end))>0
   eval(char(alphatxt1));   % loss rate coefficients: homo-collisions [cm³/s]
   eval(char(betatxt1));    % (deloading)
else
   eval(char(alphatxt2));   % loss rate coefficients: homo-collisions [cm³/s]
   eval(char(betatxt2));    % (loading)
end

% 5.1.2 OUTPUT
fprintf('\n');
fprintf('FIT PARAMETERS (homonuclear) \n');
fprintf('*********************************\n');
```

```
if parfix(1)==0
   fprintf('tau =  (%.2f +/- %.2f)',par(1),err(1));
   fprintf('s       \n');
else
   fprintf('tau =  (%.2f +/- 0)',tau);
   fprintf('s  (fixed)\n');
end
if parfix(2)==0
   fprintf('xi  =   %.4f +/- %.4f  \n',abs(par(2)),err(2));
else
   fprintf('xi  =   %.4f +/- 0  (fixed)\n',xi);
end
if parfix(3)==0
   fprintf('N0  =   %.3E +/- %.3E \n',par(3),err(3));
else
   fprintf('N0  =   %.3E +/- 0  (fixed)\n',N0);
end
if parfix(4)==0
   fprintf('y0  =   %.4f +/- %.4f\n',par(4),err(4));
else
   fprintf('y0  =   %.2f +/- 0  (fixed)\n',y0);
end
if parfix(5)==0
   fprintf('t0  =  (%.2f +/- %.2f)',par(5),err(5));
   fprintf('s  \n');
else
   fprintf('t0  =  (%.2f +/- 0)',t0);
   fprintf('s  (fixed)     \n');
end
fprintf('*********************************\n');
fprintf('DoF  =  %i\n',DoF);
fprintf('Chi² =  %.3f\n',chisq);
fprintf('Var  =  %.3f\n\n',Var);
fprintf('*********************************\n');
fprintf('n0 =   %.3E\n',n0);
fprintf('ALPHA = %.3E 1/s\n',alpha);
fprintf('BETA = %.3E cm³/s\n\n',beta);

%if ii==1
A(:,1)=x(1:length(x));
%end
A(:,2)=data(1:length(x));
save A.tab A -ascii -tabs;

pause;

% 5.1 HETERONUCLEAR COLLISIONS
```

```
%*******************************

if ii<length(t0vAB)
   int=t0vAB(ii):step:t0vAB(ii+1);
else
   int=t0vAB(ii):step:t0vAB(ii)+nfit;
end

%dTime=dTime;
x=dTimeAB(int)-dTimeAB(t0vAB(ii));
data=NdAB(int);
data=smooth(NdAB(int),smoothing);

tau=5;
xi=0.4;
N0=mhiAB;
y0=0;
t0=0;

par0   = [tau xi  N0  y0  t0];
parfix = [0   0   1   0   1];

sigN=sqrt(stdlo.^2 + c_fac^2*data.^2);
w=1./(sigN.^2);
%data=data;

loadfuntxt=('modelfun = @(par,x) w.* (par(4) + par(3).*(1-(1+abs(par(2))).*exp(-(x-
par(5))./par(1))./(1+abs(par(2)).*exp(-(x-par(5))./par(1)))));');
lossfuntxt=('modelfun = @(par,x) w.* (par(4) + par(3).*(1-abs(par(2))).*exp(-(x-
par(5))./par(1))./(1-abs(par(2)).*exp(-(x-par(5))./par(1))));');

for i=1:5
   if parfix(i)==1
      loadfuntxt = strrep(loadfuntxt,['par(',num2str(i),')'],partxt(i));
      lossfuntxt = strrep(lossfuntxt,['par(',num2str(i),')'],partxt(i));
   end
end

if (data(1)-data(end))>0
   eval(char(lossfuntxt));
else
   eval(char(loadfuntxt));
end


%[par,r,J,Sigma,MSE]=nlinfit(x,data,modelfun,par,options);
[par,r,J]=nlinfit(x,w.*data,modelfun,par0);%,options);
```

```
%ci = nlparci(par,r,'covar',Sigma);
ci = nlparci(par,r,J);
err=(ci(:,2)-ci(:,1))/2;

chisq=sum(1./(sigN.^2).*(r./w).^2);
DoF=length(data)-3;
Var=chisq/DoF;

fitvec=modelfun(par,x)./w;

intneg=t0vAB(ii)-50:step:t0vAB(ii);
xneg=dTimeAB(intneg)-dTimeAB(t0vAB(ii));

figure(2)
hold on;
plot([xneg;x],[NdAB(intneg);data],'g',[xneg;x],[mhiAB.*xneg./xneg;fitvec],'r');
xlabel('Time'); ylabel('Number of Atoms');
legend({'Li-7', 'Fits', 'Li-7 + Na'},'location','NorthEast');
hold off

figure
plot(x,data,'g',x,fitvec,'r',xneg,NdAB(intneg),'g',xneg,mhiAB,'r');
xlabel('Time'); ylabel('Number of Atoms');
legend({'Li-7 + Na', 'Fit'},'location','NorthEast');

% 5.2.1 LOSS RATE COEFFICIENTS
[VolAB,radAB]=volume('liv01.tab');
[VolB,radB]=volume('nav.tab');                    % cloud volume [cm³], cloud gauss
radius [cm]

n0txt=('n0 = par(3)/abs(VolAB);');              % cloud center density [1/cm³]
alpha1txt1=('alpha1 = 1/par(1);');                                  % decay
alpha1txt2=('alpha1 = (1-par(2))/(1+par(2)) * (1/par(1));');            % loading

for i=1:3
   if parfix(i)==1
      n0txt = strrep(n0txt,['par(',num2str(i),')'],partxt(i));
      alpha1txt1 = strrep(alpha1txt1,['par(',num2str(i),')'],partxt(i));
      alpha1txt2 = strrep(alpha1txt2,['par(',num2str(i),')'],partxt(i));
    end
end

if (data(1)-data(end))>0
   eval(char(alpha1txt1));   % loss rate coefficients: homo-collisions [cm³/s]
                     % (deloading)
else
```

```
   eval(char(alpha1txt2));   % loss rate coefficients: homo-collisions [cm³/s]
                        % (loading)
end

beta1 = (alpha1-alpha) * pi^(3/2)*radA^3*(1+(radB/radA)^2)^(3/2) / mNB;

% 5.2.2 OUTPUT
fprintf('\n');
fprintf('FIT PARAMETERS (heteronuclear) \n');
fprintf('*********************************\n');
if parfix(1)==0
   fprintf('tau =  (%.2f +/- %.2f)',par(1),err(1));
   fprintf('s       \n');
else
   fprintf('tau =  (%.2f +/- 0)',tau);
   fprintf('s  (fixed)\n');
end
if parfix(2)==0
   fprintf('xi  =   %.4f +/- %.4f  \n',abs(par(2)),err(2));
else
   fprintf('xi  =   %.4f +/- 0  (fixed)\n',xi);
end
if parfix(3)==0
   fprintf('N0  =   %.3E +/- %.3E \n',par(3),err(3));
else
   fprintf('N0  =   %.3E +/- 0  (fixed)\n',N0);
end
if parfix(4)==0
   fprintf('y0  =   %.4f +/- %.4f\n',par(4),err(4));
else
   fprintf('y0  =   %.2f +/- 0  (fixed)\n',y0);
end
if parfix(5)==0
   fprintf('t0  =  (%.2f +/- %.2f)',par(5),err(5));
   fprintf('s  \n');
else
   fprintf('t0  =  (%.2f +/- 0)',t0);
   fprintf('s  (fixed)     \n');
end
fprintf('*********************************\n');
fprintf('DoF  =  %i\n',DoF);
fprintf('Chi² =  %.3f\n',chisq);
fprintf('Var  =  %.3f\n\n',Var);
fprintf('*********************************\n');
fprintf('n0 =   %.3E\n',n0);
fprintf('ALPHA´ = %.3E 1/s\n',alpha1);
fprintf('ALPHA´-ALPHA = %.3E 1/s\n',alpha1-alpha);
```

```
fprintf('BETA´ = %.3E cm³/s\n\n',beta1);


%if ii==1
AB(:,1)=x(1:length(x));
%end
AB(:,2)=data(1:length(x));
save AB.tab AB -ascii -tabs;
function [Time,CHI,CHII,ndata] = getdata(varargin)

%clear M Time CHI CHII
warning off;

File = varargin{1};

if File(length(File)-2:length(File))==('tab')

   Tab=importdata(File,'\t');
   if size(Tab)==[1 1] Tab=Tab.textdata; end
   Tab=Tab(2:length(Tab),:);
   Tab=strrep(Tab, ',', '.');
   L=length(Tab);

   t=1;
   while t<=L
      M(t,:)=str2num(char(Tab(t,:)));
      t=t+1;
   end

   Time=M(:,1);
   CHI=M(:,2);
   CHII=M(:,3);
   ndata=length(Time);

elseif File(length(File)-2:length(File))==('dat')

   M=importdata(File,'\t');
   %M=M.data;
   ndata=length(M);
   Time=(1:ndata)';
   Time=Time./200;
   CHI=M(:,1);
   CHII=M(:,2);

end
```

```
%global M Time CHI CHII
function [Vol, rad] = volume(file)


Tab=importdata(file,'\t');
if size(Tab)==[1 1] Tab=Tab.textdata; end
Tab=Tab(2:length(Tab),:);
Tab=strrep(Tab, ',', '.');
L=length(Tab);
t=1;
while t<=L
   M(t,:)=str2num(char(Tab(t,:)));
   t=t+1;
end

Time=M(:,1);
CHI=M(:,2);
CHII=M(:,3);
ndata=length(Time);

mm=(1:2046)'*0.0131;
center=find(CHII(600:1300)==max(CHII(600:1300)));
center=599+center(1)+round(length(center)/2);

int=(center-400:center+400);

par0 = [0.17   0.01  13  1];
%      [offset   A   c   w]

myfun = @(par,x) par(1) + par(2)*exp(-((x-par(3)).^2)./(2*abs(par(4)).^2));

par=nlinfit(mm(int),CHII(int),myfun,par0);

fitvec=myfun(par,mm(int));

rad=abs(sqrt(2)*par(4));

figure;
plot(mm(int),CHII(int),mm(int),fitvec,'r');
xlabel('x [mm]'); ylabel('ccd signal [a.u.]');
legend({'data', 'Gauss Fit'},'location','NorthEast');
title(file);
text(par(3)+rad,myfun(par,par(3)+rad),['\leftarrow r = ',num2str(rad),' mm']);

rad=rad/10;                % radius in cm
Vol = pi^(3/2)*rad^3;      % Volume in cm^3
```

References

Aspect A, Arimondo E, Kaiser R, Vansteenkiste N, and Cohen-Tannoudji C (1988) Laser Cooling below the One-Photon Recoil Energy by Velocity-Selective Coherent Population Trapping, *Phys Rev Lett* **61:** 826-829.

Atutov S N, Biancalana V, Burchianti A, Calabrese1 R, Gozzini S, Guidi V, Lenisa P, Marinelli C, Mariotti E, Moi L, Nasyrov K and Pod'yachev S (2001) Sodium MOT collection efficiency as a function of the trapping and repumping laser frequencies and intensities. *Eur. Phys. J. D* **13:** 71-82.

Auböck G (2004) Light Assisted Collisions in a Combined Sodium – Lithium Magneto-Optical Trap diploma thesis (unpublished).

Auböck G, Binder C, Holler L, Wippel V, Rumpf K, Szczepkowski J, Ernst W E and Windholz L (2006) Trap loss collisions of ^{6}Li and ^{7}Li with ^{23}Na in a combined magneto-optical trap. *J Phys B: At Mol Opt Phys* **39:** S871–S879.

Band Y B, Tuvi I, Suominen K A, Burnett K and Julienne PS (1994) Loss from magneto-optical traps in strong laser fields *Phys Rev A* **50:** R2826 – R2829.

Band Y B and Tuvi I (1995) Reduced optical shielding of collisional loss for laser-cooled atoms. *Phys Rev A* **51:** R4329–R4332.

Binder C (2004) Homo- und heteronucleare, kalte Stöÿe zwischen den leichten Alkali-Atomen ^{6}Lithium, ^{7}Lithium und Natrium. *PhD. Thesis (*unpublished).

Boesten H M J M, Verhaar B J and Tiesinga E (1993) Quantum suppression of collisional loss rates in optical traps. *Phys Rev A* **48:** 1428–1433.

Bussery B, Achkar Y and Aubert -F M (1987) Long Range molecular states dissociating to the three or four lowest

asymptotes for the ten heteronuclear diatomic alkali molecules. *Chemical Physics* **116:** 319.

Chu S, Hollberg L, Bjorkholm J E, Alex C and Ashkin A (1985) Three Dimensional Viscous Confinements and Cooling of Atoms by Resonance Radiation Pressure. *Phys Rev Lett* **55:** 48-53.

Dalibard J and Cohen-Tannoudji C (1989) Laser cooling below the Doppler limit by polarization gradients: simple theoretical models. *J Opt Soc Am B* **6:** 2023–2045.

Dinneen T P, Wallace C D and Gould P L (1992) Narrow linewidth, light stable, tunable diode laser system. *Opt Commun* **92:** 277-282

Einstein (1917) *Physik*. Zeitschr. XVIII, 121.

Exciton *data sheet* http://www.excitation.com.

Frisch O R and Stern O (1933) Zeits. F. Physik **85**: 4.

Fritz T (1999) Setup of a Magneto-Optical Trap for Lithium as a Part of a Combined Na-Li MOT. *Diploma thesis* Graz (unpublished).

Gallagher A and Pritchard D (1989) Exoergic Collisions of Cold Na^*-Na. *Phys Rev* **63:** 957-960.

Hänsch T and Schawlow A (1975) *Opt Commun* **13:** 68-71.

Holland M J, Suominen K.-A., and Burnett K (1994) Cold collisions in a laser field: Quantum Monte Carlo treatment of radiative heating. *Phys Rev A* **50:** 1513–1530.

Holler F L (2004) Untersuchung von Ladevorgängen und Stoÿprozessen in einer magnetooptischen Falle für ^{7}Lithium- und ^{23}Natrium- Atome *Diploma thesis* Graz (unpublished).

Huber W (2001) Charakterisierung einer magnetooptischen Falle und díe Bestimmung der Ionisationsquerschnitte für Natrium. *Diploma thesis* Graz (unpublished).

Julienne P S and Vigue (1991) Cold collisions of ground and excited state alkali-metal atoms. *Phys Rev A* **44:** 4464 -4485.

Julienne P S, Suominen K A and Band Y (1994) Complex-potential model of collisions of laser-cooled atoms. *Phys Rev A* **49:** 3890-3896.

Julienne P S, Williams C, Dulieu O and Band Y B (1994) Calculations of collisional loss rates of trapped Li atoms. *Laser Phys* **4:** 1076–1084.

Julienne P S (1996) Cold Binary Atomic Collisions in a Light Field. *Journal of Research of the National Institute of Standards and Technology* **101:** 487-503

Marinescu M and Sadeghpour H R (1999) Long-range potentials for two-species alkali-metal atoms. *Phys Rev A* **59:** 390-404.

Metcalf H J and van der Straten P (1999) Laser cooling and Trapping. New York: Springer P 157.

Monroe C, Swann W, Robinson H and Wieman C (1990) Very cold trapped atoms in a vapor cell. *Phys Rev Lett* **65:** 1571–1574.

Phillips W D (1998) Laser cooling and trapping of neutral atoms. *Rev Mod Phys* **70:**721-741.

Prentiss M, Cable A, Bjokholm J E, Chu S, Raab E L and Pritchard D E (1988) Atomic-density-dependent losses in an optical trap. *Opt Lett* **13:** 452-454.

Pritchard D E (1986) Electron and atomic collisions. In: pp.593-604. DC. Lorents and Meyer W E and Petersen J R.

Pritchard D E, Raab EL, Bagnato V, Wieman C E and Watts R N (1986) Light traps using spontaneous forces. *Phys Rev Lett* **57:** 310-313.

Raab E, Prentiss M, Cable A, Chu S and Pritchard D (1987) Trapping of Neutral Sodium Atoms with Radiation Pressure. *Phys Rev Lett* **59:** 2631-2634.

Reinaldo L. Cavasso -F, Scalabrin A, Pereira D, and Cruz F C (2003) Observing negligible collision trap losses: The case of alkaline-earth metals Phys Rev A **67:** 021402(R)

Ritchie N W, Abraham R, Xiao Y, Bradley C and Hulet R (1995) Trap-loss collisions of ultra cold lithium atoms. *Phys. Rev. A* **51:** 890.

Santos M S, Nussenzveig P, Antunes A, Cardona P S P and Bagnato V S (1999) Hyperfine-changing collision measurements in trap loss for mixed species in a magneto-optical trap. *Phys Rev A* **60:** 3892-3895.

Scherf W (1998) Simultaneous Trapping of Lithium and Sodium in a Magneto-Optical Trap. *PhD. Dissertation* (unpublished).

Schlöder, Engler H, Schünemann U, Grimm R and Weidemüller M (1999) Cold inelastic collisions between lithium and cesium in a two-species magneto-optical trap. *Eur Phys J D* **7:** 331-340.

Sesko D W, Walker T G and Wieman C (1991) Behavior of neutral atoms in a spontaneous force trap. *J. Opt. Soc. Am. B* **8:** 946– 958.

Shore B W (1990) The Theory of Coherent Atomic Excitation, Vol.2, Wiley, New York.

Solts, Ben-Reuven R A and Julienne P S (1995) Optical collisions in ultra cold atom traps: Two-photon distorted-wave theory. *Phys. Rev. A* **52:** 4029–4042.

Suominen K -A, Holland M J, Burnett K, and P S. Julienne (1994) Excited-state survival probabilities for cold collisions in a weak laser field. *Phys Rev A* **49:** 3897–3902.

Suominen K -A, Band Y B, Tuvi I, Burnett K and Julienne P S (1998) Quantum and semi classical calculations of cold collisions in light fields. *Phys. Rev. A* **55**:3724-3738.

Szczepkowski J, Paul- Kwiek E, Auböck G, Holler L, Binder C, and Windholz L (2007) Semi classical model of magneto-optical trap depth. *Eur Phys J Special Topics* **144:** 265-271.

Telles G D, Marcassa L G, Muniz S R, Santos M S, Antunes A and Bagnato V S (2000*)* The Study of Cold Collisions Involving Different Species. *Laser Physics* **10:** 21-25.

Tuner L D, Weber K P, Hawthorn C J and Scholten R E (2002). Frequency noise characterization of narrow line width diode lasers *Opt. Commun*. **201:** 394.

Vigue J (1986) Possibility of applying laser-cooling techniques to the observation of collective quantum effects. *Phys Rev A* **34**: 4476–4479.

Walker T, Sesko D and Wieman C (1990) Collective behavior of optically trapped neutral atoms. *Phys Rev Lett* **64**: 408–411.

Walker T and Feng P (1994) Measurements of collisions between laser-cooled atoms. *Adv At Mol Opt Phys* **34**:125–170.

Wallace C D, Dinneen T P, Tan K, Grove T and Gould P (1992) Isotopic difference in trap loss collisions of laser cooled rubidium atoms**.** *Phys Rev Lett* **69**: 897-900.

Weidemüller M, Zimmermann C (2009) Cold Atom and Molecules, Physics Text Book Wiley-VCH.

Weiller M E (2007) Aufbau und Inbetriebnahme Einer Magnetooptischen Falle für Alkali-Atome. *Diploma thesis* (unpublished).

Weiner J, Bagnato V S, Zilio S C and Julienne P S (1999) Experiments and theory in cold and ultra cold collisions. *Rev Mod Phys* **71:** 1-85.

Weiner J (2003) Cold and ultra cold collisions in quantum microscopic and mesoscopic systems by Cambridge University Press.

Wieman C and Hänsch T W (1976) Doppler-Free Laser polarization spectroscopy. *Phys Rev Lett* **36:** 1170-1173.

Wieman C E and Hollberg L (1991) Using diode lasers for atomic physics *Rev Sc Instrum* **62:** 1-20.

Wieman C, Flowers G and Gilbert S (1994) Inexpensive laser cooling and trapping experiment for undergraduate laboratories. *American Journal of Physics* **63:** 317-330.

Wineland D and Dehmelt H (1975) *Bull Am. Phys. Soc* **20**: 637.

Weast (ed.) (1972-73) RC *Handbook of chemistry and physics*, Cleveland.

Wippel V, Binder C and Windholz L (2002) Cross-section for collisions of ultracold ^{7}Li with ^{23}Na. *Eur Phys J D* **21:**101-104.

Young Y E, Ejnisman R, Shaffer J P and Bigelow N P (2000) Heteronuclear hyperfine-state-changing cold collisions *Phys Rev A* **62:** 055403.